Light-emission from conjugated dendrimers and polymers

Halim, Mounir

LIGHT-EMISSION FROM CONJUGATED DENDRIMERS AND POLYMERS

Mounir Halim

A Dissertation submitted to the University of Durham

for the Degree of

Doctor of Philosophy

Department of Physics

University of Durham

January 1999

ABSTRACT

Light-Emission from Conjugated Dendrimers and Polymers

Mounir Halim: Submitted for the Degree of PhD, January 1999

This thesis reports the photophysical and electroluminescence studies undertaken on two types of material: polymeric and dendritic. The dendritic architecture is a recent concept adopted to develop new materials for light-emitting diodes. The dendritic structure offers a combination of properties of both polymers and small organic molecules whilst having their own interesting characteristic of optimising processibility, charge transport, and optical properties independently. The dendritic structure consists of functional surface groups, conjugated dendrons and a conjugated core. Initial optical (absorption and photoluminescence) studies revealed that the dendrimer emission originates from the core and is independent of excitation wavelength. This was investigated further in distyrylbenzene based dendrimers where the effect of dendrimer generation number on photoluminescence and electroluminescence properties was studied. All dendrimers emit blue electroluminescence with, in some cases, reasonable electroluminescence quantum efficiency in the range of 0.09 % and brightness up to 150 Cd m^{-2}. Having established that the funnel effect, where excitation is successfully transferred to the dendrimer core in both PL and EL, different chromophores were incorporated in the dendrimer structure. Colour control was thus demonstrated in EL devices of the different dendrimers, showing the possibility of using a large number of chromophores in a processible form for EL applications. Conjugated polymers were also studied to investigate the nature of the emitting species (poly(*p*-pyridine)) and the effect of side-chains (poly(*p*-phenylenevinylene)). In poly(*p*-pyridine) the emission was found to be strongly dependent on pyridyl ring rotation affecting the emission and its quantum yield while the side-chains in the poly(*p*-phenylenevinylene) derivatives were found to affect polymer properties such as degree of conversion of non-conjugated to conjugated polymer. The PL quantum yield system was set-up and proved useful in assessing synthesis of new materials.

DECLARATION

The work described in this thesis was carried out at the Department of Physics, University of Durham between October 1995 and December 1998.

The material in this thesis has not been submitted for the examination for any other degree, or part thereof at the University of Durham or any other institution. The material contained in this thesis is the work of the author except where formally acknowledged by reference.

Mounir Halim, January 1999

ACKNOWLEDGEMENTS

I would like to thank my supervisor Dr I. D. W. Samuel for his continued support, encouragement and fruitful discussions throughout this project.

My gratitude also goes to my second supervisor Dr A. P. Monkman for his guidance and advice on physics and five-a-side football, but certainly not on driving around tight corners!

I am indebted to Jonathan Pillow and Dr Paul Burn for their magic chemistry that has produced many colourful trees without which I could never have seen any 'dendritic trees' glowing! I also deeply acknowledge the chemists of Durham: Dr Eymard Rebourt for his efficient PPY and French sense of humour and Dr Lockhart Horsburgh for his even brighter PPY and 'Jal frezi' recommendation. I would also like to thank Patricia Marr and Dr Joe Crayston at St Andrews University for supplying the PPV derivatives. The research group have certainly offered me much useful advice, especially on how to adapt to the Geordie lifestyle. I am also very grateful to Dr Andy Beeby for letting me use the facilities in his laboratories and to Dr Graham Cross for making me welcome in his clean room. The list should in no way forget Norman Thompson and David Pattinson for their continuous help and genius ideas, although I am not so sure about 'Mr Muscle oven cleaner'. A special thank you to Dr Mariana Vaschetto for her help with the colour printing. I would like to thank the University of Durham, Department of Physics for funding my PhD.

*And finally a **HUGE THANK YOU** to my dearest wife who has helped, supported, and cooked a LOT!*

DEDICATION

To my beloved parents,

without whom none of this would have been possible.

CONTENTS

Chapter 1

Introduction

Electroluminescence (EL), defined as the occurrence of light emission as a result of opposite charge recombination, has been observed in a large number of different materials, such as inorganic phosphors [1] and organic molecular crystals [2,3]. Commercial light-emitting diodes (LEDs) have been fabricated using inorganic semiconductors for many years and have been used in a variety of applications. Ideally, the emitting material should fulfil many criteria such as high luminescence efficiency, the availability of a broad range of colours, good stability, and a low manufacturing cost. Further criteria arise depending upon the commercial application. For example, in colour displays a reasonably fast luminescence response time is required, preferably with a narrow emission spectrum. Existing commercial materials for LEDs are struggling to meet the increasing number of demands: for example blue

emission from inorganic LEDs has until recently proven to be relatively difficult to achieve, while cost is still high compared to other LEDs emitting longer wavelengths. The deposition techniques, such as sublimation and vapour deposition, used for manufacturing semiconducting LEDs are relatively expensive and not well suited for the fabrication of large-area panel displays.

In 1990 a research group at the University of Cambridge discovered how conjugated polymers could be used as the emissive layer in light-emitting diodes [4]. The discovery of the 'plastic sandwich' has brought conjugated polymers to challenge other materials used for light-emitting applications. This has attracted a great deal of interest in the scientific community and initiated an increasing number of publications reporting that a number of desirable properties have been developed and improved [5,6].

Conjugated polymers are an interesting class of material with an extended system of delocalised π-electrons, hence attractive optical and electronic properties. In general, these materials display a weak inter-chain coupling and so they are considered to behave as one-dimensional semiconductors. Conjugated polymers offer many advantages over the conventional inorganic semiconductors which makes them of considerable interest for commercial display applications. The polymeric structure provides these materials with desirable mechanical and morphological properties. For example, flexibility is an important advantage for potential future flexible displays. They are easy to process and hence simple techniques are used for fabrication of plastic devices such as spin coating and casting. This, as well as maintaining a low manufacturing cost, offers the possibility of fabricating large-area displays. For colour display applications, it is important to be able to obtain different colours throughout the visible spectrum. This is achieved in conjugated polymers by chemical modification to the polymer structure. Moreover, the wide choice of materials available and multiple ways of synthesis can offer a large number of materials with different individual properties.

Although conjugated polymers seem to be very promising candidates for use in LEDs, a few characteristics of these materials have proven to be disadvantageous, such as photo-degradation and the difficulty in obtaining pure blue emission. Hence more research is in progress in order to eliminate or overcome such problems.

Dendrimers or dendritic molecules, known also as starburst dendrimers, are another interesting family of molecules. Dendrimers have several uses and are the focus of research projects mainly in biological applications, such as the dendritic box [7] demonstrated by E. W. Meijer *et al* where a different, smaller molecule was enclosed, and possibly transported, in the cavity of the dendrimer.

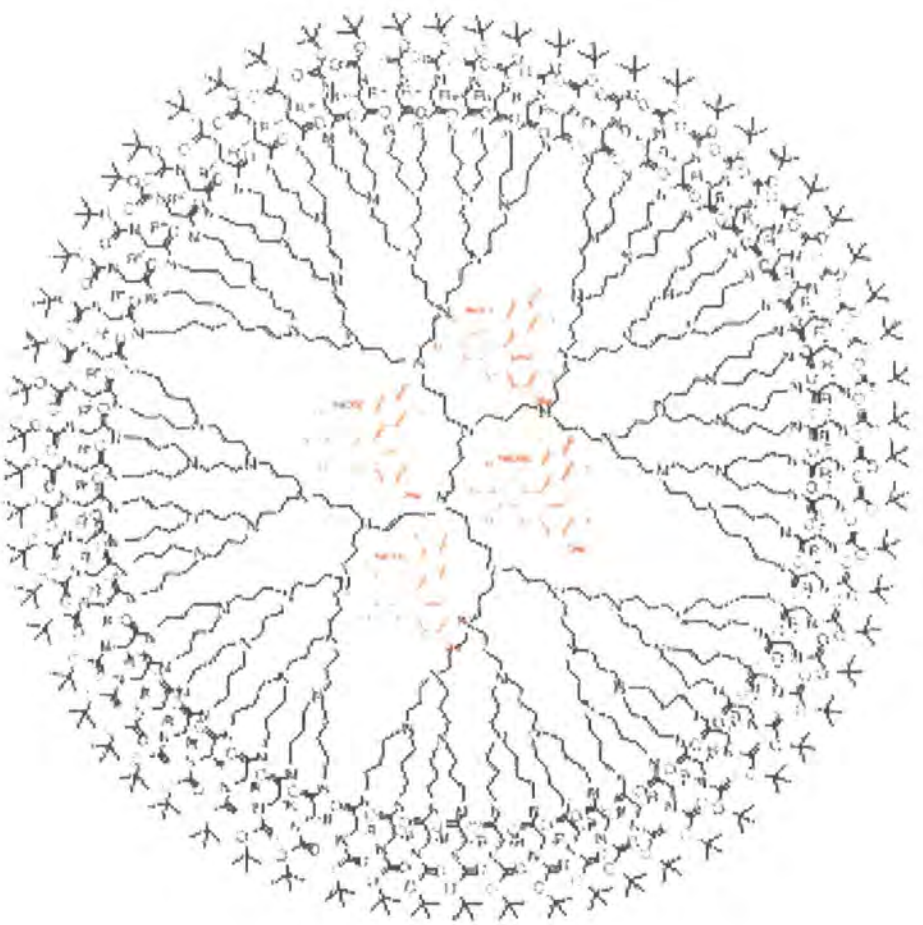

FIG. 2.1 *The dendritic box (taken from reference [7]).*

More recently, dendritic molecules have been used in light-emitting materials research as a charge transporting layer [8]. Recently a research group from the University of Illinois have used, for the first time, an anthracene based dendrimer as the active layer in LEDs. I will now briefly outline the contents of this thesis.

Chapter two provides a brief overview of the basic optical and electronic properties of conjugated polymers, starting from the simplest conjugated polymer, trans-polyacetylene. This chapter lays the groundwork for the explanations proposed in the following chapters.

Chapter three outlines the experimental techniques used to study and characterise the different polymers and dendrimers. Experiments such as the absolute quantum yield and electroluminescence characterisation are discussed.

Chapter four discusses the use of novel materials as the active layer in LEDs. Photophysical investigations were carried out on a trans-distyrylbenzene (DSB) based dendrimer in order to study the nature of the emitting species. These studies revealed that the excitonic species recombine in the central core. Higher generations of the DSB-based dendrimer were also studied to investigate the effect of generation number. DSB-based dendrimer LEDs were fabricated and were emitting in the blue part of the visible spectrum.

The fifth chapter describes how different colours were obtained in dendritic molecules. This was simply achieved by replacing the central core, which controls the colour, while the other parts of the dendrimer (branches and surface groups) are kept intact to preserve the processing properties of the molecules. Both photoluminescence and electroluminescence were demonstrated in the anthracene-derivative and porphyrin dendrimers. The demonstrated pure red emission in the porphyrin was further tuned to obtain different 'reds' by incorporating different metals in the porphyrin cavity.

Chapter six discusses the photophysical properties of PPY. The luminescence in solution and solid state is reported. Using the integrating sphere, the quantum yield of PPY films as a function of time in different atmospheres was carried out for a photo-stability study. The photophysical study also included the absorption and photoluminescence of PPY films, blended with a host polymer, doped with different acids, or as a function of temperature. The different studies allowed a greater understanding of the emission process in PPY. Different PPV derivatives were also studied to investigate the effect of side-groups on the polymer optical and processing properties.

The final chapter summarises the work described in this thesis by presenting general conclusions drawn from the results reported within this dissertation.

Publications that have been produced as a result of the work presented in this thesis are listed in the appendix.

References

1. J. W. Allen, *J. Luminescence,* **1994**, 60-61, 912.
2. M. Pope, H. P. Kallmann and P. Magnante, *J. Chem. Phys.,* **1962**, 38, 2042.
3. M. Pope and C. E. Swenberg, "Electronic Processes in Organic Crystals" **1982**, Clarendon Press, Oxford.
4. J. H. Burroughes, D. D. C. Bradley, A. R. Brown, R. N. Marks, R. H. Friend, P. L. Burn and A. B. Holmes, *Nature,* **1990**, 347, 539.
5. R. H. Friend, D. D. C. Bradley and A. B. Holmes, *Phys. World,* **1992**, 5, 42.
6. A. Kraft, A. C. Grimsdale and A. B. Holmes, *Angew. Chem. Int. Ed.,* **1998**, 37, 402.
7. E. W. Meijer *et al*, Polym. Mater. Sci. Eng., 1995, 73, 123.
8. Y. Kuwabara, H. Ogawa, H. Inada, N. Noma and Y. Shirota, *Adv. Mater.,* **1994**, 6, 677.

Chapter 2

Optical and Electronic Properties of Conjugated Materials

2.1 Introduction

The purpose of this chapter is to outline the basic physical properties of conjugated polymers. It begins with defining conjugation in molecular materials and by explaining the simplest conjugated polymer, the widely studied *trans*-polyacetylene. The following sections will discuss basic concepts of energy levels, optical transitions and photoexcitations within conjugated systems. Finally, a brief description of the electroluminescence process, from injection to electron-hole recombination, in these conjugated molecules will be presented.

2.2 Conjugated Molecules

The term 'conjugated' or 'conjugation' is a way of expressing the nature of some bonding between atomes due to electron delocalisation along these molecules. In ethene (C_2H_2), for example, each carbon atom is bonded to two hydrogen atoms and to the other carbon atom. The electronic configuration of the ground state of the carbon atom is $1s^2 2s^2 2p^2$ and the two p electrons in the outer electronic level are unpaired. In this case, the carbon atom's electronic configuration can mix the 2s orbital with two of the 2p orbitals to give three equivalent hybridised orbitals termed sp^2. These orbitals lie in a plane and are directed about 120° apart from each other; the bonds formed from these orbitals are called σ-bonds or alternatively 'single' bonds and are shown in figure 2.1. The remaining p orbital is unhybridised and is normal to the plane of the σ-bonds, hence is termed a p_z orbital.

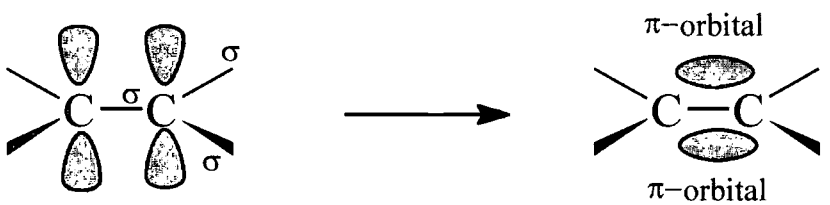

FIG. 2.1 *The formation of the π-bond (cloud) in ethene. The σ-bonds are represented with straight lines.*

There will be some overlap between the p_z orbitals of the neighbouring carbon atoms due to the fact that the atoms are close to each other. This electronic overlap will lead to the formation of a new bond above and below the σ-bonds of the same neighbouring atoms. This new bond is termed a 'pi (π)' bond, and collectively with a σ-bond they form what is called a 'double' bond.

If more than two carbon atoms are bonded together in the same electronic configuration, their p_z orbitals will overlap along the carbon atoms forming extended π-bonding or π-electron delocalisation. The system is termed π-conjugated, or often

just conjugated. Thus increased π-electron delocalisation is observed with an increasing number of carbon atoms as shown in figure 2.2 in the anthracene molecule.

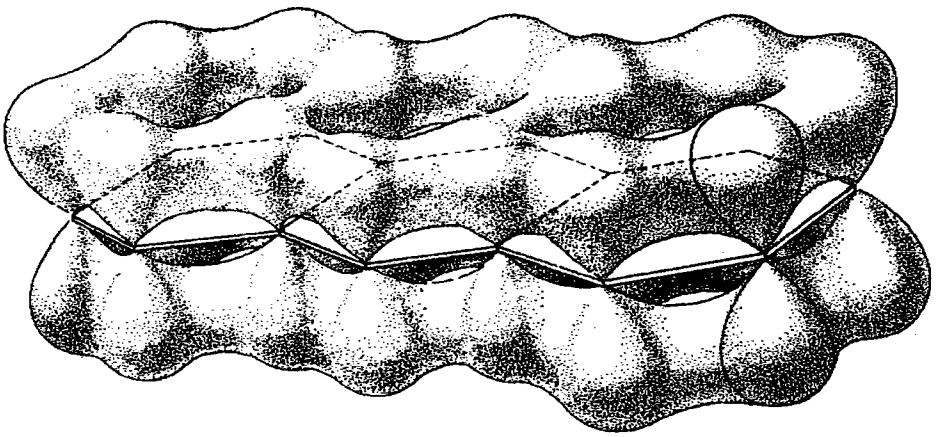

FIG. 2.2 *π-conjugation in the anthracene molecule (source: Pope and Swenberg, 1982).*

2.2.1 Polyacetylene

Trans-polyacetylene is, structurally, the simplest conjugated polymer and as such has been studied extensively both theoretically and experimentally. Its chemical structure is shown in figure 2.3 and consists of a chain of carbon atoms connected by alternating single and double bonds. In each carbon atom three electrons in the outer shell are in sp^2 hybridised electronic orbitals which form the σ-bonds. The fourth is in a π-orbital. The π-orbitals do overlap which leads to extensive electron delocalisation along the carbon atom chain.

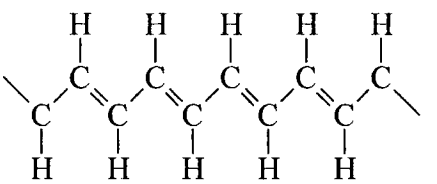

FIG. 2.3 *Trans-polyacetylene.*

2.2.2 The model

A single-electron model has been developed by Su, Schrieffer and Heeger (SSH) [1,2] for *trans*-polyacetylene and subsequently extended to other materials. The SSH approach involves tight-binding calculations for a polymer chain with cyclic boundary conditions, neglecting the electron-electron interactions.

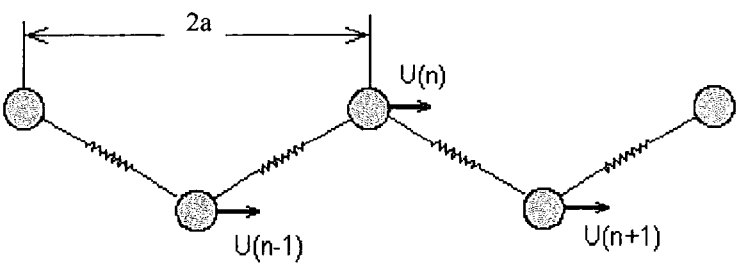

FIG. 2.4 *The displacement parameter 'u' as defined for trans-polyacetylene.*

The bonding between the carbon atoms in the polymer chain is represented as a spring (constant *k*). In the undimerised structure the carbon atoms would be spaced at regular intervals (a), measured parallel to the chain direction, so that the actual bond length would be $2a/\sqrt{3}$ (assuming 120° bond angles). The distortion is expressed using a set of displacement parameters (u_n), where u_n is the displacement of the n^{th} carbon atom (see figure 2.4).

However, the one-dimensional metal is unstable to dimerisation, and hence undergoes a Peierls transition [3] to the dimerised form. Experimental evidence of the dimerisation has been observed experimentally using NMR [4] and X-ray [5] techniques.

A special feature of *trans*-polyacetylene is the degenerate ground state. This means that the two alternative senses of bond alternation (single and double bonds), shown in figure 2.5, have identical energy.

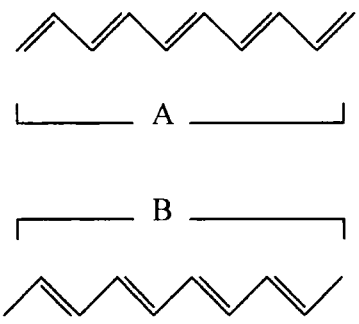

FIG. 2.5 *The two degenerate phases of trans-polyacetylene.*

2.2.3 Bond alternation defects

In a $(CH)_n$ chain with an odd number of carbon atoms, a bond alternation defect must occur to preserve the theoretical constraints of boundary conditions. The defect will separate the two equal energy phases of the *trans*-polyacetylene (A and B), as can be shown in figure 2.6, to result in a carbon atom with a p_z electron of non-bonding character. The defect is known as a soliton.

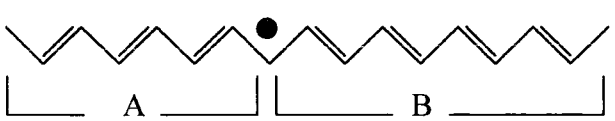

FIG. 2.6 *Bond alternation defect on a trans-polyacetylene chain.*

The soliton is expected to be mobile and free to move along the polymer chain, hence delocalised over several carbon atoms. The length of soliton delocalisation has been calculated resulting in the conclusion that the phase change extends over approximately 14 bonds [6]. Therefore, the soliton is spread far more than is shown in figure 2.6. The soliton introduces a localised state in the middle of the energy gap,

which can be occupied by 0, 1, or 2 electrons to form a negative, neutral, or positive soliton respectively (see figure 2.7). Note that since the energy required to create a soliton defect [7] is lower that that required to create an electron or a hole state at the band edge, the soliton is expected to be the most dominant species produced by photo or electro-excitation. Further detailed theoretical and experimental studies of solitons in trans-polyacetylene are reviewed by A. J. Heeger *et al* [8].

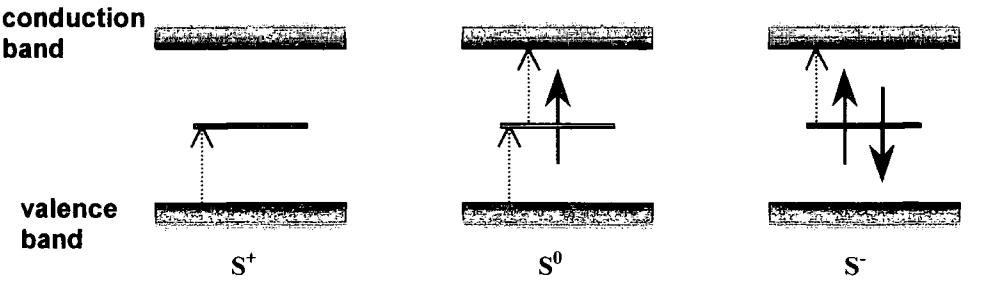

FIG. 2.7 *The mid gap states in trans-polyacetylene: positive (S^+), neutral (S^0), and negative (S^-) soliton. The dotted arrows represent the new optical transitions.*

2.3 Non-Degenerate Ground State Polymers

Most of the conjugated polymers prepared to date do not support isolated bond alternation. Unlike trans-polyacetylene, the reversal of the sense of bond alternation causes a change in energy in most conjugated polymers and hence they have a preferred sense of bond alternation. For example, in poly(*p*-phenylene) (PPP), the ground state corresponds to the benzenoid form while a reversal of the sense in the bond alternation gives the higher energy, thus less favoured, quinoid form. The two phases are shown in figure 2.8.

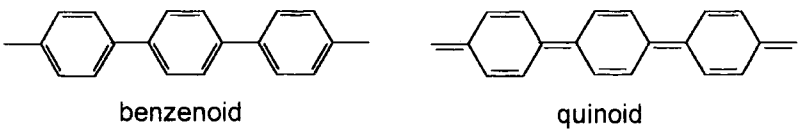

FIG. 2.8 *The two alternative senses of bond alternation in PPP.*

The non-degenerate ground state polymers also differ from the degenerate polymers in terms of the nature of the bond alternation defects and the consequent sub-gap states. In these materials a soliton would separate two phases with different energies and will, therefore, be expected to migrate to the end of the polymer chain in order to minimise the extent of the higher energy form. As a result, bond alternation defects are only stable in non-degenerate polymers if they are created in pairs. These defects are termed polaron, bipolaron, or polaron-exciton according to their occupancy.

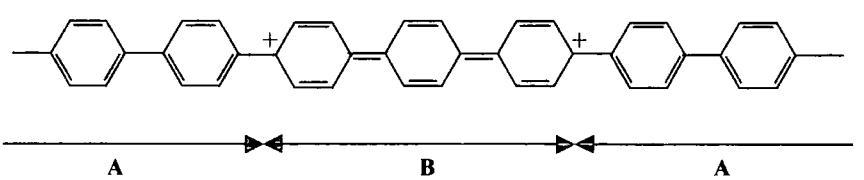

FIG. 2.9 *A schematic structure of a bipolaron in PPP. The soliton pair separates the benzenoid and quinoid forms.*

Polarons and bipolarons give rise to new energy levels within the band gap which are symmetrically placed around the centre of the gap, in a similar manner to that seen with solitons in *trans*-polyacetylene. The energy levels, of positive and negative polarons and bipolarons, are schematically shown in figure 2.10. These states give rise to new allowed optical transitions which can be detected using spectroscopic techniques.

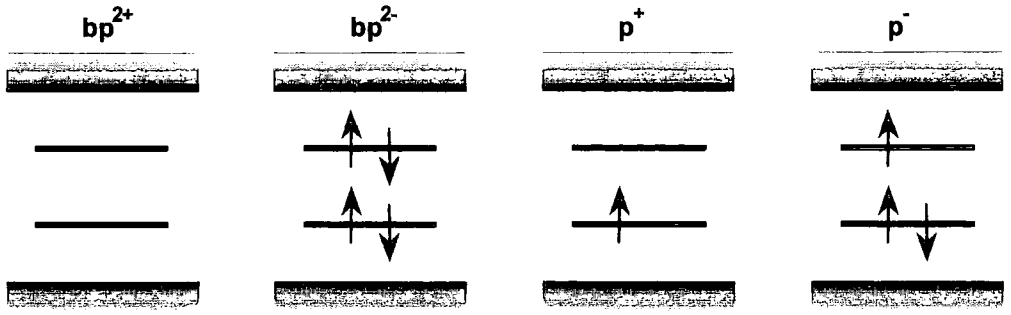

FIG. 2.10 *The energy levels of positive (p^+) and negative (p^-) polaron and positive (bp^{2+}) and negative (bp^{2-}) bipolaron.*

In the study of light-emitting polymers neutral polaron-excitons, which are another sub-gap defect, are of particular interest. This is mainly because they can be formed by either photoexcitation or a combination of positive and negative polarons, as is the case in the electroluminescence process [9]. After being created, the singlet polaron-exciton, henceforth referred to as excitons, may decay radiatively by emitting light.

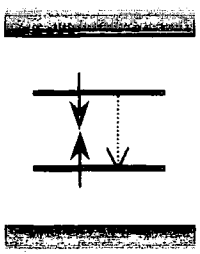

FIG. 2.11 *The neutral polaron-exciton.*

Charge storage in conjugated polymers in the appropriate soliton and polaron states is always energetically favoured over the occupation of the extended band states. Hence the intra-gap states are an important parameter for understanding the physics and the chemistry of these materials. As mentioned earlier these defects can be created in different ways, the most relevant to the work in this thesis are photo and electro-excitation which will follow.

2.4 Photoexcitation

In the solid state, conjugated polymers are very different from the idealistic one-dimensional configuration used in the SSH model. Further phenomena become operative in the solid state, such as inter-chain processes that could be predominant in determining the nature of photoexcitation and consequently affect the properties of the polymer, e.g. quantum yield. Hence, direct optical excitation is one of the most convenient ways to generate excitons in order to be able to study the nature of the photoexcitations in these conjugated molecules.

2.4.1 Emission process

A schematic diagram of the transitions that give rise to the absorption and emission spectra is shown in figure 2.12. In these materials the electronic transitions are strongly coupled to the vibrational modes, which leads to the vibronic structure in the absorption and emission profiles. Since electronic transitions take place on a much faster time scale ($\sim 10^{-15}$ s) than the nuclear motions ($\sim 10^{-13}$ s), most electronic transitions are completed before the nuclei can alter its configuration. Thus the electronic transitions are represented by vertical, or so called Franck-Condon, transitions as shown in figure 2.12. Because of the time scale of these electronic transitions the absorption and emission take place at the lowest vibrational levels, leading, as can be seen in figure 2.12 and 2.13, to mirror symmetry between the two spectra. Thus within this framework there is an energy shift between all various possible electronic transitions in absorption and emission which results in a shifted emission spectrum. This is termed the Stokes' shift and is evidence of excitonic emission.

Typically the observed absorption spectra of conjugated polymers are significantly broader and possess less vibronic structure than the emission spectra [10-12]. The exact energy of the electronic transitions for a given section of polymer will be determined by several factors, such as the local environment of the conjugated segments in the polymer chain. For a given polymer, there is likely to be a range of

electronic transition energies available due to the random distribution of conjugation length. Optical absorption occurs throughout the sample, sampling all the conjugation segments, and hence will result in a broad spectrum.

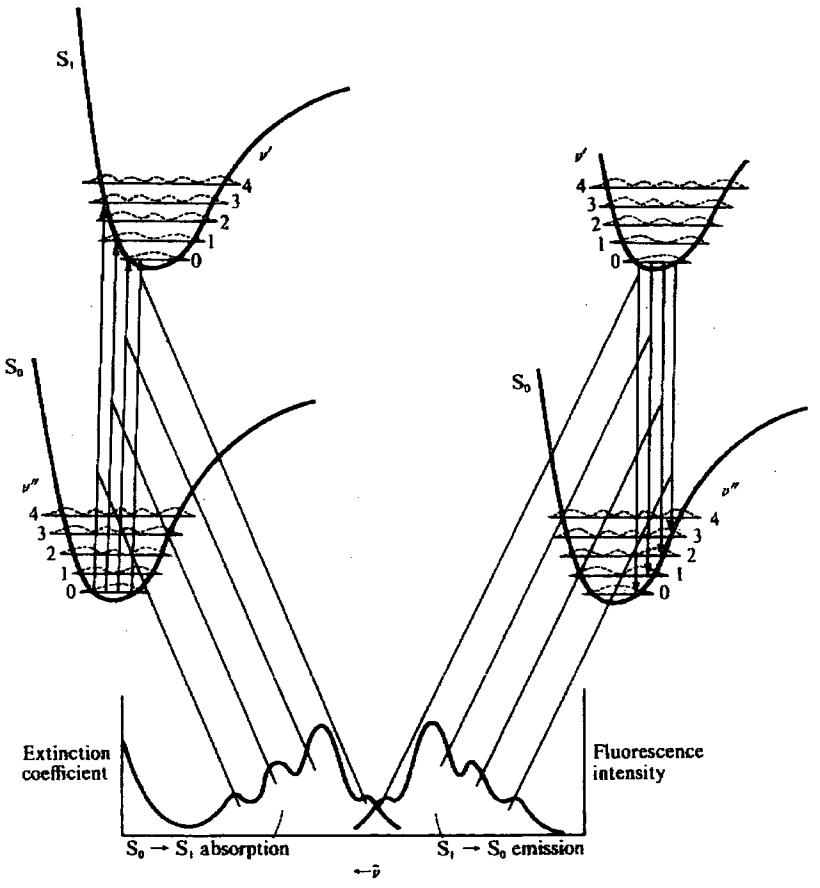

FIG. 2.12 *Absorption and emission transitions between the S_0 and S_1 electronic states of an organic molecule (from Kearwell and Williamson [13]).*

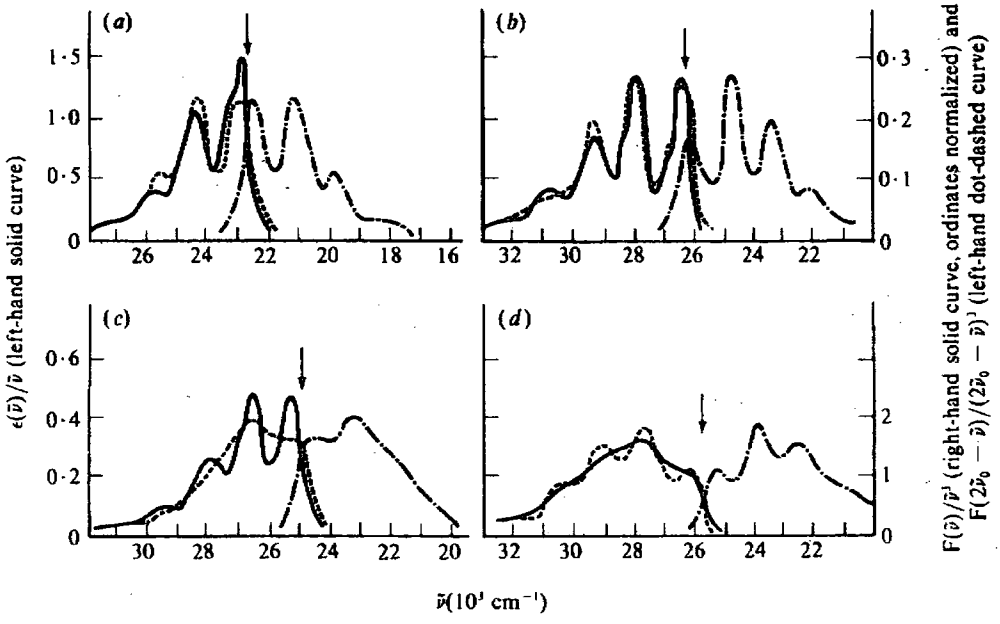

FIG. 2.13 *Mirror symmetry relationship and Stokes' shift (taken from reference [14]).*

2.4.2 Excitons in conjugated materials

In conjugated materials, if an electron is placed in the conduction band while a hole is placed in the valence band, it is possible that they will form a bound state known as an exciton. This species is a well known state in many solid sate systems, such as III-V semiconductors and molecular organic crystals [15,16]. In the context of organic molecular crystals there are two different types, or extremes, of excitons. If the electron and hole are bound on the same molecule with a relatively small radius (< 5 Å), then the exciton is known as a Frenkel exciton. The other extreme is when the exciton is delocalised over more than one order of magnitude of the intermolecular separation with a radius ranging between 40 to 100 Å. The exciton in this case is termed a Wannier-Mott exciton. There is another possible intermediate situation

where the extent of an exciton is approximately two times the nearest-neighbour intermolecular distance and is termed a charge-transfer exciton.

In the Wannier-type of exciton, the intervening medium between the electron and the hole may be treated approximately as a dielectric continuum and, therefore, the large radius exciton can be seen as a positronium atom. Optical transitions of such excitations are then considered to resemble Rydberg transitions in the hydrogen atom which result in a series of energy levels given by

$$E = E_G - \frac{G}{n^2} \qquad n=1, 2 \ldots, \qquad eq.\ 2.1$$

where E_G is the energy required to ionise the molecule in the solid and G is the binding energy of the exciton [14].

The existence of excitonic electronic states in conjugated polymers and their study has been the focus of extensive investigation by several researchers [17,18]. The Stokes' shift between the absorption and photoluminescence spectra was observed in many conjugated polymers [19-22]. For example, Bradley and co-workers [6,23,24] reported the Stokes' shift in PPV (figure 2.14) and have proposed that the electronic excited states responsible for emission were associated with excitons. The other difference between the emission and absorption spectra of PPV is the less pronounced structure in the absorption spectrum and its relative broadness. This is common behaviour in conjugated polymers and is in sharp contrast to the 'mirror-image' spectra observed in organic molecules. As mentioned earlier, this was attributed to the disordered nature of conjugated polymers. Optical absorption reflects contributions from all chains, including the many local environments within every chain, giving rise to a number of electronic structures, each with a different absorption spectrum. The absorption spectrum of the polymer, can then be imagined as a superposition of the contributions from the various environments in the polymer backbone. In fact, polyenes of up to 240 bonds were studied by Samuel *et al* and have shown a relatively featureless absorption in THF solutions. Kohler and Samuel [25] have shown that

these polyene absorption spectra could be understood as a sum of absorption spectra of shorter oligomers (see section 3.4). Excitons in PPV have a typical lifetime in the range of 70-250 ps at room temperature [26,27] and are believed to be a mobile species, capable of diffusing between different sections of the conjugation during this lifetime. The excitons will then migrate to the lowest energy sites prior to undergoing radiative relaxation. It is energetically preferable for these excitons to move to the longest sections of conjugation, which correspond to the low energy transitions. Emission therefore originates from only a section of conjugated segments in the polymer chain which explains the narrow nature of the emission spectrum with respect to the absorption spectrum.

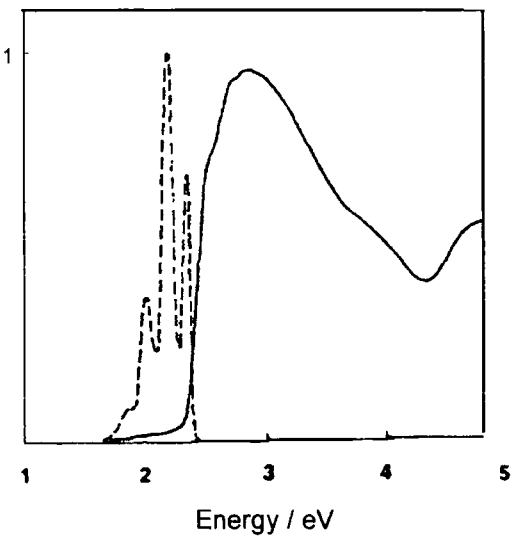

FIG. 2.14 *Normalised absorption (continuous) and emission (dashed) spectra of PPV.*

Further evidence of the exciton diffusion in these conjugated systems is provided by the site-selective fluorescence (SSF) experiments of Rauscher *et al* [28]. They have used different excitation energies to photo-excite a PPV film, the energy of the 0-0 emission peak was recorded as a function of the excitation energy and is shown in figure 2.15. By measuring the emission profile when photo-exciting the PPV at the edge of its absorption, only the lowest energy PPV conjugated segments are excited. Moreover, exciting the low energy segments inhibits the exciton migration since

adjacent segments are of higher energy. After a threshold energy (or localisation threshold), excitons are created in different environments of high energy and therefore can hop to other neighbouring conjugated segments of lower energy.

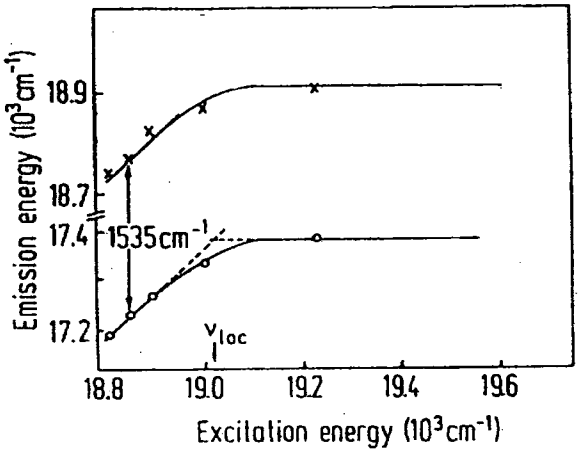

FIG. 2.15 *Variation of the emission energy as a function of the excitation energy (taken from Rauscher et al [28]).*

As mentioned earlier, the loss of the mirror-image between absorption and emission spectra in conjugated polymers is a result of structural disorder in the polymer backbone. By reducing the inhomogeneity of the absorption spectrum in a PPV derivative (poly(2-methoxy,5-(2'-ethyl-hexyloxy)-*p*-phenylenevinylene, MEH-PPV), Hagler *et al* [29] have provided experimental evidence of mirror-imaging between absorption and emission spectra. Unusually, the MEH-PPV used was gel-processed in polyethylene (PE), and Hagler was therefore able to stretch and align blends of the two polymers to stretch ratios in excess of 200, and consequently stretch-orientate the MEH-PPV creating a different environment. As a result, the absorption and emission spectra show mirror-image characteristic.

2.4.3 Non-radiative decay

The emission from conjugated polymers is agreed to be a result of the radiative decay of singlet excited states. However, this is not the only process taking place, as the

decay of the excited state occurs by a combination of radiative and non-radiative pathways with different decay rates (see section 3.5). The non-radiative decay channels are of considerable importance, as they will compete with the desired radiative processes and consequently affect the luminescence quantum yield. Unfortunately though, our understanding of many of these channels is very limited. R. H. Friend *et al* have listed a number of alternative decay mechanisms running in parallel to the radiative decays which could be responsible for the low efficiency in fluorescence [24]: for example charge separation, which is believed to predominantly be through inter-chain transfer, initially gives polarons and also bipolarons. However, in PPV this was not thought to be a very efficient process, as singlet excitons are the dominant species of photoexcitation [30], and so will not significantly affect the quantum yield or decay kinetics of the luminescence. Multiple phonon emission is also known as a non-radiative process. Danielsen and Ball [31] have reported the possibility of the multiple phonon emission process and believe it would be very rapid. It is also believed that the decay rate of this process is dependent on the number of phonons required. This process is known in semiconductors where the energy released will raise the temperature of the lattice. Migration to recombination centres such as quenching of charges (singlet-singlet annihilation) is, for example, another possible non-radiative channel for this decay. Inter-system crossing to a low-lying triplet state can also quench the luminescence: triplets act as efficient quenchers of singlet excitons. In this case the singlet passes its energy to the triplet. The reverse process, namely, transfer of triplet energy to the singlet exciton, is spin-forbidden. Photoinduced absorption is a useful technique for studying the triplets in conjugated polymers [6].

The recombination of the singlet excitons in conjugated polymers is believed to be influenced by some or all of these quenching mechanisms, depending on the material and experimental parameters such as temperature, excitation energy, and disorder in the solid state.

2.5 Electroluminescence

The previous section concentrated on the common method – photoexcitation – for creating singlet excited states. These are also believed to be created by electro-excitation where it is possible to generate individual positive and negative charges, electrons and holes, in the emissive material by charge-injection from contacts (figure 2.16).

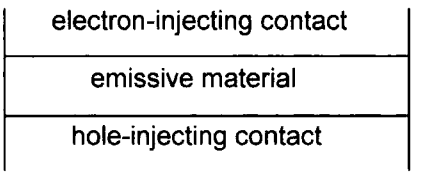

FIG. 2.16 *A basic electroluminescent device.*

The electrons and holes are injected by the contacts in different regions of the emissive material and are subsequently transported, under the influence of the applied electric field, to different regions of the material where they meet and may form electron-hole pairs and excitonic bound state. Any singlet excited states so formed have the potential of decaying by emitting light known as electroluminescence.

The electroluminescence process consists of three important stages: the injection of electrons and holes, their transport, and finally their radiative recombination. A brief background on these mechanisms will therefore follow.

2.5.1 Charge injection

Early polymer devices used PPV as the emissive layer [32], while a semi-transparent oxidised aluminium layer was used as the hole injecting electrode. Electrons were injected using aluminium contacts. These devices were inefficient and suffered from several problems [33]. Since then, ITO has become the most frequently used hole injector in polymer/organic LEDs.

The injection of charge carriers may occur either by quantum mechanical tunnelling or by a thermionic emission mechanism. The current will be dominated by one of these mechanisms depending on many parameters, such as the nature of the barrier or strength of the applied electric field.

In the thermionic emission case, the current across a barrier of height ϕ, in the absence of space charge and trapping sites, will be given by the Dushman-Richardson equation [34]:

$$I \propto T^2 e^{-\phi/kT} \qquad \textit{eq. 2.2.}$$

The barrier height is a function of the applied electric field across the device and therefore the current is field dependent. Note that the diffusion of the charges back to the injecting metal is a common undesirable feature. Typically in conjugated polymers such as PPV, the charge mobility is not high enough to remove the injected carriers from the vicinity of the metal-polymer interface which results in a back-diffusion into the electrode. This phenomenon is particularly important at low bias.

In the tunnelling case, also referred to as field emission, the injection of the carrier is modelled by assuming tunnelling through a triangular barrier. Fowler-Nordheim theory, based on this model, predicts a current of

$$I \propto F^2 \exp\left(\frac{-8\pi\sqrt{2m^*}\phi^{\frac{3}{2}}}{3qhF}\right) \qquad \textit{eq. 2.3}$$

where m^* represents the effective mass [35]. The field emission is known to be important at low temperatures or for large barriers at high fields [36].

Although these injection mechanisms show different characteristics, it is not very clear which one will dominate for a given device. I. D. Parker [35], for example, has used field emission to model the injection current in MEH-PPV devices at room

temperature. The possibility of the two mechanisms running in parallel to model the injection of the majority carriers was also proposed in organic hole transporting materials by H. Vestweber and co-workers[37]. These basic processes are often governed by the individuality of the systems, such as metal-material interface, making the whole process of a complex nature.

Generally, in semiconductor devices, the nature of the interface is the major limiting factor on the current across the device. This could also be applicable to polymer devices and so could have a significant influence on device performance. In polymer/organic LEDs, where there is an intimate contact between the emissive layer and the metal contact, a potential barrier is created due to the workfunction differences of the two materials. This barrier will therefore affect the charge injection into the bulk, and hence affect many properties such as efficiency and brightness of devices. It is also possible, depending on conditions used to fabricate the cathodes, to form oxides between the metal and the active layer. This is likely to influence the barrier properties.

The nature of this interface has been extensively studied [38]. Charge build-up at this interface will result in the coincidence of the Fermi levels of the two materials. In semiconductors, it is known that if the Fermi energy of the semiconductor is larger than the workfunction of the electrode, then the contact is considered ohmic. In the opposite case, where the Fermi level of the semiconductor is lower than the metal workfunction, the resulting contact is known as a Schottky barrier. Most of the work on modelling the metal-polymer interfaces has been based on these semiconductor models. It is, however, still unclear as to what extent these electrode-emitter interfaces in conjugated materials differ from those in conventional inorganic materials.

Ideally these organic materials are considered intrinsic semiconductors. However, despite the considerable care taken in their processing, small amounts of impurities are present in the bulk, usually considered as dopants. For example, PPV is thought to be slightly *p*-doped, possibly due to the presence of residuals of precursor units, or perhaps because of some oxygen defects. Some attempts have been carried out to

determine the dopant concentration: in PPV estimates of 10^{14} and 10^{17} cm^{-3} were deduced from conductivity measurements [39] and from LED characterisation [40] respectively. The concentration of dopants is believed to vary strongly, depending on the synthesis and processing of the materials.

2.5.2 Charge transport

In molecular crystals the carrier mobility is typically in the range 10^{-2}-10^{1} cm^2 V^{-1} s^{-1} [14] and is known to be limited by a hopping process of the charge between conjugated units. In conjugated polymers, hole mobility has been found to be around 10^{-4} cm^2 V^{-1} s^{-1} [41-43]. The charge transport in these conjugated materials, according to Time-of-Flight (TOF) measurement, is highly dispersive, as is generally expected in disordered systems [44]. The low mobility is believed to be due to larger hopping distances, increased disorder, and also to the effects of traps. The electron mobility, compared to mobility of the holes, is found to be at least two orders of magnitudes lower [42]. This is usually attributed to the trapping of electrons at defect sites [40]. Two principal models have been proposed to explain the observed transport properties of conjugated materials. The first, known as the 'polaron model', is based on the assumption of a thermally activated hopping process [45]. The activation energy for a given 'hop' is determined by the lattice distortion associated with the charge on the chain and the overlap integral between the adjacent sites. The other model, known as the 'disorder model', assumes that the disorder in the material is the major factor controlling the charge transport [46]. The dispersive nature of the charge transport in these materials can not be explained with the polaron model alone. Disorder theory predicts that a reduction of the hopping rate with time after charge injection occurs as the charge carriers relax into thermal equilibrium. This model is similar to that used in explaining the diffusion of excitons in disordered systems.

The temperature and field dependence of the mobility predicted by the two different models are not the same.

2.5.3 Charge recombination

In an electroluminescent device, charges of opposite sign are injected from two electrodes situated at either side of the active layer. The capture of these charges to form a bound, singlet exciton state is often referred to as recombination. Due to the non-geminate nature of the injected charges and to the threefold degeneracy of the triplet state, the ratio of triplet to singlet exciton generated should be 3:1. This figure is usually used to predict the maximum of electroluminescence quantum efficiency for the LED of 25 % if the triplets are bound at room temperature.

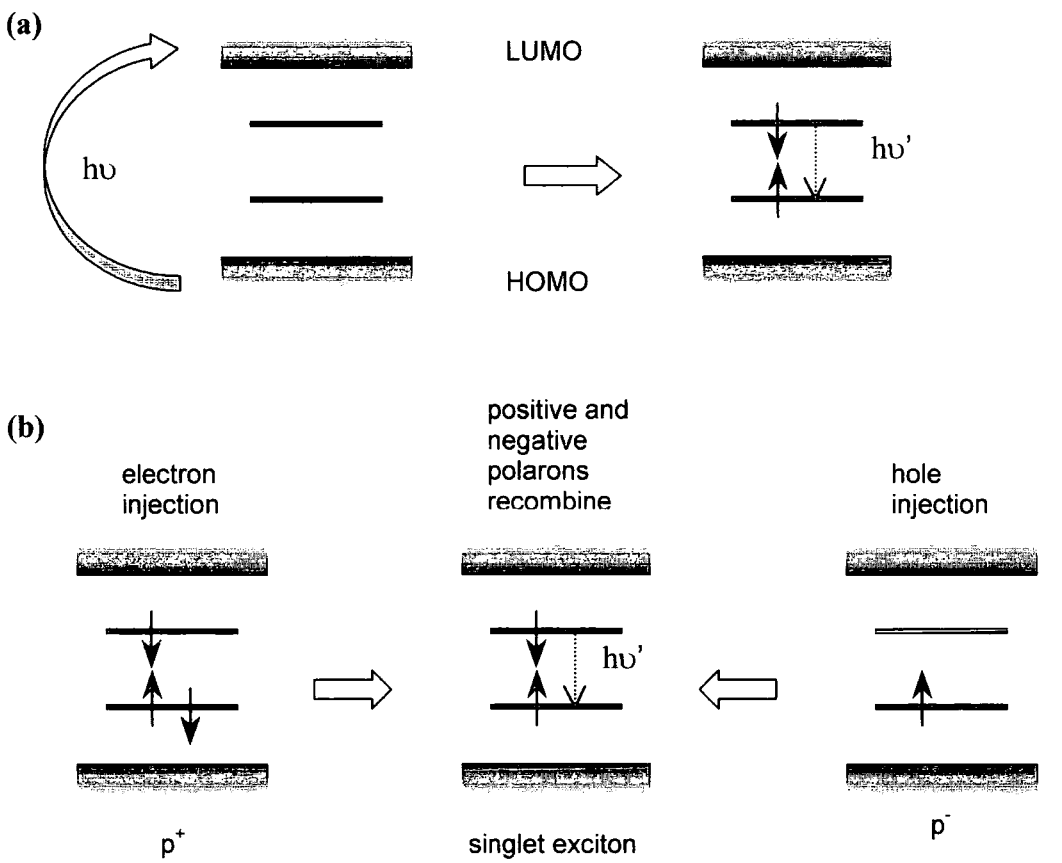

FIG. 2.17 *Scheme of (a) photoluminescence and (b) electroluminescence processes.*

It is clear, from figure 2.17, that both process – photoluminescence and electroluminescence are similar. This is also apparent when comparing the PL and EL spectra which are usually of the same shape and their comparison could give useful information about the process of emission and the nature of emitting species in polymer LEDs (figure 2.16). The comparison of the two spectra can also show their non-similarities which could indicate important facts such as different emission zones: in the PL measurement the emission is believed to occur from the bulk of the emissive material whereas in the EL process, the emission zone is believed to be close to the metal/emissive material interface. This is influenced by the mobility of the opposite charges in the material. The recombination zone can be moved away form the metal vicinity by introducing a further layer between the metal and the active layer (bilayer LEDs). The added layer acts as an electron transporter and could also control the injection for improved efficiencies.

2.6 Summary

Radiative decay of singlet excited states in conjugated organic molecules is an interesting stage of light-emission in both photoluminescence and electroluminescence processes. The similarity of the two processes makes photoluminescence an important technique for investigating the singlet excited states in conjugated systems that could also be responsible for emission in LEDs. The concepts reported in this chapter form the basis of discussions that will arise in following chapters, and are necessary in developing more efficient devices.

References

1. W. P. Su, J. R. Schrieffer and A. J. Heeger, *Phys. Rev. Lett.*, **1979**, 42, 1698.
2. W. P. Su, J. R. Schrieffer and A. J. Heeger, *Phys. Rev. B*, **1980**, 22, 2099.
3. R. E. Peierls "Quantum Theory of Solids" **1955**, Oxford University Press.
4. C. Fincher, C. E. Chen, A. J. Heeger, A. G. McDiarmid and J. B. Hastings, *Phys. Rev. Lett.*, **1982**, 48, 100.
5. C. S. Yannoni and T. C. Clarke, *Phys. Rev. Lett.*, **1983**, 51, 1191.
6. N. F. Colaneri, D. D. C. Bradely, R. H. Friend, P. L. Burn, A. B. Holmes and C. W. Spangler, *Phys. Rev. B*, **1990**, 42, 11670.
7. S. A. Brazovskii and N. N. Kirova, *JETP Lett*, **1981**, 33, 4.
8. A. J. Heeger, S. Kivelson, J. R. Schrieffer and W. P. Su, *Rev. Mod. Phys.*, **1988**, 60, 781.
9. D. D. C. Bradley, A. R. Brown, P. L. Burn, J. H. Burroughes, R. H. Friend, A. B. Holmes, K. D. MacKay and R. N. Marks, *Synth. Met.*, **1991**, 41-43, 3135.
10. A. B. Holmes et al, *Synth. Met.*, **1993**, 55-57, 4031.
11. S. W. Jessen, J. W. Blatchford, L. B. Lin, T. L. gustafson, J. Partee, J. Shinar, D. K. Fu, M. J. Marsella, T. M. Swager, A. G. MacDiarmid and E. J. Epstein, *Synth. Met.*, **1997**, 84, 501.
12. P. L. Burn, A. B. Holmes, A. Kraft, D. D. C. Bradley, A. R. Brown and R. H. Friend, *J. Chem. Soc. Chem. Comm.*, **1992**, 1, 32.
13. A. Kearwell and F. Wilkinson, "Transfer and Storage of Energy by Molecules" **1969**, Wiley, New York.
14. M. Pope and C. E. Swenberg "Electronic processes in organic crystals." **1982**, Clarendon Press, Oxford.
15. J. T. Devreese and F. Peeters. "Polarons and Excitons in polar semiconductors and ionic crystals." **1984**, Eds., Nato ASI Series B.
16. D. C. Reynolds and T. C. Collins. "Excitons, their Properties and Uses." **1981**, Academic Press, New York.
17. K. Harigaya, *J. Phys. Cond. Mat.*, **1997**, 9, 5253.
18. S. V. Frolov, M. Liess, P. A. Lane, W. Gellermann, Z. V. Vardeny, M. Ozaki and K. Yoshino, *Phys. Rev. Lett.*, **1997**, 78, 4285.

19. See for example chapter 7 in N. S. Sariciftci, "Primary Photoexcitations in Conjugated Plymers: Molecular Exciton versus Semicondictor Band Model" **1997**, *World Scientific Publishing Co. Pte. Ltd.*, Singapore.
20. F. Garten, A. Hilberer, F. Cacialli, E. Esselink, Y. V. Dam, B. Schlatmann, R. H. Friend, T. M. Klapwijk and G. Hadziioannou, *Adv. Mater.*, **1997**, 9, 127.
21. A. P. Monkman, M. Halim, S. Dailey, I. D. W. Samuel, M. Sluch and L. E. Horsburgh, *SPIE*, **1997**, 3148, 82.
22. S. T. Kim *et al*, *Adv. Mater.*, **1996**, 8, 979.
23. D. D. C. Bradley and R. H. Friend, *J. Mol. Elec.*, **1989**, 5, 19.
24. R. H. Friend, D. D. C. Bradley and P. D. Townsend, J. *Phys. D: Appl. Phys.*, **1987**, 20, 1367.
25. B. E. Kohler and I. D. W. Samuel, *J. Chem. Phys.*, **1995**, 103, 6248.
26. I. D. W. Samuel, B. Crystall, G. Rumbles, P. L. Burn, A. B. Holmes and R. H. Friend, *Chem. Phys. Lett.*, **1993**, 213, 472.
27. U. Lemmer, R. F. Mahrt, Y. Wada, A. Greiner, H. Bassler and E. O. Gobel, *Appl. Phys. Lett.*, **1993**, 62, 2827.
28. U. Rauscher, H. Bassler, D. D. C. Bradley and M. Hennecke, *Phys. Rev. B*, **1990**, 42, 9830.
29. T. W. Hagler, K. Pakbaz, K. F. Voss and A. J. Heeger, *Phys. Rev. B*, **1991**, 44, 8652.
30. N. C. Greenham, I. D. W. Samuel, G. R. Hayes, R. T. Phillips, Y. A. R. R. Kessner, S. C. Moratti, A. B. Holmes and R. H. Friend, *Chem. Phys. Lett.*, **1995**, 241, 89.
31. P. L. Danielsen and R. C. Ball, *J. Physique*, **1985**, 46, 1611.
32. J. H. Burroughes, D. D. C. Bradley, A. R. Brown, R. N. Marks, R. H. Friend, P. L. Burn and A. B. Holmes, *Nature*, **1990**, 347, 539.
33. Adam Brown, PhD Thesis, **1992**, Cambridge.
34. S. M. Sze, "Physics of Semiconductor Devices" **1981**, Wiley, New York.
35. I. D. Parker, *J. Appl. Phys.*, **1994**, 75, 1656.
36. K. C. Kao, and W. Hwang, "Electrical Transport in Solids" **1981**, Pergamon Press, Oxford.

37. H. Vestweber, J. Pommerehne, R. Sander, R. F. Mahrt, A. Greiner, W. Heitz and H. Bassler, *Synth. Met.*, **1995**, 68, 263.

38. See for example K. C. Kao, and W. Hwang, "Electrical Transport in Solids" **1981**, Pergamon Press, Oxford. R. H. Williams, "Semiconductor Contacts" **1989**, Clarendon Press, Oxford. S. M. Sze, "Physics of Semiconductor Devices" **1981**, Wiley, New York.

39. S. Karg, W. Reiβ, V. Dyakonov and M. Schwoerer, *Synth. Met.*, **1993**, 54, 427.

40. R. N. Marks, J. J. M. Halls, D. D. C. Bradley, R. H. Friend and A. B. Holmes, *J. Phys. Con. Mat.*, **1994**, 6, 1379.

41. T. Takiguchi, D. H. Park, H. Ueno, K. Yoshino and R. Sugimoto, *Synth. Met.*, **1987**, 17, 657.

42. J. Obrzut, M. J. Obruzt and F. E. Karasz, *Synth. Met.*, **1989**, 29, 103.

43. N. T. Binh, L. Q. Minh and H. Bassler, *Synth. Met.*, **1993**, 58, 39.

44. R. Richert, L. Pautmeier and H. Bassler, *Phys. Rev. Lett.*, **1989**, 63, 547.

45. L. B. Schein, *Phil. Mag. B*, **1992**, 65, 795.

46. H. Bassler, *Phil. Mag. B*, **1984**, 65, 347.

Chapter 3

Experimental Techniques from Synthesis to Characterisation through Device Fabrication

3.1 Introduction

The first section of this chapter is concerned with the synthesis of some conjugated polymers used in this thesis. Different laboratories have supplied us with different materials: PPV-THT leaving group precursor was supplied by Cambridge Display Technology (CDT), MEH-PPV was provided by Hoechst in Germany while PPY was synthesised in our laboratories. The dendrimers were made at the Dyson Perrins Laboratory in Oxford by Jonathan Pillow and Dr Paul Burn. The following section will be focused on the device preparation, describing step by step the techniques used for the fabrication of a polymer or dendrimer emitting device. Following this, I will be discussing the experimental optical and electronic techniques used to characterise these devices.

3.2 The Processing of Conjugated Polymers

Conjugated polymers are not easily processed due to a tendency to adopt a planar configuration of the conjugated backbone to maximise overlap of p_z orbitals. Hence, they are usually rigid-rod and some are therefore insoluble in common organic solvents (chloroform, toluene ...). Some examples of well studied conjugated polymers are shown in figure 3.1.

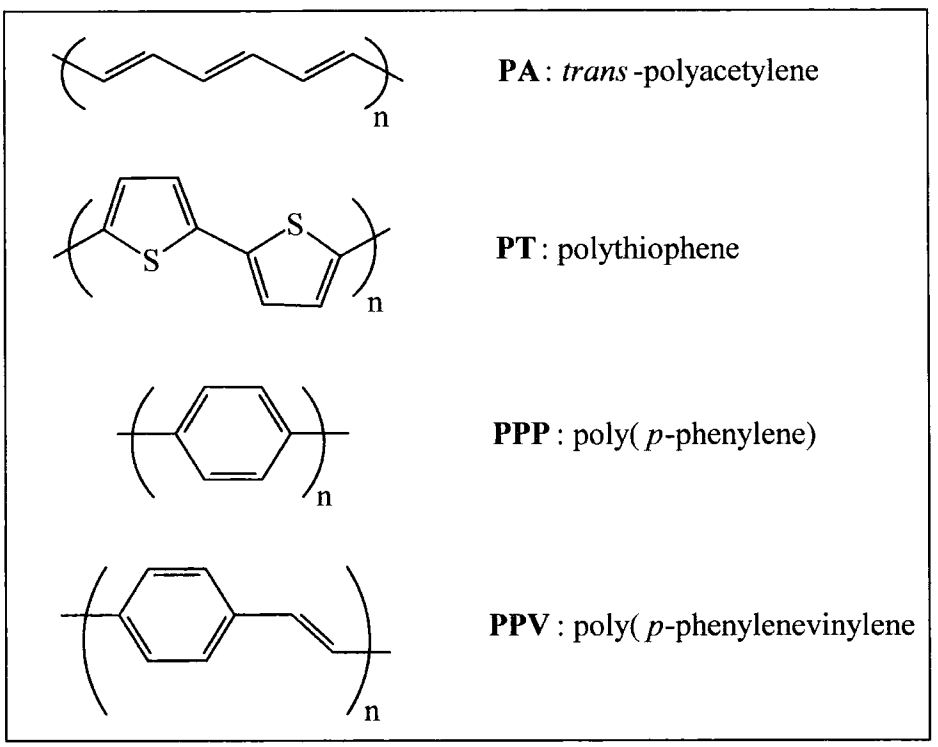

FIG. 3.1 *Chemical structures of some commonly studied conjugated polymers.*

Various approaches have been adopted to overcome the processing problems of these polymers, of which two have proved to be the most efficient and useful for the fabrication of polymer films suitable for use in electrical devices.

The first method of synthesis consisted of using a precursor route in which a soluble non-conjugated 'precursor' polymer is produced. The precursor polymer can be processed and spin coated on suitable substrates, to form films which subsequently are converted to the final conjugated polymer films either by thermal or chemical

elimination of the leaving groups. A typical example of this precursor route is the Durham route used by Feast and co-workers to synthesise polyacetylene [1] and Wessling [2] or sulphonium polyelectrolyte [3] precursor routes for the synthesis of PPV. The precursor route offers many advantages such as the possibility to produce thin films for optical studies [4-6]. There are other advantages to be gained using the precursor-based polymers such as the fact that after converting the precursor films, the fully converted conjugated polymer films are insoluble in most organic solvents and hence allows a subsequent deposition of further layers [7,8] to prepare multilayer LEDs. They also demonstrate thermal stability up to 400 °C [7] and have good mechanical properties.

However, it is also desirable to synthesise conjugated polymers which are soluble in organic solvents. This was typically achieved by the use of side groups or side chains attached to the polymer backbone (see figure 3.2). Poly(2-methoxy-5-(2'-ethyl-hexyloxy)-*p*-phenylenevinylene) (MEH-PPV) is a typical example of soluble conjugated PPV derivative [9].

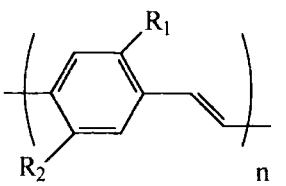

FIG. 3.2 *2,5 substituted PPV.*

The advantage that this method has over the precursor route is that it is time efficient, as one less LED fabrication step is needed. Moreover, it allows the purification of the final polymer in solution, which is a great advantage and offers the possibility of controlling the molecular weight. However, the introduction of the side-solublising groups often yield a softer material which can prove to give some difficulties while being handled and tend to make the polymer chains more flexible which reduces the π-electron delocalisation, and hence results in a material with different electronic properties.

3.2.1 THT precursor route to PPV

Figure 3.3 outlines the tetra-hydrathiophenium (THT) leaving group precursor route to PPV [10]. The disalt monomer (II) is prepared from α,α'-dichloro-*p*-xylene (I), and is polymerised by the slow addition of aqueous sodium hydroxide at 0 °C. The precursor polymer is then dialysed for three days in order to eliminate monomeric impurities.

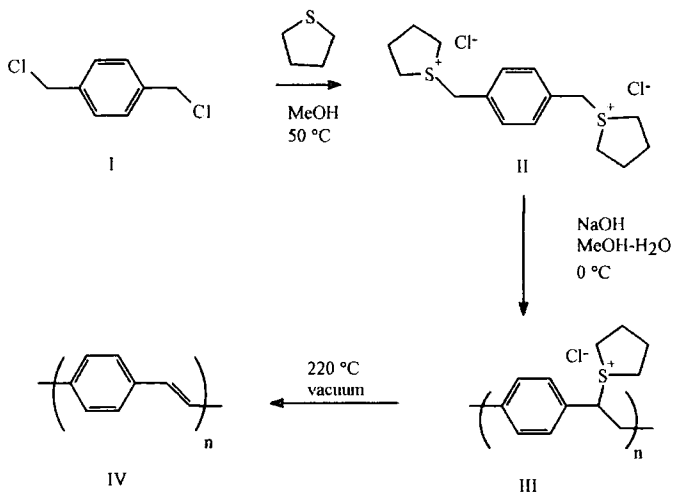

FIG. 3.3 *The THT precursor route to PPV [10].*

The final precursor polymer is soluble in methanol and so it was possible to spin coat thin films which were converted to the final conjugated polymer films (IV) by thermal treatment at 220 °C in a vacuum for 12 hours. The storage of the precursor polymer solution is a crucial matter as the precursor is thermodynamically unstable even at room temperature. Therefore the solution was exposed to light as little as possible and stored below freezing temperature at all times.

3.2.2 Synthesis of PPV-based soluble polymers

Although the precursor route has its advantages, it is often preferable to work with soluble polymers, for the reasons mentioned above. The standard way of synthesising soluble PPV-based polymers is to substitute alkoxy or dialkoxy side groups to the phenylene ring. Figure 3.4 shows the synthetic routes to dialkoxy substituted PPV.

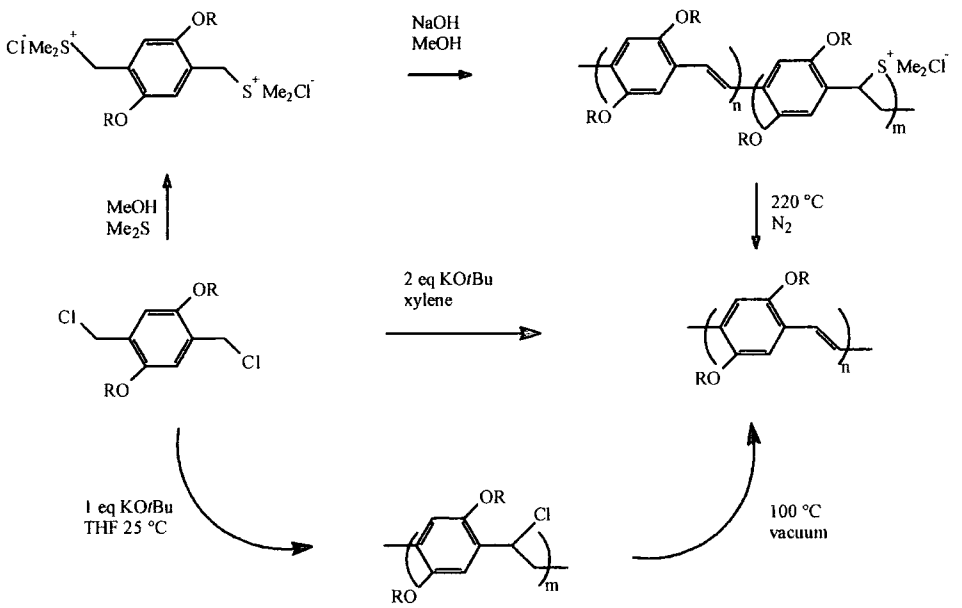

FIG. 3.4 *Synthetic routes to PPV-based substituted polymers.*

Several research groups have reported the synthesis of dialkoxy substituted PPVs [11-14]. The final substituted polymer can been obtained through several pathways either involving direct synthesis (route 3) or using precursor alternatives (1 and 2). One attractive feature of these synthetic routes is the possibility of tuning the electronic properties by using different side groups. For example the alkoxy substitution of PPV as in MEH-PPV gives a characteristic orange emission [15]. Another example is the use of cyano groups on the vinylene units which gives CN-PPV an electron withdrawing property together with other interesting properties [16,17].

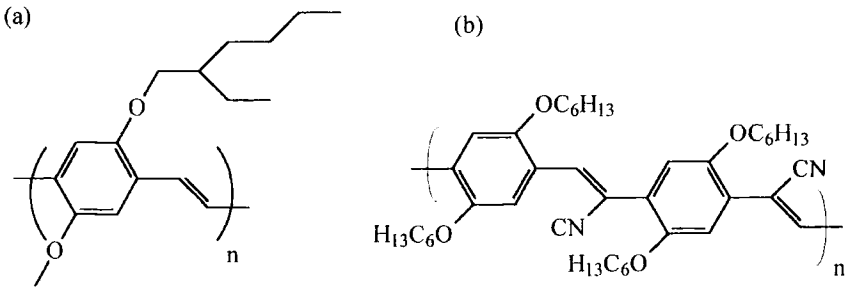

FIG. 3.5 *Chemical structure of (a) MEH-PPV and (b) CN-PPV.*

It is important to mention that the polymer (or dendrimer) in its realistic configuration could be drastically different from the chemical formula (e.g. fig 3.5) or the three-dimensional drawings presented in this thesis. This is mainly due to conformational disorder such as twists and bends of the polymer chain. Conformational disorder can also occur in conjugated dendrimers. Defects could also be chemical such as saturated units or chain branches created during the synthesis. Ideally the polymer is conjugated all along the polymer chain, however due to the twists in the chain the conjugation is broken and finally the chain has a distribution of conjugation lengths. The difference in the polymer chain length and the effective conjugation length is that the latter one is the length of the monomer units where the conjugation is not perturbed while the polymer chain length is the overall number of repeating monomer units in the polymer chain.

Kohler and Samuel [18] have studied a number of well defined linear polyenes (28 – 240 double bonds) in order to extract the distribution of conjugation lengths using their absorption spectra. This distribution was found to be dominated by short conjugation lengths, which is in agreement with the assumption that short conjugated segments, possibly created by broken conjugations due to twists or folds in the polymer chain, exist.

3.3 Device Fabrication

A simple polymer LED consists of a polymer film sandwiched between two electrodes (figure 3.6). At least one of the electrodes has to be semi-transparent so that the light generated in the polymer bulk, can be viewed. The indium-tin oxide (ITO) coated glass is the widely used transparent anode substrate in various flat panel display technologies [19] and in polymeric LEDs [20-22]. Other groups have reported the use of other polymers [23], e.g. pani, as the anode to avoid problems that could occur from the use of ITO [24]. The ITO used in this thesis was supplied by Balzers in the form of 30 cm x 30 cm sheets and had a surface resistance of 20 Ω/square. The sheets were cut into 12 mm x 12 mm substrates which was the standard size used for our LEDs.

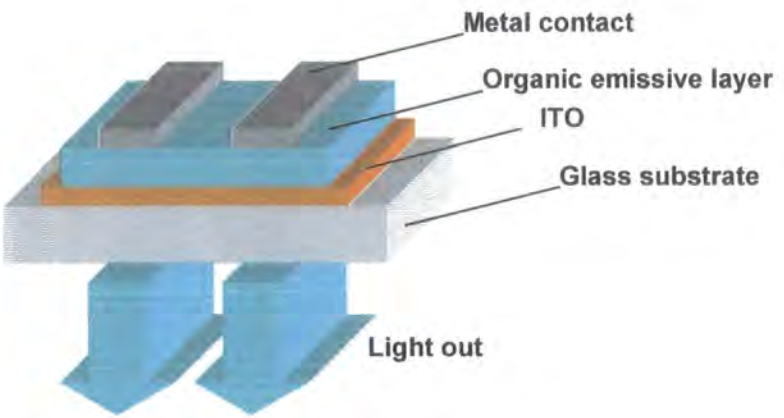

FIG. 3.6 *The basic structure of a monolayer organic LED.*

Electrical contacts to top and bottom electrodes were made via metallic pins. However these metallic pins are prone to penetrating the soft polymer layer causing the device to short circuit. To overcome this problem a narrow strip of ITO was etched away from the two opposing sides of each substrate as illustrated in figure 3.7. The etching was carried out originally using a nail polish to cover a strip in the middle of the substrate. By immersing the substrates in 1 M HCl solution at 60 °C for 20 minutes, the ITO is etched away from the non-masked areas. A commercial pen was also used to etch the ITO. This was achieved by following the same procedure and then

immersing the substrates in 1:1 (HCl : water) solution for 20 minutes without any thermal treatment. Both etching materials (nail polish and pen) were soluble in acetone which was used to remove the mask. The substrates were then cleaned in an ultrasonic bath to eliminate any surface contamination: they were immersed in acetone for approximately 5 minutes, and then in propan-2-ol for a similar period. The substrates were then dried using a nitrogen gas line. It is worth mentioning that other techniques have also been used to avoid the direct contact of the electrodes and consequent short circuits. The ITO was not etched away but instead a polyimide layer was placed between the ITO and the polymer layer [17].

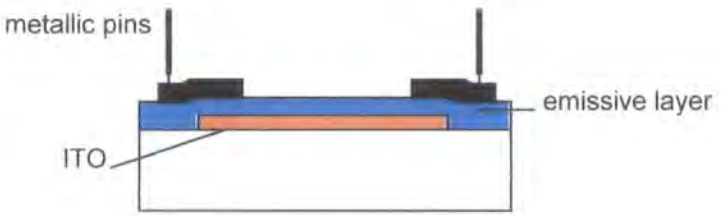

FIG. 3.7 *Illustration showing the ITO etched away from the two sides of the substrate.*

It is crucial that films to be used in the fabrication of polymer LEDs should be of good quality – that is uniform, pin hole free etc. The morphology of films is strongly dependent on the way they have been deposited, and depends on factors such as care taken during deposition and also the solvent used for spin-coating. D. Braun *et al* [25] has reported that some surface ripples could develop in thin films spin-coated from very volatile solvents. These ripples were a few hundred angstroms in size which is likely to influence the operation of thin polymer LEDs.

To deposit the films we used the spin coating technique which is a reliable and well used technique for polymer deposition. The substrate is first covered completely with the solution before being spun at a constant speed for a certain time period. When spreading the solution on top of the substrate, care was taken not to create air bubbles on the surface as this could affect the quality of the film. The thickness of the film, as reported by Zse [26], is proportional to the concentration of the solution and inversely

proportional to the spin speed and so either factor can be exploited to obtain a desirable polymer thickness. The typical thickness used for our polymer devices was in the range of 100 nm. The film thicknesses were measured using an alpha step surface profile machine by measuring the depth of the step caused by scratching or removing a small area of the polymer. Figure 3.8 shows a typical print of the thickness measurement.

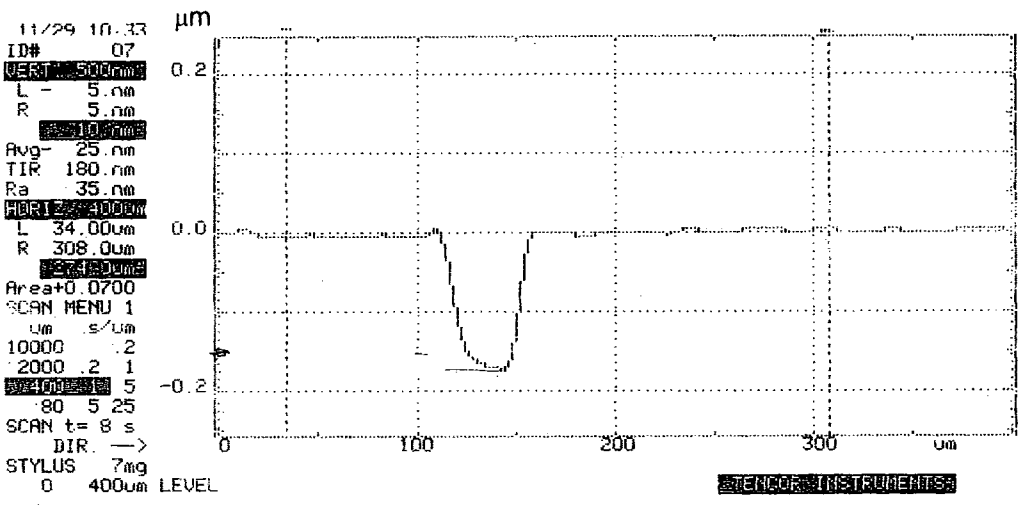

FIG. 3.8 *A print from a thickness measurement.*

When PPV was used the spin coated precursor films were converted at 220 °C in vacuum for 12 hours as described in section 3.3. The samples were allowed to cool down before removal from the oven.

The devices were then placed in an evaporator where the top electrodes were deposited on the polymer surface by a thermal evaporation. The evaporation was carried out in vacuum, at pressures typically of order $1x10^{-6}$ mbar. Tungsten filaments were used to hold and heat the aluminium. Initially the crucible for calcium granules was a cone made of quartz but more recently a tungsten boat has been used. This allows the use of only one or two calcium granules making the pressure in the evaporator more controllable. The thickness of the metal contacts was monitored continuously during evaporation using a crystal oscillator. Deposition rates in the

range of 1 nm s^{-1} were used to achieve a typical metal film thickness of 80 nm. The calcium contacts are known to be unstable in air and very reactive and so devices where calcium was used as the top electrode required a further layer of aluminium, to cap the calcium layer and prevent it from degradation. Both aluminium and calcium were stored in a nitrogen atmosphere in the glove box. After removing the devices from the evaporator chamber they were either transferred directly to the testing chamber (vacuum) or stored in the dark in the glove box.

3.4 LED Characterisation

After the devices had been transferred into the testing chamber (see figure 3.9), the chamber was evacuated immediately to prevent the devices from degrading, particularly important for those devices with calcium electrodes. Typical pressures in the chamber were in the range of 2.5×10^{-5} mbar. The chamber has a glass window which allows the light emitted in the forward direction to escape, and either viewed by the operator or collected using a silicon photodiode. The current in the photodiode was converted into voltage which was measured using a Keithley 196 digital multimeter. The Keithley 2000 is a source-measure unit and was used to drive the polymer LEDs and also to measure the current flowing through them. The experimental set-up was computer controlled via an IEEE interface card.

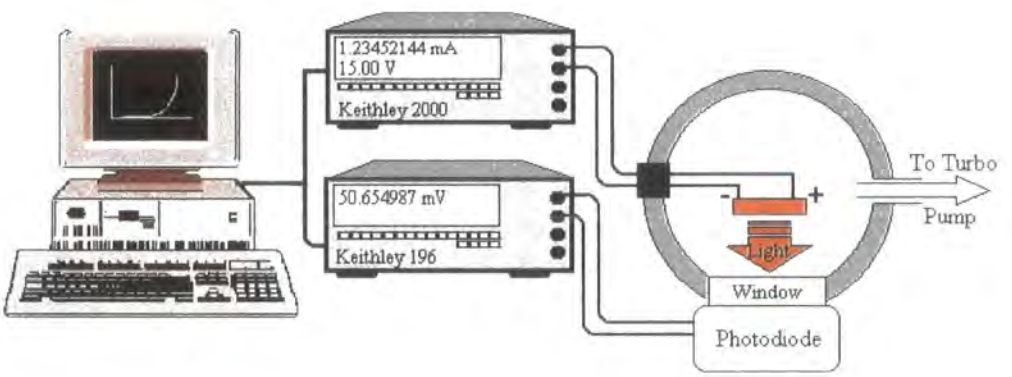

FIG. 3.9 *Experimental set-up used to measure current and light output as a function of the applied voltage.*

3.5 Photoluminescence Quantum Yield Measurement

3.5.1 Definition

The photoluminescence quantum yield of a sample is defined as the number of photons emitted by the sample divided by the number of photons absorbed. Luminescence in conjugated polymers is believed to be the result of radiative decay of singlet excitons. This radiative decay is also in competition with a non-radiative process as shown in figure 3.10.

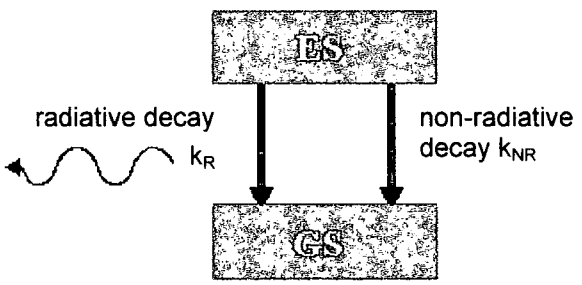

FIG. 3.10 *Decay of the excited state.*

The rates (k_R and k_{NR}) of both processes (radiative and non-radiative) determines the efficiency of the luminescence. For example, a weak luminescence efficiency could be the result of a very fast non-radiative decay channel dominating the decay processes: the excited species will decay non-radiatively before they can have the time to emit light. If these decays are monomolecular processes, and assuming that the emitted light originates from a single species, then the rate of decay of a number of excitations, N, following a short pulsed excitation is given by

$$\frac{dN}{dt} = -(k_R + k_{NR}) \times N \qquad \textit{eq. 3.1.}$$

The overall luminescence decay will be exponential with a life time, τ, given by

$$\tau^{-1} = \tau_r^{-1} + \tau_{nr}^{-1} \qquad eq.\ 3.2$$

where τ_r (k_R^{-1}) and τ_{nr} (k_{NR}^{-1}) are the natural decay life times of the radiative and non-radiative processes. The photoluminescence quantum yield is then given by

$$\phi_{PL} = \frac{k_R}{k_R + k_{NR}} = \frac{\tau}{\tau_R} \qquad eq.\ 3.3.$$

The overall life time, τ, and the PL quantum yield, ϕ_{PL}, are measurable values. The time-correlated single photon counting is a widely used technique for the measurement of the luminescence lifetime in molecular materials [27-29], while ϕ_{PL} is measured using the integrating sphere technique which will be discussed in the next section. It is quite clear that, knowing τ and ϕ_{PL} which should have been measured on the same or identical samples, one can deduce both rate constants from equation 3.2 and 3.3.

While it is widely believed that the dominant species in conjugated polymers such as PPV are singlet intra-chain excitons [30,31], Rothberg and co-workers [32,33] have been arguing, based on the results from picosecond stimulated-emission spectroscopy, that only a small fraction, n, of the absorbed photons leads to the formation of singlet excitons while the dominating states are inter-chain polaron pairs which are non-emissive. They suggested that only 10 % of the species generated in PPV are singlet excitons and hence n should be equal to 0.1. Equation 3.3 where n is assumed to be 1 should be written as :

$$\phi_{PL} = \frac{k_R}{k_R + k_{NR}} \times n = \frac{\tau}{\tau_R} \times n \qquad eq.\ 3.4$$

where $0 \le n \le 1$.

However, N. C. Greenham *et al* [34] report a life time of 320 ps measured on PPV samples at 2.25 eV which when combined with the radiative life time of at least 1.2 ns gives a value of 0.28 for the ratio τ/τ_r. They have measured ϕ_{PL} of PPV films and found it to be 0.27 which suggests that the fraction of singlet excitons generated by the absorbed photons is very close to 1. However the weakness of Greenham's argument consists in the use of two values τ and τ_r measured on different samples. This could easily create room for error as the luminescence life time is very sensitive to the structural conditions of the polymers studied. Furthermore, the excitation used for the life time and the quantum yield measurement were different (405 and 458 nm) which could cause some differences especially in systems where more than one specie is responsible for the emission. In PPV, however, the use of different excitation energy seems to have little effect on the photoluminescence quantum yield .

3.5.2 Absolute measurement

Measurement of absolute PL quantum yield on solid state films was performed using a 'Bentham IS4' integrating sphere. An integrating sphere is a hollow sphere, the interior of which is painted with a highly diffusive and very reflecting material. The sphere was used in this set-up to collect all the emitted light from the sample, not just in the forward direction. The experimental set-up of this measurement is shown in figure 3.11.

Thin films of conjugated materials were deposited by spin coating on 12 mm diameter quartz discs. The films used for this study were quite absorbing at the excitation wavelength, typical optical densities were in the range of 1, or preferably higher. The samples were then placed at the centre of the sphere (1) using a small sprung clip. The excitation energy was provided by the visible lines of a water cooled argon ion laser (2). Metal neutral density filters (3) were used to achieve a desirable incident laser power (in the range of 1 mW). The filtered power entered the sphere from the entrance port which is a small hole in the sphere wall (4).

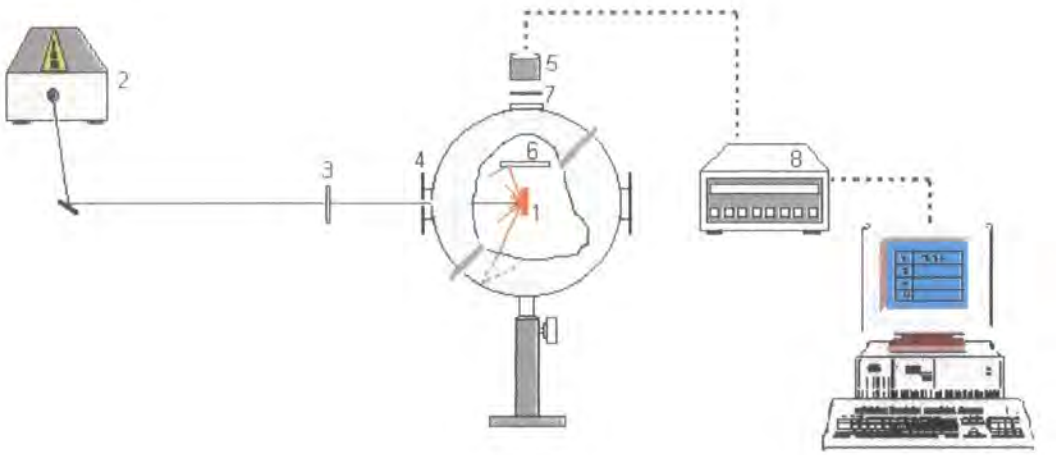

FIG. 3.11 *Quantum yield measurement experimental set-up.*

The laser line strikes the sample which emits light in all directions, which in turn starts bouncing from the sphere walls. A silicon photodiode (5) with a known quantum efficiency was placed at the exit port (top of the sphere) to collect the luminescence of the sample. This was proportional to the overall luminescence generated inside the sphere. To stop the light from the sample directly reaching the detector, a baffle (6), painted with the same diffusive substance as the sphere walls, was placed between the sample and the detector. To stop the laser light inside the sphere escaping from the exit port and allow only the emitted light to be detected, a suitable cut-off filter (7) was placed in front of the silicon photodiode. N. C. Greenham and co-workers [34] found that Schott glass filters contributed to the detected signal due to their luminescence properties, and therefore they were replaced by Kodak Wratten Gelatin filters which resolved their problem. Hence the same type of filters were used in this set-up. All the signals detected by the photodiode were transferred to a computer controlled Keithley multimeter (8).

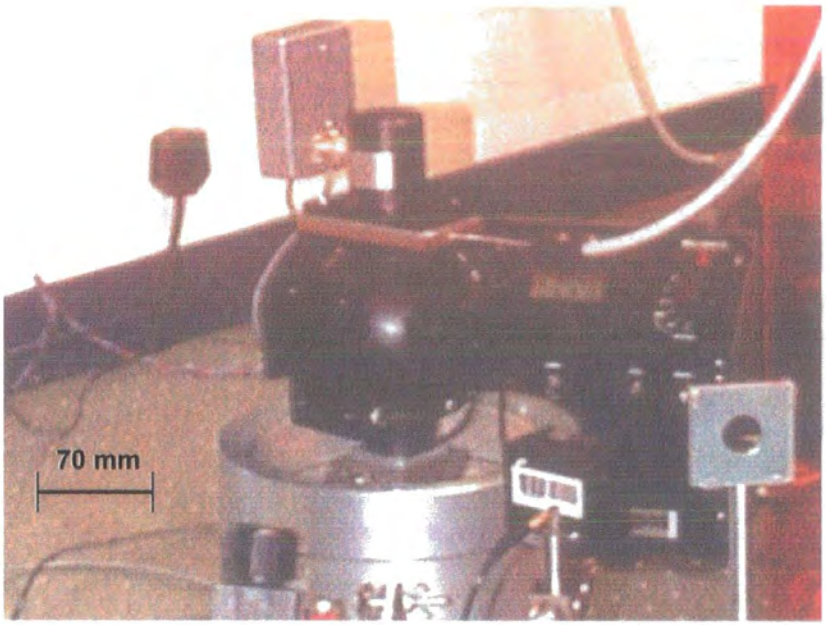

Photograph 3.1 *The integrating sphere.*

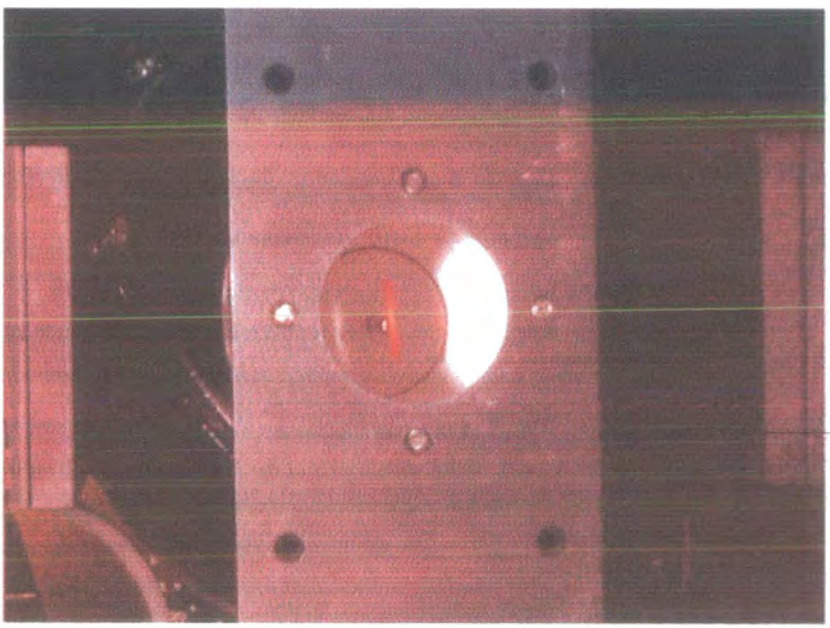

Photograph 3.2 *A fluorescing sample held inside the integrating sphere. The diameter of the port is 1 inch.*

In principle, the PL quantum yield, ϕ_{PL}, should be equal to the signal from the sample divided by the signal from the laser source.

$$\phi_{PL} = \frac{X_{Sample}}{X_{Laser}} \qquad eq.\ 3.5.$$

The signal due to the laser beam (X_{Laser}) is measured by removing both the sample and the filter and pumping the same amount of energy inside the sphere. However, due to sample re-absorption of the reflected laser beam, one could be over-estimating the sample luminescence. To correct for this term (X_{Sphere}), one has to estimate the amount of light that could be re-absorbed by the sample. In fact, this can be measured by using the same details as when measuring X_{Sample} but, instead of having the laser projected into the sample, it will first hit and bounce off the sphere wall before being absorbed by the sample. Equation 3.5 becomes

$$\phi_{PL} = \frac{X_{Sample} - (R+T)X_{Sphere}}{X_{Laser}(1-R-T)} \qquad eq.\ 3.6$$

where R and T are the reflectance and the transmission of the sample respectively. Further corrections had to be taken into consideration because of the response of the sphere and the non-uniform response of the calibrated photodiode across the UV-visible range. The spectral distribution of a tungsten lamp was measured before it was used to illuminate the sphere, for the purpose of the sphere calibration. The lamp was set-up to illuminate the sphere from the entrance port while the signal was detected at the exit port. The correction term is then given by

$$c = \frac{\int \frac{S_{Sphere}(\lambda)L(\lambda)G(\lambda)F(\lambda)}{S_{Lamp}(\lambda)} d\lambda}{\frac{S_{Sphere}(\lambda_{ex})G(\lambda_{ex})}{S_{Lamp}(\lambda_{ex})} \int L(\lambda)d\lambda} \qquad eq.\ 3.7$$

where S_{Sphere} and S_{Lamp} are the output of the lamp inside and outside the sphere respectively. $G(\lambda)$ is the quantum efficiency of the calibrated photodiode, $F(\lambda)$ is the transmission of the filter, $L(\lambda)$ is the emission profile of the sample measured using the same excitation (λ_{ex}). The absolute PL quantum yield is then given by

$$\phi_{PL} = c^{-1} \times \left(\frac{X_{Sample} - (R+T)X_{Sphere}}{X_{Laser}(1-R-T)} \right) \qquad eq.\ 3.8.$$

It is of importance to mention that a reasonable decrease in the quantum yield for most of the common light-emitting polymers was observed, if these samples were left lying around in air or under exposure to light. This is believed to be due to ageing and photo-oxidation of the polymers. Hence the samples used in this measurement were preferably 'fresh' in order to obtain adequate quantum yields. Otherwise, the samples were stored in the dark in a nitrogen atmosphere to prevent photo-oxidation. Readings of the signals had to be taken as soon as the laser beam struck the sample. The reason for this being that most of the conjugated polymers are very sensitive to oxygen and hence the sample will start degrading (in air) very rapidly and consequently a delayed reading (in the range of 1 s) would under estimate the PL quantum yield. This decay was found to be dependent on the polymer (some polymers are more stable than others), the laser power (the more powerful the laser, the faster the decay), and whether the laser beam is directly striking the polymer surface or through the glass side of the sample.

Different samples with a known photoluminescence quantum yield were used to verify the values obtained using this method. PPV and MEH-PPV are well-known conjugated polymers as is their ϕ_{PL} which is reported to be in the range of 0.27 and 0.10-0.15 respectively [34]. The values we have obtained were 0.24 and 0.13 for PPV and MEH-PPV respectively and are clearly in the same range as those in the literature. The small difference in PPV could only be due to the different samples as a combination of different factors: synthesis of the materials, conversion conditions, where the samples have been stored and for how long.

There is a large number of interesting emitting materials that absorb only at high energies (UV) and therefore the measurement was extended to be measured with excitations in this range. The samples were excited with the UV lines of the argon ion laser which offers the possibility of using a small entrance port to avoid loss of reflected laser beam and sample fluorescence. The integrating sphere response was re-measured using the same procedure as in the visible measurement, but using a Xenon lamp. Note that one must use a sample of optical density greater than 0.4.

Because most conjugated materials are very sensitive to oxygen and degrade rapidly in air (see section 6.2), a continuous flow of nitrogen was introduced into the sphere from the top port. The experiment was further 'upgraded' to measure the temporal dependence of the luminescence in order to investigate the photo-stability of the emitting materials. This was achieved by using a data logger which monitors the signals from the photodiodes as a function of time. To further control the atmosphere within the sphere, a cut-to-size bell jar was used in a vacuum experimental set-up shown in figure 3.12. Since the bell-jar is cylindrical, a quartz window had to be implemented in the cylinder surface to allow full transmission of the laser beam.

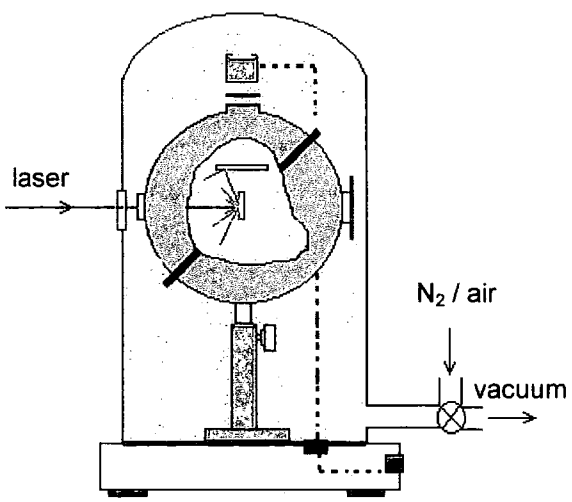

FIG. 3.12 *Measurement in different atmospheres.*

A rotary pump was used to create a primary vacuum inside the bell-jar and the pressure was $1x10^{-1}$ mbar. The signal was transmitted to the computer controlled data

logger which was also monitoring any changes in the laser power using a reference beam. The readings were taken every 100 ms.

The experiment was also used to measure quantum yields of solutions. A 12 x 12 x 10 mm glass cuvette was placed in the centre of the sphere. A similar procedure to the solid state case was carried out. Preliminary measurements on Rhodamine 101 (Rh101) in ethanol solutions gave values in the range of 0.77 which is low compared to the expected quantum yield of 1 [35]. This was believed to be due to oxygen quenching in the solution. Therefore the freeze-pump-thaw-technique was used to remove the present oxygen. This involved sealing the solution off from a low pressure vacuum line, and then freezing it by immersing in a liquid nitrogen bath. Once the solution was frozen the vacuum line was opened to evacuate the solution container. The tube was sealed off again and the solution was allowed to melt. The process was repeated at least three times before transporting the solution to the integrating sphere. The quantum yield was then measured and found to be very close to unity (0.98). This was also used to measure MEH-PPV solution quantum yield which was found to be 0.35 ± 0.02.

3.5.3 CCD method

The CCD method is a recently developed technique [36] for the measurement of the PL quantum yield. It is based on the same experimental set-up described in the previous section, with a few modifications. The signals at the exit port of the integrating sphere were transferred to a CCD spectrograph, instead of a calibrated photodiode, via a quartz fibre. This has the added benefit of being able to distinguish between the luminescence originating from the sample and the laser signal without having to use a cut-off filter. This, of course will also reduce any contribution in the detected signal from the filter luminescence and/or transmission.

The measurement was split into three experiments (figure 3.13). The first measurement (a) consists of illuminating the sphere with the laser through the entrance port and recording the laser profile using the CCD spectrograph. In the

second experiment (c) the sample is placed in the centre of the sphere and excited using the same energy and power as in the first experiment. The laser and emission profile are recorded at the same time and using identical parameters such as the exposure time and slit widths etc. Finally (b) the sample is rotated slightly so that the laser beam will miss the sample.

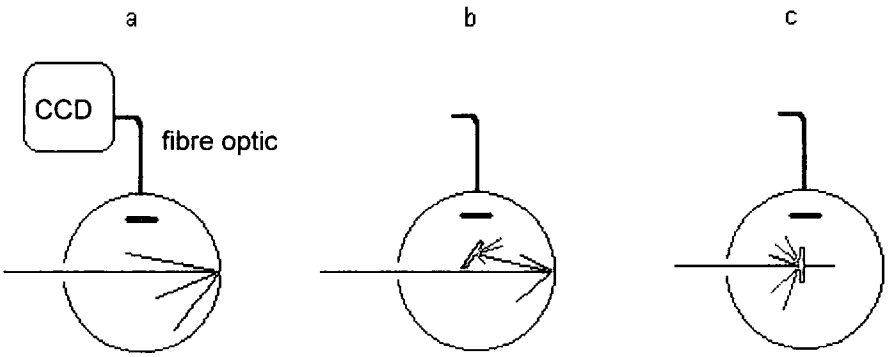

FIG. 3.13 *Diagram illustrating the three steps for measuring the photoluminescence quantum yield using a CCD spectrograph.*

Let L and P be the area under the laser and emission profile respectively. In experiment (b), it is assumed that a fraction μ of the diffused laser will be absorbed by the sample. In experiment (c) where the laser directly strikes the sample, a fraction A will be absorbed by the sample and hence $(1\text{-}A)$ is the fraction of the laser that is transmitted and/or reflected by the sample.

Thus

$$L_b = L_a(1-\mu) \qquad \textit{eq. 3.9}$$

$$L_c = (1-A)(1-\mu) \qquad \textit{eq. 3.10}$$

where L_a, L_b, and L_c are the area under the laser profile in experiment a, b, and c respectively. From equation 3.9 and 3.10 one can deduce the fraction of absorbed light:

$$A = (1 - \frac{L_c}{L_b}) \qquad eq.\ 3.11.$$

The laser light scattered from different points on the sphere wall is assumed to contribute to the same signal and has been verified by J. C. deMello to an accuracy of 2 % [36].

The signal detected in experiment (b), $L_b + P_b$, has two origins, which are the detected laser light (L_b) scattered from the sphere walls and the sample luminescence (P_b). The sample in this case is excited indirectly by the laser light scattered by the reflecting sphere walls. However, when the sample is illuminated directly with the laser beam (experiment c), a fraction of this laser light is absorbed while *1-A* is reflected and/or transmitted. This latter term will be scattered by the sphere walls and strike the sample again to contribute to the detected signal (P_c) in experiment (c). This contribution is given by $(1\text{-}A)(L_b + P_b)$ while the other term contributing to P_c is originating from the directly absorbed light ($\phi_{PL} L_a A$). Therefore, the signal in experiment (c) can be expressed as

$$L_c + P_c = (1 - A)(L_b + P_b) + \phi_{PL} L_a A \qquad eq.\ 3.12$$

and hence the PL quantum yield can be written as

$$\phi_{PL} = \frac{P_c - (1 - A)P_b}{L_a A} \qquad eq.\ 3.13.$$

Therefore this method should, in principle, give similar results compared to the first method. This was verified for films and solutions of MEH-PPV where quantum yields

of 0.11 and 0.34 were obtained respectively. Values of similar samples measured using the calibrated photodiode were 0.15 for film and 0.35 for solution.

As mentioned earlier, using the CCD spectrometer instead of the calibrated photodiode offers extra advantages such as the fact that filters are not used to stop the laser reaching the detector, therefore the laser profile and the sample luminescence are measured at the same time which should eliminate any contribution from the filters transmission and/or luminescence. Furthermore problems due to laser fluctuation can also be avoided. An added benefit of the CCD technique is the possibility of measuring quantum yields of scattering samples, such as powders, or some free-standing films which is not possible using the standard technique where it is difficult to measure their reflectance in order to determine the fraction of emitted light, due to the re-scattered laser beam. This is not the case for the CCD method as one does not need to measure the reflectance nor the transmission of the sample since their sum is expressed by *1-A*, which could be deduced directly from the measurement.

3.5.4 Solution measurement

The measurement of the PL quantum yield for solutions is relatively simple. This is mainly because one can assume an isotropic angular distribution of light, hence does not need an integrating sphere to collect all the emitted light. All that is required is to record the emission profile of the solution, and then compare it to the emission profile of a standard solution of a known quantum yield. The spectra must be measured using the same geometry. This is not usually a problem for commercial fluorimeters, however when using a CCD one has to make sure that the two measurements are identical. The quantum yield of an unknown solution Q_X is calculated according to the equation [37]

$$Q_X = Q_R \times \frac{A_R}{A_X} \times \frac{E_X}{E_R} \times \frac{I}{I_X} \times \frac{n_X^2}{n_R^2} \qquad \textit{eq. 3.14}$$

where Q_R is the quantum yield of the standard, A is the absorbance of the solution at the excitation wavelength, E is the relative intensity of the emitted light, and n is the refractive index of the solution. Subscripts R and X correspond to the standard and unknown solution respectively. By using the same solution optical densities, and the same excitation wavelength, one can eliminate A and I from equation 3.14. The quantum yield is then given by

$$Q_X = Q_R \times \frac{E_X}{E_R} \times \frac{n_X^2}{n_R^2} \qquad \textit{eq. 3.15.}$$

Note one should use very dilute solutions (< 0.05 optical density) in order to avoid formation of quenching sites such as aggregate states. The standards used are usually of a very high quantum yield. Rhodamine 101 is known to be 100 % efficient [35] while quinine sulfate has a quantum yield of 59 % [37].

Although this technique is simpler than the integrating sphere, its weakness consists in the fact that the quantum yields obtained using this method are relative, not absolute. The use of the same technique for films is a challenge as finding the right standards is difficult. Furthermore, the isotropic angular distribution of the emitted light does not make this method first choice for quantum yield measurement of films.

3.6 Optical Spectra

Solutions and thin films of conjugated polymers or dendrimers were characterised by measuring the standard optical spectra. These are the absorption, excitation and emission profiles. The absorption was measured using a Perkin Elmer λ19 dual-beam spectrometer while excitation and emission profiles were carried out on a LS 50B fluorimeter, with a 90° geometry. When measuring spectra for spin coated thin films, the films were slightly turned to thwart reflected excitation beam from reaching the detector. Xenon and tungsten lamps were used to provide excitation across the UV and visible region of the spectrum. Note that the spectra had to be corrected using a

calibration curve supplied by the manufacturer. A CCD spectrograph was also used to measure the emission profile of the materials. The excitation, in this case, was provided by a water cooled argon ion laser. Optical filters were used to prevent any laser light from reaching the CCD spectrograph.

In LEDs, the EL spectrum was measured using the CCD spectrograph with a quartz fibre coupled to the entrance (detection) window. The LED was mounted in the testing device chamber, as illustrated in figure 3.9, while the fibre was positioned at the window of the chamber. This allows us to carry out measurements in a vacuum, which was found to be of use for unstable devices, especially when long exposure times were required. The CCD spectrograph was originally calibrated by the manufacturer at two centre wavelengths, however for some emission ranges new calibrations were needed. This was carried out using a tungsten lamp. Firstly the lamp was measured at the two calibrated centre wavelengths, then spectra positioned at different wavelengths were measured and compared to those that had been calibrated. The ratio of these was used as the calibration of the specific centre wavelength.

3.7 The C.I.E. System

The emission spectrum of a given material is useful information in terms of studying and characterising the material. However for technological applications a more practical and precise method is needed to express the details of the emitted light, such as the colour, purity, and dominant wavelength. This is achieved using the system of colorimetry which was adopted in 1931 by the C.I.E. (Comission Internationale d'Eclairage) [38]. This was the first system to be agreed on internationally for specifying colours without the need to refer to a set of samples, and remains today the international system for quantitatively specifying colours [39]. The C.I.E. system provides a way of converting spectrum into perceived colour. It uses the fact that the eye has detector cones sensitive to three different colours. The procedure involves estimating overlap spectrum with the response function of the eye.

3.7.1 Chromaticity Diagram

The C.I.E. system is based on converting the emission spectrum into three values, called CIE co-ordinates, which are based on the average response of the human eye. The first two co-ordinates can be located in the chromaticity diagram e.g. XYZ colour diagram shown in figure 3.14. In this diagram, the primary colours *R*, *G*, and *B* are situated on the perimeter of the diagram forming a triangle that defines any possible combination of the three primary colours. This range of colour is known as the gamut and is important information for accessing the performance of display technology, such as RGB monitors.

To specify the colour emitted by a device, one begins by calculating the tristimulus values, *X*, *Y*, and *Z* which is achieved by integrating the energy distribution spectrum, S_λ, in turn with the three colour-matching functions $\bar{x}(\lambda)$, $\bar{y}(\lambda)$, and $\bar{z}(\lambda)$:

$$X = k\int S(\lambda)\bar{x}(\lambda)d\lambda$$

$$Y = k\int S(\lambda)\bar{y}(\lambda)d\lambda$$

$$Z = k\int S(\lambda)\bar{z}(\lambda)d\lambda$$

The chromaticity co-ordinates are then

$$x = X/(X+Y+Z); \qquad y = Y/(X+Y+Z); \qquad z = Z(X+Y+Z).$$

Since $x + y + z = 1$, two of these quantities are enough to determine the corresponding colour. x and y are the usual co-ordinates chosen by the CIE to represent the chromaticity in the C.I.E. diagram (see figure 3.14). Note that the colour matching functions are based on the primaries selected and are shown in figure 3.13. The co-ordinates of the RGB primaries in the XYZ system are:

R (700 nm):	x = 0.73467	y = 0.26533
G (546.1 nm):	x = 0.27376	y = 0.71741
B (435.8 nm):	x = 0.16658	y = 0.00886

In figure 3.16, which is the XYZ chromaticity diagram, *W* is known as the achromatic point and corresponds to the white emission. Its (*x, y*) co-ordinates are (1/3, 1/3).

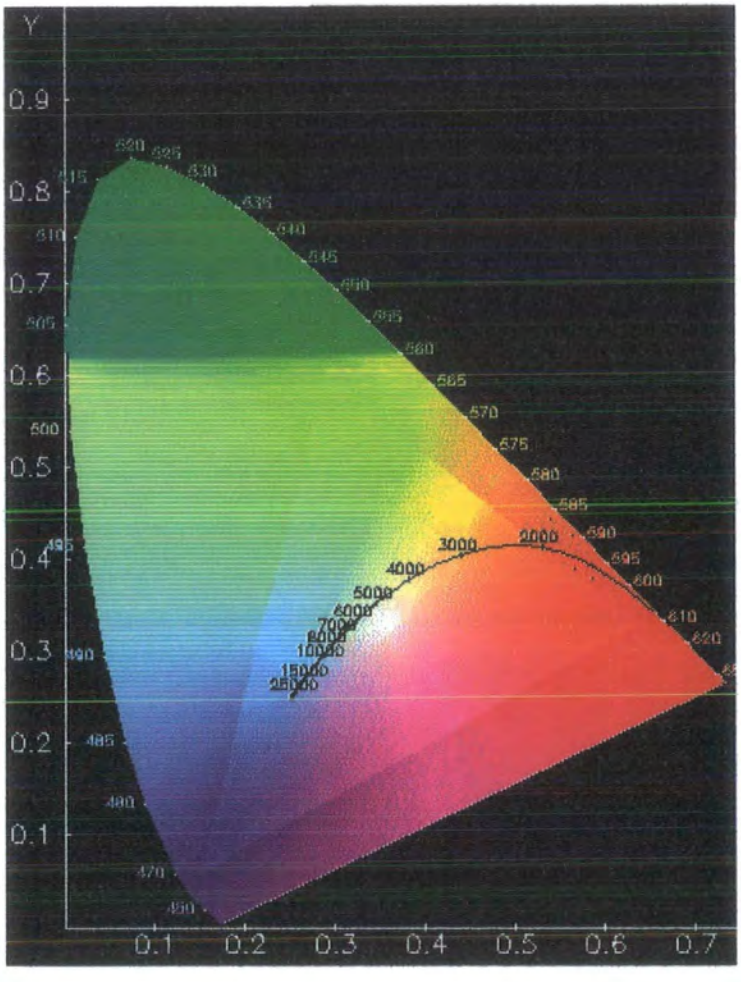

FIG. 3.14 *The chromaticity diagram which depends on the primaries used.*

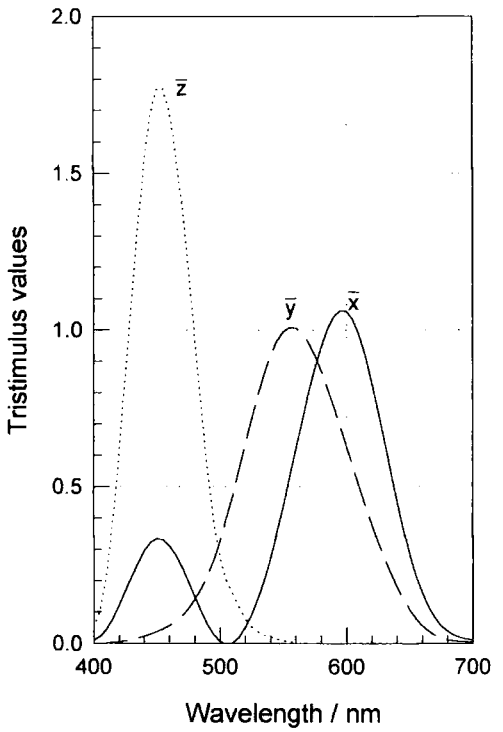

FIG. 3.15 *The colour matching functions of the 1931 CIE system of colorimetry (taken from reference [38]).*

3.7.2 Purity and dominant wavelength

The emitted light can also be characterised using parameters other than C.I.E. co-ordinates. These are the dominant wavelength, λ, and the colour purity, p, providing the achromatic point has been defined (W in fig 3.16). The dominant wavelength of a given source of light (M) represented in figure 3.16 is defined as the projection of the line passing through W and M on the perimeter of the chromaticity diagram. The purity of the colour, p, is defined as the ratio of the distance between the achromatic point and the chromaticity, to the length of the line drawn between the achromatic point and the perimeter passing through the point representing the colour (WM/WM'). The purity of a given colour is clearly dependent on the shape of the emission

spectrum. In principal, the broader the emission spectrum the poorer is the purity and vice versa. Hence in colour display technology, the pure colour emitters are very desirable, because of the large gamut they can provide.

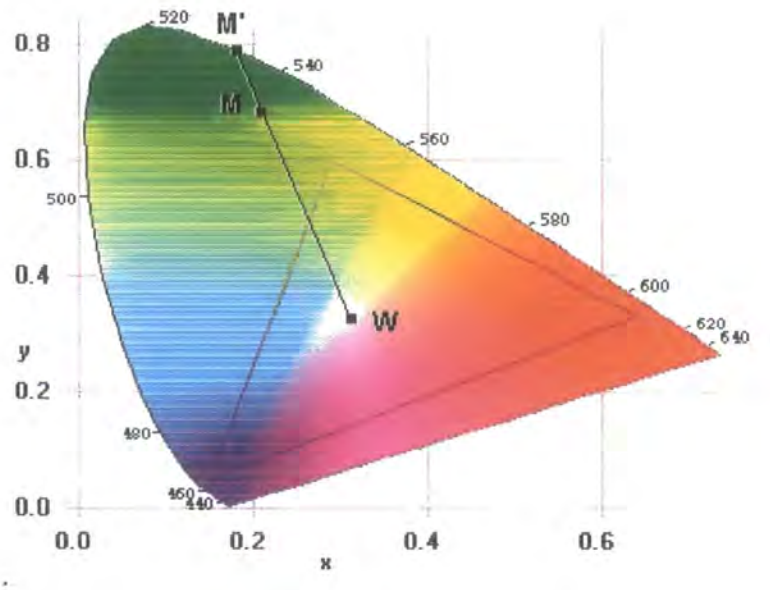

FIG. 3.16 *The definition of dominant wavelength and colour purity.*

For reference, CN-PPV luminescence (0.65, 0.30), is situated in the orange-red region of the chromaticity diagram [40]. The dominant wavelength of the emission is in the range of 600 nm and the colour purity is 0.85. Clearly the pure colour will be 1 and CN-PPV exhibits a reasonably pure emission, which makes it a desirable red-emitter for colour displays.

References

1. J. H. Edwards and W. J. Feast, *Polymer,* **1980**, 21, 595.
2. R. A. Wessling, *J. Polym. Sci. Polym. Symp.,* **1985**, 72, 55.
3. M. Kanbe and M. Okawara, *J. Polym. Sci.,* **1968**, 6, 1058.
4. P. D. Townsend and R. H. Friend, *Synth. Met.,* **1987**, 17, 36.
5. P. D. Townsend and R. H. Friend, *Phys. Rev. B,* **1989**, 40, 3112.
6. J. H. Burroughes, C. A. Jones and R. H. Friend, *Nature,* **1988**, 335, 137.
7. D. D. C. Bradley, *J. Phys. D,* **1987**, 20, 1389.
8. S. Dailey, M. Halim, E. Rebourt, I. D. W. Samuel and A. Monkman, *J. Phys. Cond. Mat.,* **1998**, 10, 5171.
9. D. Braun and J. Heeger, *Appl. Phys. Lett.,* **1991**, 58, 1982.
10. P. L. Burn, D. D. C. Bradley, A. R. Brown, R. H. Friend and A. B. Holmes, *Synth. Met.,* **1991**, 41-43, 261.
11. S. Tokito, T. Monii, H. Murata, T. Tsutsui and S. Saito, *Polymer,* **1990**, 31, 1137.
12. I. Murase, T. Ohnishi, T. Nogushi and M. Hirooka, *Synth. Met.,* **1987**, 17, 639.
13. S. Antoun, F. E. Karasz and R. W. Lenz, *J. Polym. Sci. A,* **1988**, 26, 1809.
14. P. C. Marr, J. A. Crayston, M. Halim and I. D. W. Samuel, *In press.*
15. M. I. Sluch, C. Pearson, M. C. Petty, M. Halim and I. D. W. Samuel, *Synth. Met.,* **1998**, 94, 285.
16. N. C. Greenham, S. C. Moratti, D. D. C. Bradley, R. H. Friend and A. B. Holmes, *Nature,* **1993**, 365, 628.
17. N. C. Greenham, PhD Thesis, **1995**, University of Cambridge.
18. B. E. Kohler and I. D. W. Samuel, *J. Chem. Phys.,* **1995**, 103, 6248.
19. R. Tueta and M. Bragueir, *Thin Solid Films,* **1981**, 80, 143.
20. P. May, *Physics World,* **1995**, March, 52.
21. P. L. Burn, A. B. Holmes, A. Kraft, D. D. C. Bradley, R. H. Friend and R. W. Gymer, *Nature,* **1992**, 356, 47.
22. M. Berggren, O. Inganas, G. Gustafsson, J. Rasmusson, M. R. Andersson, T. Hjertberg and O. Wennerstrom, *Nature,* **1994**, 347, 539.

23. S. A. Carter, M. angelopoulos, S. Karg, P. J. Brock and J. C. Scott, *Appl. Phys. Lett.*, **1997**, 70, 2067.

24. C. Pearson *et al, to be published.*

25. D. Braun, G. Gustafsson, D. McBranch and A. J. Heeger, *J. Appl. Phys.*, **1992**, 72, 564.

26. Zse, "Semiconductor devices: physics and technology." Bell Telephone Laboratories Inc. New York, **1985**.

27. I. D. W. Samuel, B. Crystall, G. Rumbles, P. L. Burn, A. B. Holmes and R. H. Friend, *Chem. Phys. Lett.*, **1993**, 213, 472.

28. I. D. W. Samuel, G. Rumbles, C. J. Collison, B. Crystall, S. C. Moratti and A. B. Holmes, *Synth. Met.*, **1996**, 76, 15.

29. D. V O'Connor and D. Phillips "Time-correlated Single Photon Counting" **1984**, *Academic Press*, New York.

30. R. H. Friend, D. D. C. Bradley and P. D. Townsend, *Appl. Phys. Lett.*, **1987**, 20, 1367.

31. Z. G. Soos, D. S. Galvao and S. Etemad, *Adv. Mater.*, **1994**, 6, 280.

32. M. Yan, L. J. Rothberg, F. Papadimitrakopolous, M. E. Galvin and T. M. Miller, *Phys. Rev. Lett.*, **1994**, 72, 1104.

33. J. W. P. Hsu, M. Yan, T. M. Jedju, L. J. Rothberg and B. R. Hsieh, *Phys. Rev. B*, **1994**, 49, 712.

34. N. C. Greenham, I. D. W. Samuel, G. R. Hayes, R. T. Phillips, Y. A. R. R. Kessner, S. C. Moratti, A. B. Holmes and R. H. Friend, *Chem. Phys. Lett.*, **1995**, 241, 89.

35. K. H. Drexhage, "*In Dye Lasers*" **1973**, Springer, Berlin.

36. J. C. deMello, H. F. Wittmann and R. H. Friend, *Adv. Mater.*, **1997**, 9, 230.

37. A. T. R. Williams, S. A. Winfield and J. N. Miller, *Analyst*, **1983**, 108, 1076.

38. Y. Le Grand, "*Light Colour and Vision*" **1957** Chapman and Hall Ltd. London.

39. R. M. Boynton, "*Encyclopedia of lasers and optical technology*".

40. D. R. Baigent. PhD Thesis, **1993**, University of Cambridge.

Chapter 4

Conjugated Dendrimers for Light-Emitting Diodes: Effect of Generation

4.1 Introduction

Since electroluminescence was first discovered in poly (*p*-phenylenevinylene) (PPV) [1] much interest has been shown in ways of using different conjugated polymers and improving device performance. Conjugated polymer-based light-emitting diodes (LEDs) offer many potential advantages over conventional inorganic LEDs such as their processibility [2], the potential for the fabrication of flat large-area displays [3] and the possibility of tuning the colour by simple chemical modifications [4].

However, polymer LEDs emitting blue light have proved to be the most difficult to make due mainly to the large energy gap of the emitting materials. Hence, particular interest has been shown by many research groups in the aim of obtaining enhanced blue emission from conjugated polymeric systems. They have used various ways to

achieve this, such as introducing non-conjugated units into the polymer backbone [5-7]. Others used small organic molecules that are readily available, although they seem to suffer from poor stability with a tendency to crystallise at the operating temperatures of LEDs, mainly due to their low glass transition temperature (Tg). Strategies consist of dispersing the molecular materials in polymer matrices [8,9], or the use of short aromatic segments (e.g. distyrylbenzene) as functional groups attached to an inert polymer was also explored [10].

Our approach was to combine the properties of small organic molecules, such as colour, and conjugated polymers, such as processibility. This was achieved in one molecular system by using a new class of macromolecular architecture called conjugated dendrimers.

In this chapter, I shall describe the photo-physics of one family of the dendrimers, studied in this thesis, both in their solution and solid states, and present the results obtained when these dendrimers were used as the active part in a single layer light-emitting diode configuration. I will then describe the effect of the number of generation on its optical and electroluminescent properties.

4.2 Dendrimer Concept

The continued interest in developing new conjugated organic materials has been spurred on by the discovery that they can be used as the light-emitting layer in light-emitting diodes (LEDs) [1,11]. The materials investigated fall into two main classes – molecular and polymeric. Low molecular weight materials are generally processed into the device structures by evaporation under high vacuum. In contrast, light-emitting polymers have the advantage that they can be deposited simply by spin-coating or even printing [12]. Excellent progress has been made in the areas of device efficiency and lifetime, and control of colour using both low molecular weight materials and polymers. However, one of the main disadvantages of using low molecular weight compounds and (co)polymers is that chemical modification of a

material to realise a particular electronic property may also substantially change the processing properties.

There has been remarkable progress in the synthesis of dendrimers leading to routes which give rapid access to large and complex molecules [13]. There is now a growing awareness that the field could develop from understanding the synthetic routes to, and properties of, dendrimers, to functional materials [14], and a few studies of electroactive dendrimers have been reported [15-20]. Hence, conjugated dendrimers are a promising new class of material for organic LEDs. They can be thought of as a conjugated light-emitting core, conjugated branches, and surface groups as illustrated in figure 4.1.

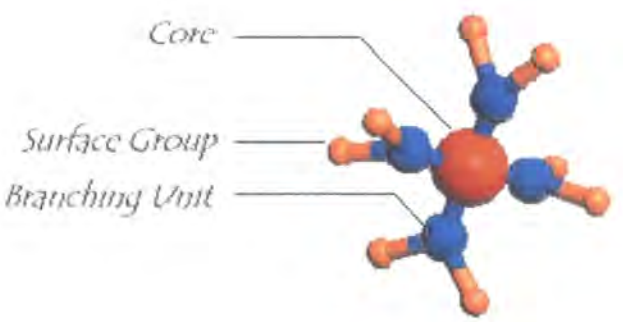

FIG. 4.1 *Schematic diagram of a first generation dendrimer.*

Such materials can be designed so that the core defines the colour of light-emission, the surface groups control the processing properties, and the branches allow transport of charge to the core. There are a number of potential advantages of this approach over molecular materials and polymers. Firstly, it provides the light-emitting chromophore in a solution processible form and gives the opportunity to optimise the electronic and processing properties independently: the colour of light-emission can be controlled by selection of the core, whilst the surface groups can be selected to control solubility. Secondly, the dendritic architecture provides a way of controlling interactions between molecules: in a high generation dendrimer it would only be the surface groups and/or outer branches which come into contact with each other. This

should alleviate the problems observed for blue and red emission in some polymeric systems. Finally, the branches can be chosen to have a wider HOMO-LUMO energy-gap near the surface with a narrower HOMO-LUMO energy gap near the core so as to funnel charge and excited states towards the core thus trapping charge in a similar manner to multilayer LEDs.

There have been a number of reports of conjugated dendrimers being used in LEDs with most of these focusing on materials for charge transport layers [16,17]. However, a more recent report describes the use of a dendrimer with an anthracene core and phenylacetylene dendrons as the light-emitting layer in an LED [18]. Electroluminescence spectra of the devices were given but neither efficiencies nor brightnesses were reported.

4.3 New Conjugated Dendrimers

Blue emission has been obtained for some time from molecular materials [21,22]. However in easily processed polymers, it has been a difficulty. The first conjugated dendrimers I have studied, were designed to approach this particular problem (blue emission). The dendrimer had to be a good blue emitter as well as having similar processing properties as polymers. It was necessary for the dendrimer to have conjugated segments in order to enhance the charge transport along the branches and to have an emissive core.

1-*ter*P is a first generation dendrimer based on the terphenyl molecule which is the central core of this dendrimer (see figure 4.2.). The branches are made of stilbene units and the surface groups (tertiary butyls) terminate the dendrimer structure. The second dendrimer, 1-DSB, was very similar in that it is also first generation with the same branches and surface groups, but has the *trans*-distyrylbenzene as the central core.

1-*ter*P

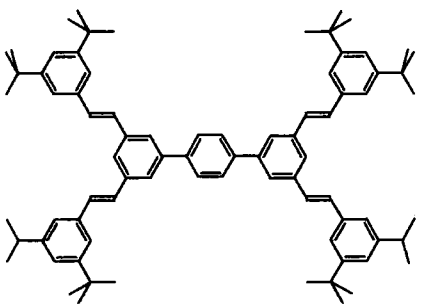

1-DSB

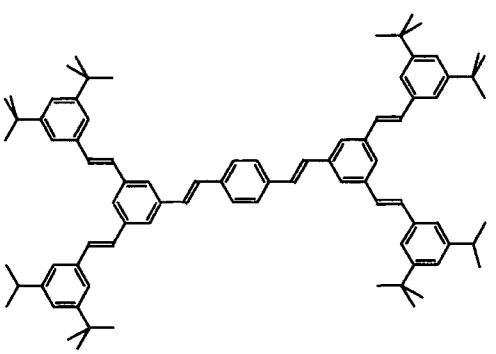

FIG. 4.2 *Chemical structures of 1-terP and 1-DSB.*

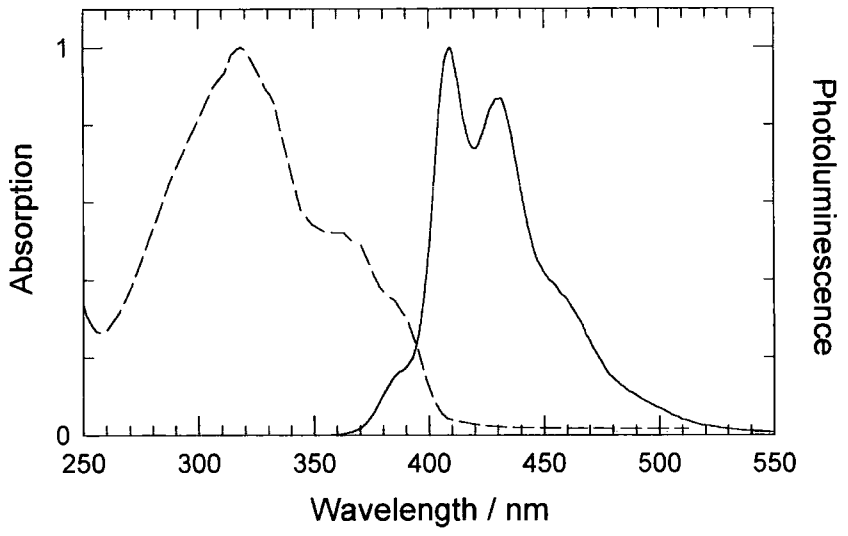

FIG. 4.3 *Absorption (dashed) and photoluminescence (continuous) spectra of 1-DSB in chloroform solution. PL was measured at 360 nm excitation wavelength.*

4.3.1 Optical characterisation

These dendrimers are soluble in most organic solvents due to their surface groups. Chloroform ($CHCl_3$) was used to make solutions, typically of concentrations 4 mg/ml.

The absorption spectrum of 1-DSB, shown in figure 4.3, could be divided into two parts: the first is where the maximum absorption occurs at around 320 nm and the second is the vibronic structure appearing at longer wavelengths with two shoulders at around 360 and 386 nm. The absorption spectrum of 1-*ter*P has one major feature at 320 nm, relatively similar to the band seen in 1-DSB absorption at the same wavelength. This suggests, considering that the two dendrimer molecules possess some similarities in structure, that these bands are of similar origin. Photoluminescence of the two different solutions were measured in a 90° geometry as described in the previous chapter. The PL spectra were recorded on solutions using the same excitation wavelengths (330 nm). The two solutions were found to emit strongly in the blue region of the visible spectrum and moreover, the two spectra are very similar.

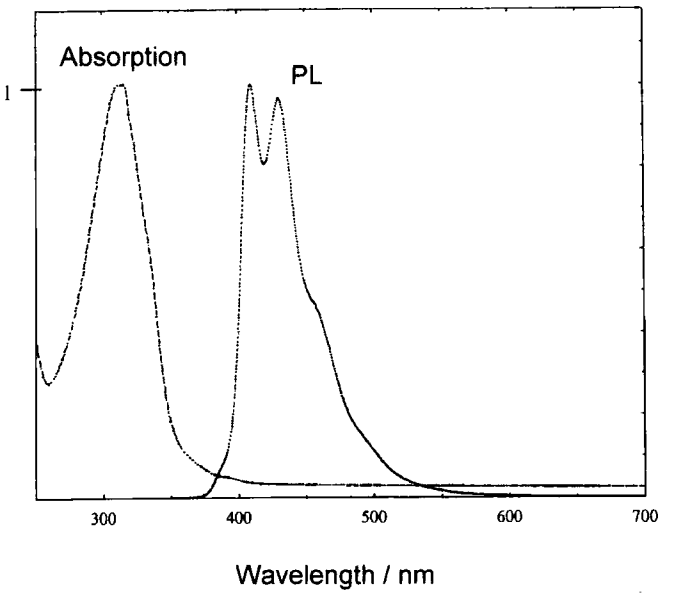

FIG. 4.4 *Absorption and photoluminescence spectra of 1-terP in chloroform solution.*

It was possible to spin coat directly from these dendrimer solutions to form thin uniform films and therefore to investigate and compare the optical properties of the corresponding materials. Microscope slide glass was used as substrates, with typical spinning speeds of 1600 rpm for 60 seconds, resulting in approximately 120 nm thick films. Films of these materials appeared to be colourless and transparent to the naked eye. The absorption and photoluminescence spectra of a 1-DSB film are shown in figure 4.5. The absorption spectrum was similar to that of the dendrimer solution with two major structures. The first is a band peaking at 320 nm while the other feature consists of the two shoulders lying at higher wavelengths. The film was excited at 330 nm and the PL spectrum shows a blue-emission with a peak at 475 nm. It is red-shifted with respect to the 1-DSB solution emission profile, and has lost the vibronic structure. The modest change can be due to increased conjugation in the film and could also be a result of a distribution of environments. This is not unusual for conjugated polymeric systems. Aggregation due to π-stacking of the molecules in the

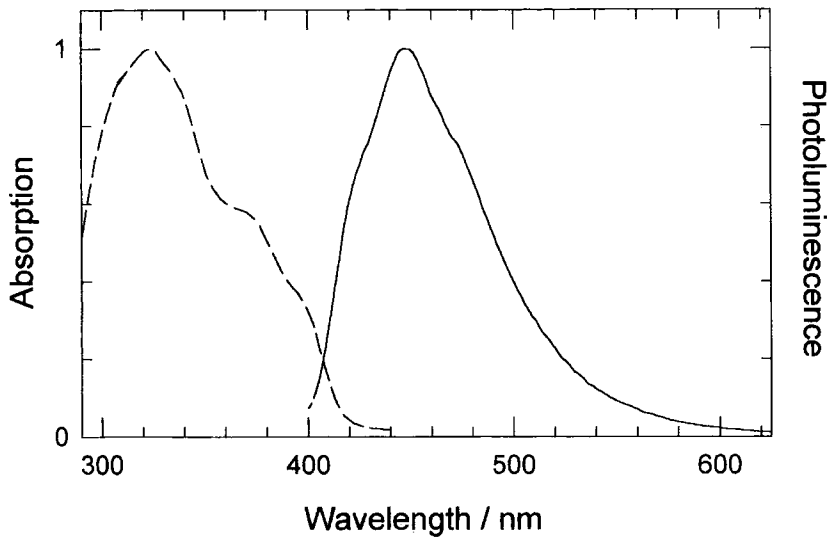

FIG. 4.5 *Absorption (dashed) and photoluminescence (continuous) of 1-DSB film (λ_{ex} =330 nm).*

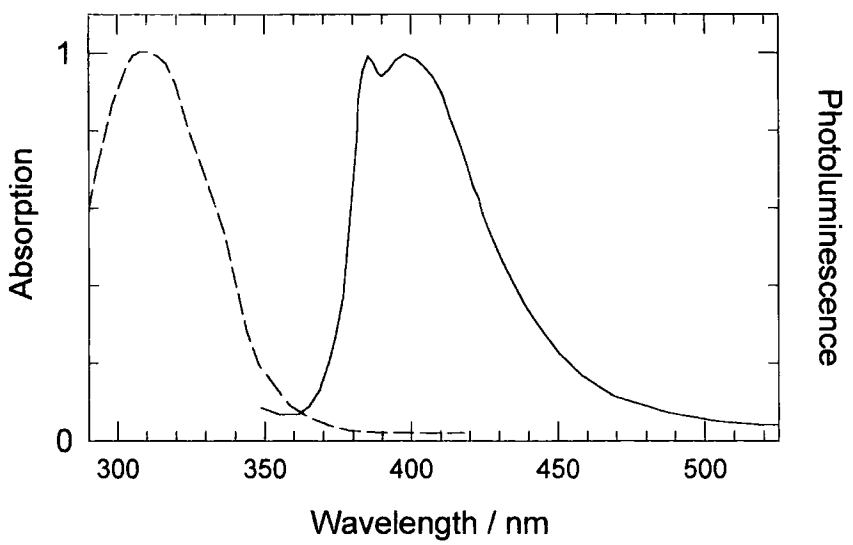

FIG. 4.6 *Absorption (dashed) and photoluminescence (continuous) of 1-terP film (λ_{ex} = 330 nm).*

solid state could also contribute to the observed change. The absorption of the 1-*ter*P film is shown in figure 4.6 together with its PL. The absorption of the film is similar to that of the solution with a peak at 320 nm. Films of 1-*ter*P were also excited at 330 nm which resulted in a PL spectrum with two peaks at 386 and 401 nm. The 386 nm feature seen in the 1-*ter*P film emission profile is possibly due to an impurity. However, it is unclear as to why the PL spectrum of the 1-*ter*P dendrimer film is blue-shifted by approximately 10 nm with respect to the emission profile of the corresponding solution. A possible explanation for this behaviour could be related to the spacing of the molecules in the solid state phase: since the core is a terphenyl, the molecular arrangement of these molecules could be different to that in the 1-DSB case and therefore create a different environment with an average shorter effective conjugation length, hence the blue-shift.

As will be discussed later in this chapter (figure 4.25), these dendrimer molecules prefer a rather planar arrangement – at least for early generations – which will probably cause the molecule to π-stack in the solid state, and possibly form aggregates or excimers [23]. This could alter the optical properties and could lead to undesirable characteristics for future applications. Therefore, by making the dendrimer structure bulkier – using either bigger branching units or central cores, or even using multiple core configuration – one could hopefully avoid any formation of aggregate state.

The opportunity was taken to pursue a primary investigation on another distyrylbenzene type of dendrimer. This particular dendrimer (0-3DSB), unlike the previous two, has a three-part central core and is a zero generation dendrimer. This is because it does not have a layer of branching units, hence the 'zero' in its name. In this case methoxy (OMe) groups were used as the functional surface groups. The chemical structure of this dendrimer is shown in figure 4.7.

Like many small organic molecules, 0-3DSB does not form good quality films when spin coated directly from chloroform solutions and therefore we had to disperse this dendrimer in a polymer matrix. For this task, poly(methylmethacrylate) (PMMA) is

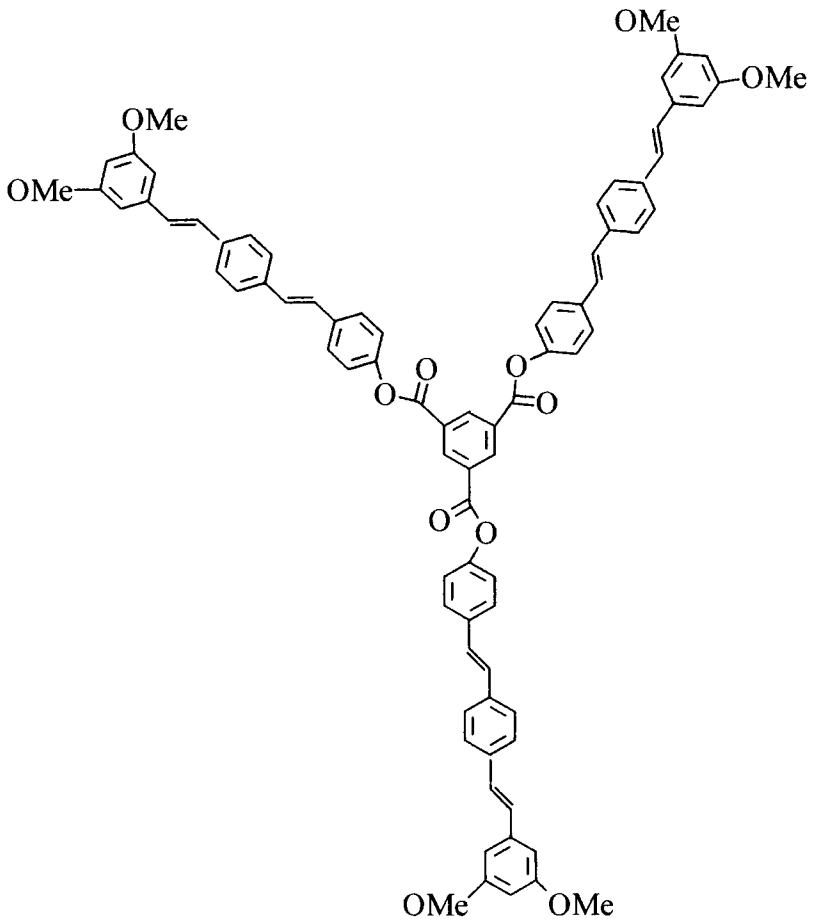

FIG. 4.7 *Chemical structure of 0-3DSB.*

the best candidate as it is an insulator with saturated carbon-carbon bonds and a large band gap (~ 5 eV, see figure 4.8), hence electrically inert.

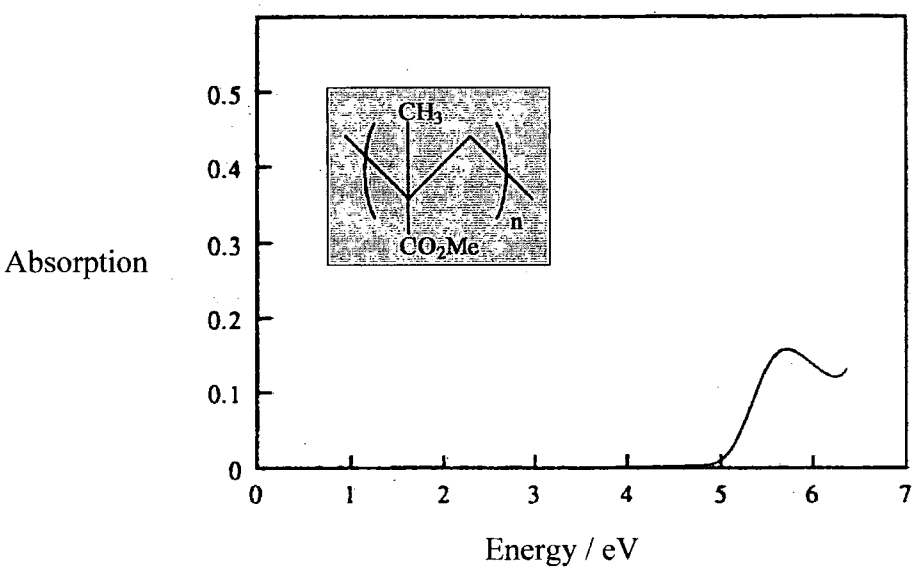

FIG. 4.8 *Absorption and chemical structure of PMMA.*

5 mg of 0-3DSB was dissolved in 1ml of chloroform to which 25 mg of PMMA was added. Spin coating from the blend solution at 1500 rpm / 60 s gave film thicknesses of around 100 nm. To understand more about the photophysics of this dendrimer it was necessary to run a comparative study on one of the constituents of this dendrimer (to be referred to hereafter as the dendrimer arm). The chemical formula of the arm is shown in figure 4.9.

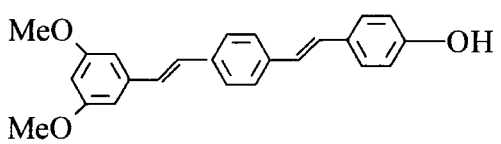

FIG. 4.9 *Chemical structure of the arm.*

Initial investigations were focused on looking at the optical absorption of the 0-3DSB dilute solution and comparing it to that of its arm. The absorption spectra of the solutions are shown in figure 4.10 and indicate that there is a degree of similarity between the two spectra, especially at longer wavelengths. 0-3DSB has two shoulders

in its absorption spectrum which lie at around 370 and 390 nm. This is very close (within a few nm) to the main absorption band peak and the lower energy shoulder of the dendrimer arm. Clearly this suggests that the component in the absorption spectrum of 0-3DSB at lower energy originates from the arms of the molecule and that there is a slight alteration of the π-π^* transition energy between the arm and the dendrimer.

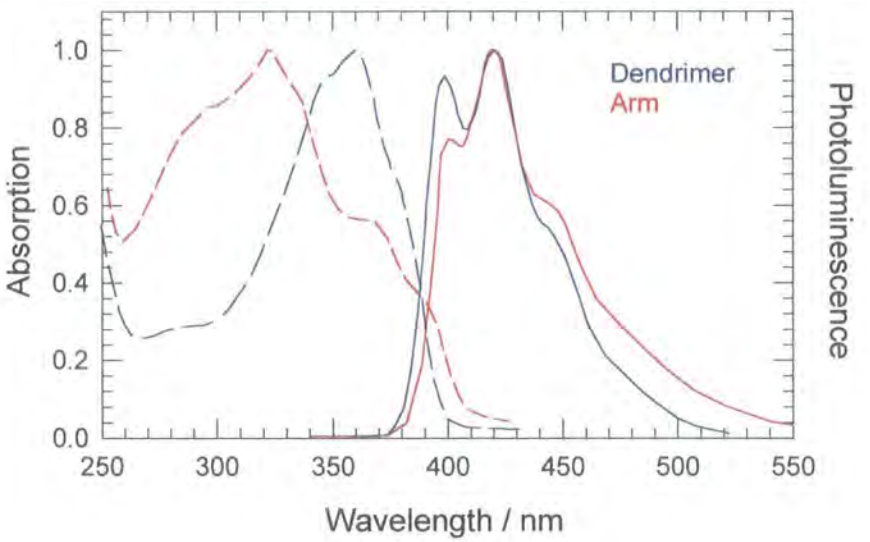

FIG. 4.10 *Normalised absorption (dashed) and photoluminescence (continuous) of the arm and dendrimer solutions. Photoluminescence was measured with 330 nm excitation wavelength.*

The similarity between the arm and the dendrimer is also reflected in their emission profiles. The dendrimer, when excited, emits strongly in the blue with a spectrum that peaks at 430 nm. The PL spectrum also has another peak at around 410 nm and a low energy shoulder at around 460 nm. The emission profile of the arm was almost identical, although it seems slightly blue-shifted by approximately 10 nm with respect to PL spectrum of 0-3DSB. The shape of the arm PL is slightly different as the ratio intensity of the two peaks changes. This is possibly due to self absorption of the arms. Figure 4.11 compares the different photoluminescence excitation (PLE) spectra of the dendrimer for emission monitored wavelengths corresponding to the peaks and

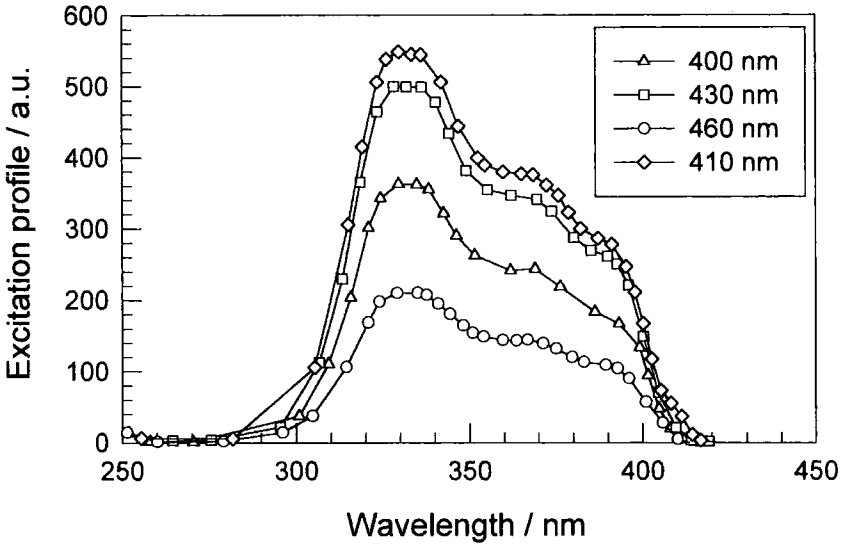

FIG. 4.11 *Excitation spectra of the dendrimer solution monitored at different emission wavelengths.*

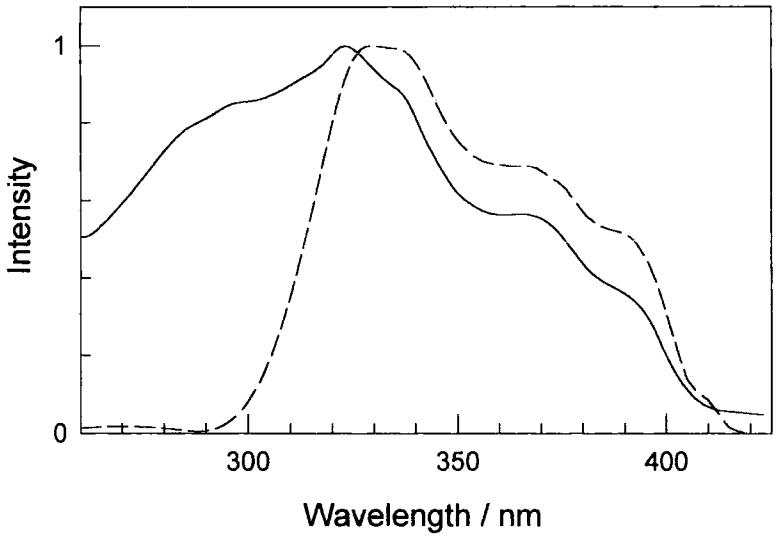

FIG. 4.12 *Normalised absorption (continuous) and PLE (dashed) spectra of 0-3DSB solution.*

shoulders of its PL spectrum. Clearly, all spectra are identical and very similar to the absorption of the dendrimer, especially above 325 nm. Therefore there is only one species responsible for the emission in the dendrimer. The PLE was also measured for the dendrimer arm solution (figure 4.13). As expected the PLE spectrum is very similar to the absorption spectrum of the arm.

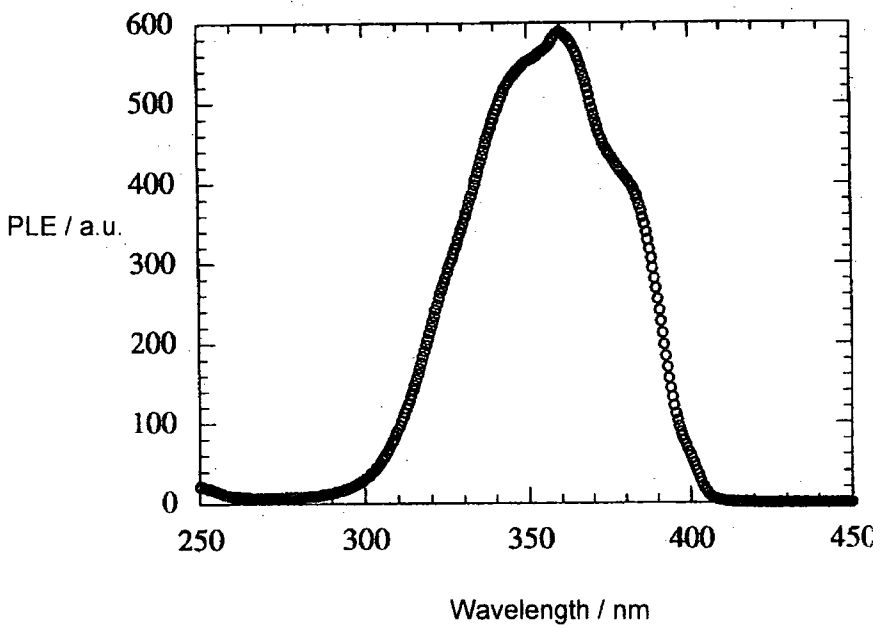

FIG. 4.13 *PLE spectrum of the arm solution (λ_{em} = 430 nm).*

Thin films of the 0-3DSB were spin coated on microscope slide glass substrates as described in a previous section. The films also emit blue light when excited in their absorption band. The PL spectrum of the film is shown in figure 4.14.

It is clear from the figure that there is evidence for vibronic structure in the film PL spectrum. Furthermore, the spectrum is very similar to the solution emission profile, with a negligible shift. This is in contrast to 1-DSB and 1-*ter*P films in which the PL tended to shift to longer wavelengths with respect to the solution PL (1-DSB) or have a completely different profile (1-*ter*P). This was explained as a consequence of a π-stacking of the molecules and the different environment in the solid state. Very likely

this is not the case for this zero generation dendrimer which is probably due to a twist across the ester linkage or because of the star-like shape of the molecules occupying a much larger space and therefore does not aggregate. Using a molecular shape to minimise aggregation may be an important direction for obtaining purer (blue) emission in dendritic systems.

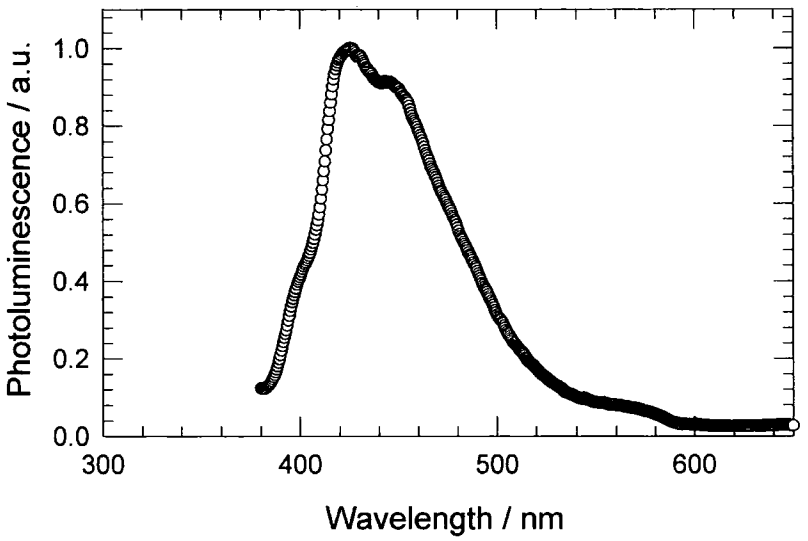

FIG. 4.14 *Photoluminescence of 0-3DSB spin coated film excited at 360 nm.*

4.3.2 Electroluminescence attempt

Films of 1-DSB, 1-*ter*P, and 0-3DSB were spin coated from chloroform solutions onto ITO coated glass substrates. Single layer LEDs using either calcium or aluminium as the top electrode were made following the standard procedure.

In dendrimer devices where aluminium was used to inject electrons into the dendrimer bulk, no diode characteristics were found. In fact the current-voltage (*I-V*) characteristics were either of typical ohmic behaviour or an open circuit. Sometimes because of poor ITO etching, a short circuit was observed. However using calcium as the top electrode resulted in some of the 1-DSB LEDs to function "glow" as they

emitted visible blue light. The *I-V* characteristics are non-linear and the current through the diode is observed to increase significantly above 6 volts (see figure 4.15). The difference between devices made with each contact is due to the difference in workfunctions of metals (ϕ_{Ca} = 2.9 and ϕ_{Al} = 4.28 eV): a higher workfunction providing a higher barrier for electron injection.

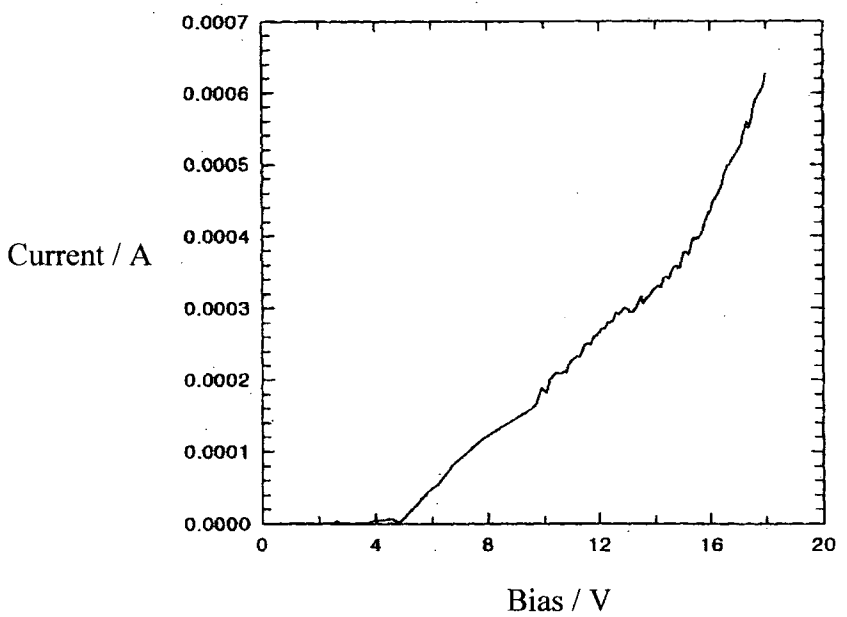

FIG. 4.15 *I-V characteristics of ITO/1-DSB/Ca diode.*

4.4 Distyrylbenzene-Based Dendrimers

It is evident from the preliminary results presented so far that distyrylbenzene based dendrimers could provide an alternative or replacement for polymeric LEDs. The combination of the properties of a small organic molecule and the polymer-like processing is a strong advantage. Furthermore, it has been reported [24-26] that the dendritic structure tends to harvest the energy from the surface groups through the

branches towards the central core. This will certainly be a key point in dendrimers for LEDs where many essential properties could be tuned separately and independently.

Deb *et al* have studied some similar dendritic systems (PPV dendrimers) and have found that the dendrimer properties depend strongly on the generation number [20]. The solution PL quantum yield of their compounds increases with the generation number (up to n = 4). The shape of the emission profile, as shown in figure 4.16, has also changed with higher generation number which was mainly due to a steric hindrance effect becoming more effective at high generations.

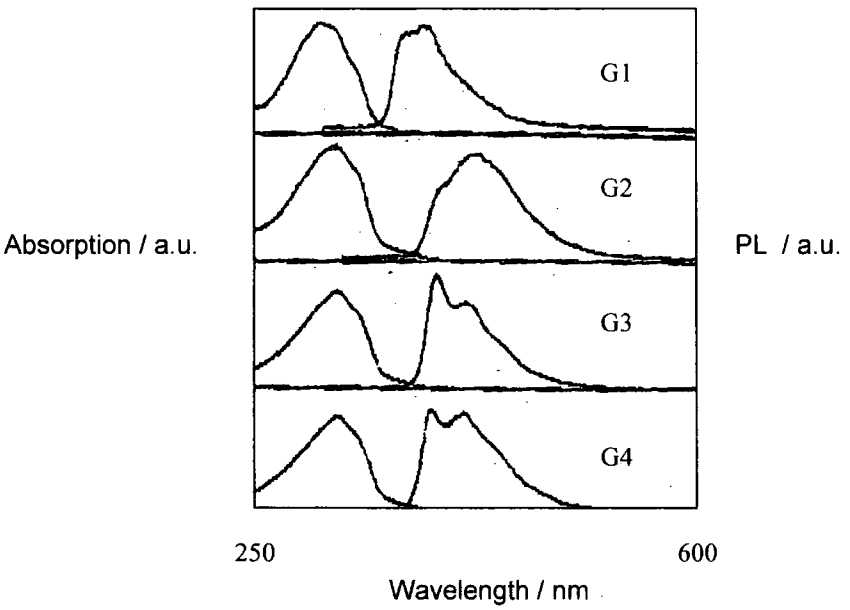

FIG. 4.16 *Normalised absorption and fluorescence spectra of different generations of PPV dendrimers (taken from reference [20]).*

In the next section of this chapter I will be investigating the effect of the generation number on the photophysical and electroluminescence properties of the distyrylbenzene based dendrimers, both in solution and solid state. The data shown on 1-DSB dendrimers are measured using a different batch from the one used in the previous section.

4.4.1 Synthesis

The distyrylbenzene dendrimers were synthesised according to the scheme shown in figure 4.17 and is published by J. Pillow *et al* [27]. Firstly, an iterative repetition of the Wittig and Heck reactions formed the three generations of aldehyde-focused dendrons by a convergent methodology. The aldehyde dendrons were then coupled to a central core to form the final luminescent dendrimer.

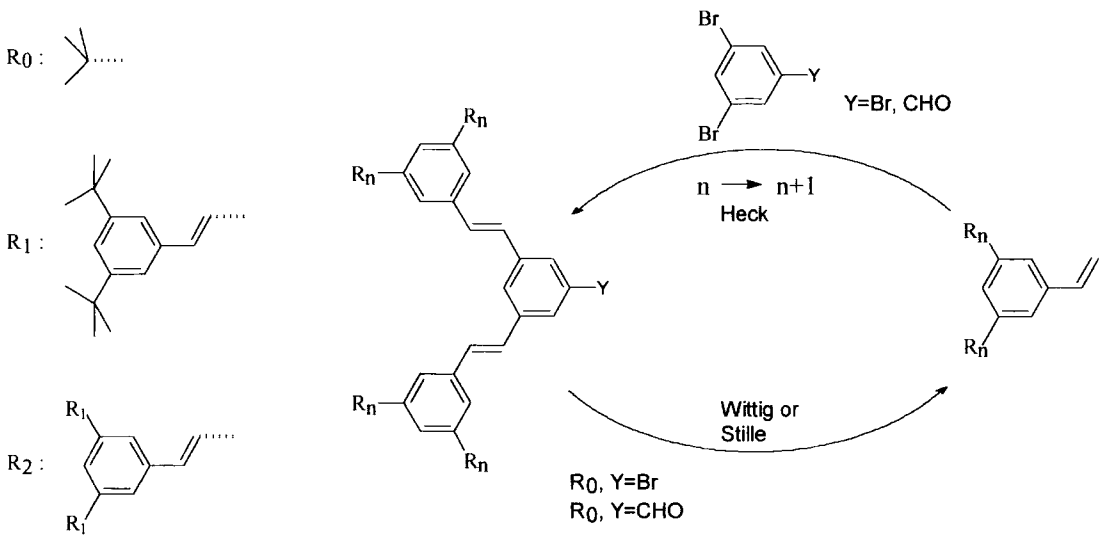

FIG. 4.17 *DSB-dendrimer synthesis [27].*

The 3,5-di-*t*-butylbenzaldehyde (1) starting material was prepared according to a literature procedure. The Wittig reaction was then performed, reacting aldehyde (1) with the yield formed from methyltriphenylphosphonium iodide in potassium *t*-butoxide in dry tetrahydrofuran, to form the styrene (2). The Heck reaction was then performed between styrene (2) and 3,5-dibromobenzaldehyde (3), formed according to a literature procedure. The Heck coupling used the palladacycle catalyst (4), and used the methodology given by Herrmann *et al.* 2,6-Di-*t*-butyl-4-methylphenol was added as a radical inhibitor to prevent the polymerisation of styrene.

A mixture of 2 and 3, along with catalyst 4, sodium carbonate as the base and radical inhibitor 5 in *N,N*-dimethylacetamide was heated at 130 °C for 26 hours under argon. First generation aldehyde was then isolated in a 69% yield.

The distyrylbenzene dendrimer was prepared using the Wadsworth-Emmons coupling of the aldehyde dendrons with a 1,4-phenylene with potassium *t*-butoxide in dry tetrahydrofuran.

The dendrimers were purified by column chromatography. In addition, the DSB dendrimers required isomerisation with catalytic iodine in refluxing toluene overnight to remove unwanted *cis* isomers.

4.4.2 Funnel effect

There have been reports on some dendritic systems where there was a potential light harvesting or directional energy transfer unit. It was possible to transfer charges towards the centre of the dendrimer, which will be the focal point, creating a funnel effect. Thus, by choosing the right parameters, charge recombination could take place in the central core of the dendrimer.

1-DSB has shown a strong luminescence in the blue region (section 4.3.1) and also promising results as a dendrimer LED. The luminescence in 1-DSB and 0-3DSB was found to resemble luminescence of their central cores. Further investigation of the origin of luminescence in this dendrimer was carried out in solution. The absorption spectrum of a new batch of 1-DSB (first generation dendrimer) in chloroform (5 mg/l) is shown in figure 4.19 and compared to the absorption spectra of its fragments, these being the stilbene (dendrons) and *trans*-distyrylbenzene (central core). Their structure is shown in figure 4.18.

The two main features of the absorption spectrum of 1-DSB are at a maximum at 320 nm, and two shoulders at approximately 370 and 385 nm. Since the conjugation in dendrimer structure (figure 4.2) is broken at the branching point, due to a *meta*

arrangement of the dendron links, it was expected that the observed absorption spectrum of 1-DSB would consist of a superposition of the absorptions, due to the stilbene dendrons and the distyrylbenzene core. This is partly true as comparison of the absorption spectrum of 1-DSB with that of distyrylbenzene and stilbene (figure 4.19) shows that the absorption maximum at 320 nm is possibly associated with stilbene units in the dendrons, and that the shoulders are due to the distyrylbenzene core. However, it is interesting to note that that absorption due to the distyrylbenzene core is slightly blue-shifted from the dendrimer absorption spectrum. This small shift indicates that although the stilbene dendrons are *meta* linked, they still allow a small amount of π-electron delocalisation beyond the distyrylbenzene core.

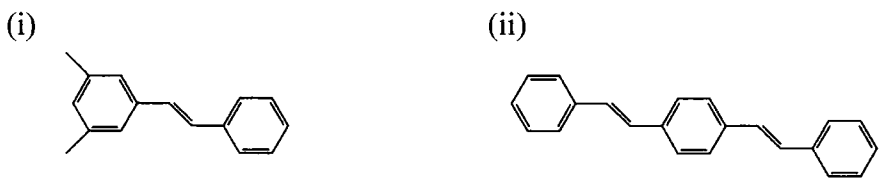

FIG. 4.18 *Chemical structure of the dendrimer fragments: (i) stilbene and (ii) trans-distyrylbenzene.*

The 1-DSB emission spectrum shows two major peaks in the blue region of the visible spectrum. One occurs at 409 nm and the other with less intensity is at 430 nm. The distyrylbenzene solution emission profile was similar to that of 1-DSB solution, although slightly blue-shifted (~15 nm) with respect to the dendrimer PL. The emission from the 1-DSB solution was also measured as a function of the excitation wavelength across the absorption band. The PL spectra are shown in figure 4.20 and look identical.

This clearly means that the emission in this dendrimer system is independent of the excitation energy.

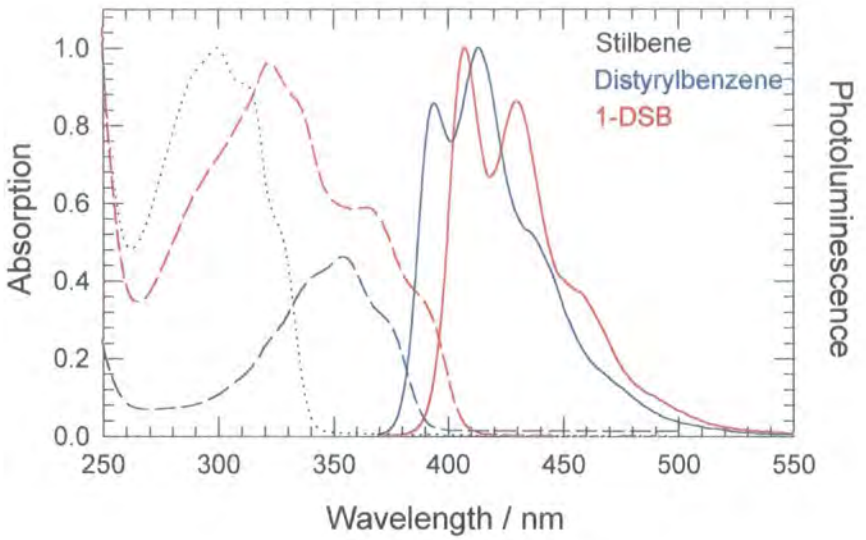

FIG. 4.19 *Absorption spectra of distyrylbenzene (dashed), stilbene (dotted) and 1-DSB (dashed) solution and photoluminescence spectra of distyrylbenzene (continuous) and 1-DSB (continuous) solution, both measured with excitation at 360 nm.*

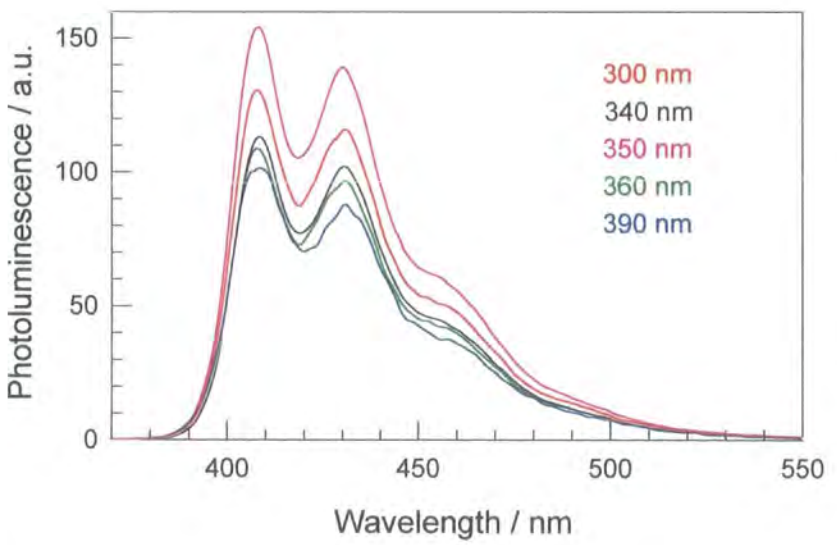

FIG. 4.20 *Photoluminescence spectra of 1-DSB solution excited with different wavelengths.*

The PLE measurements were performed on dendrimer solutions to see whether the luminescence peaks are due to the same species. The results were compared to the absorption spectrum and are shown in figure 4.21. It is clear that the PLE spectra are identical at the different wavelengths, and were also similar to the absorption spectrum of the same solution. This indicates that the two peaks in the emission profiles are originating from the same species. Similar measurements were carried out on the dendrimer core (distyrylbenzene). As shown in figure 4.22 the PLE spectra for emission monitored at 390, 419, and 440 nm are identical and very similar to the absorption of the same solution.

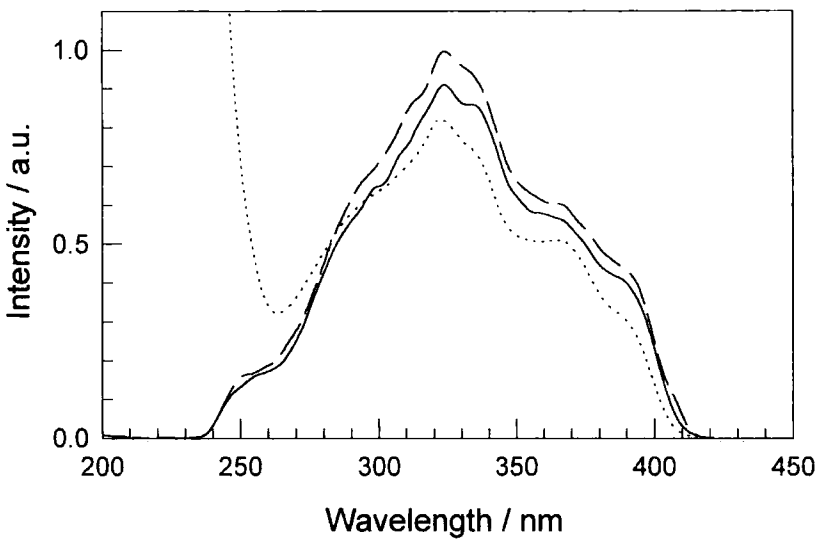

FIG. 4.21 *Photoluminescence excitation spectra of 1-DSB solution measured at 430 (continuous) and 408 nm (dashed). The dotted curve is the absorption of 1-DSB solution for comparison.*

As mentioned before, the absorption of the distyrylbenzene dendrimer resembles a superposition of the stilbene (branching units) and distyrylbenzene (central core), although there are small differences in details. The photoluminescence of the dendrimer measured for different excitation wavelengths were identical, and also similar to the luminescence of the dendrimer core. This is clearly evidence of the emitting chromophore in the dendrimer resembling distyrylbenzene, although the shift between the PL spectra of the dendrimer and distyrylbenzene in solution suggests

more extensive electron delocalisation. The fact that the dendrimer emission was independent of the excitation wavelength over the absorption band means that energy transfer or exciton migration from stilbene to the chromophore is very rapid. Moreover, the peaks of 1-DSB luminescence were due to the same species as shown in the PLE spectra.

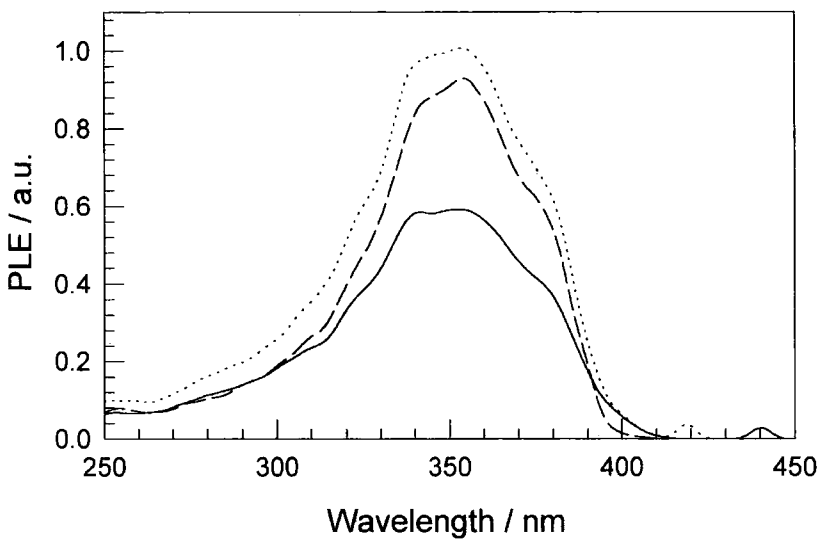

FIG. 4.22 *PLE spectra of distyrylbenzene solution measured at 440 (continuous), 419 (dashed), and 390 nm (dotted).*

It is clear that the funnel effect or the light harvesting property has been demonstrated in this dendrimer type. The core of 1-DSB is certainly behaving as the chromophore in the molecules with little interference from the branching units.

4.4.3 Optical characterisation

Different generations of the DSB dendrimer were synthesised by J. Pillow [27] at the Dyson Perrins Laboratory, Oxford using very similar methodology to 1-DSB (figure 4.17), although the purification tends to become more difficult with increasing generation number. The structures of the second (2-DSB) and third generation (3-DSB) molecules of the distyrylbenzene based dendrimers are shown in figure 4.23.

2-DSB

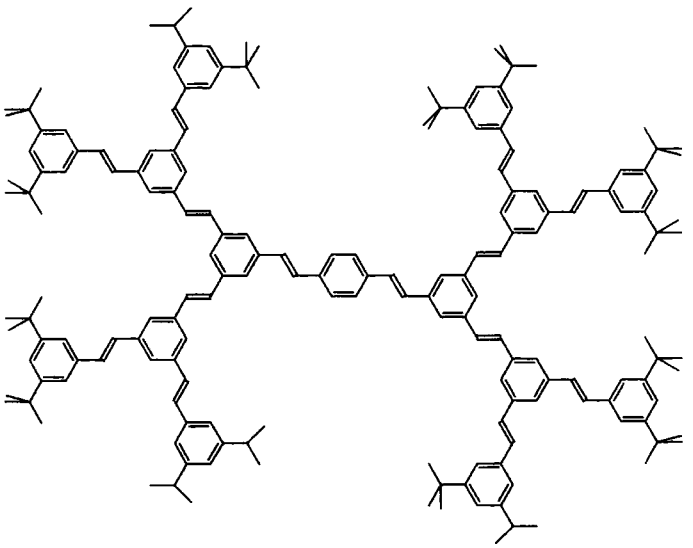

3-DSB

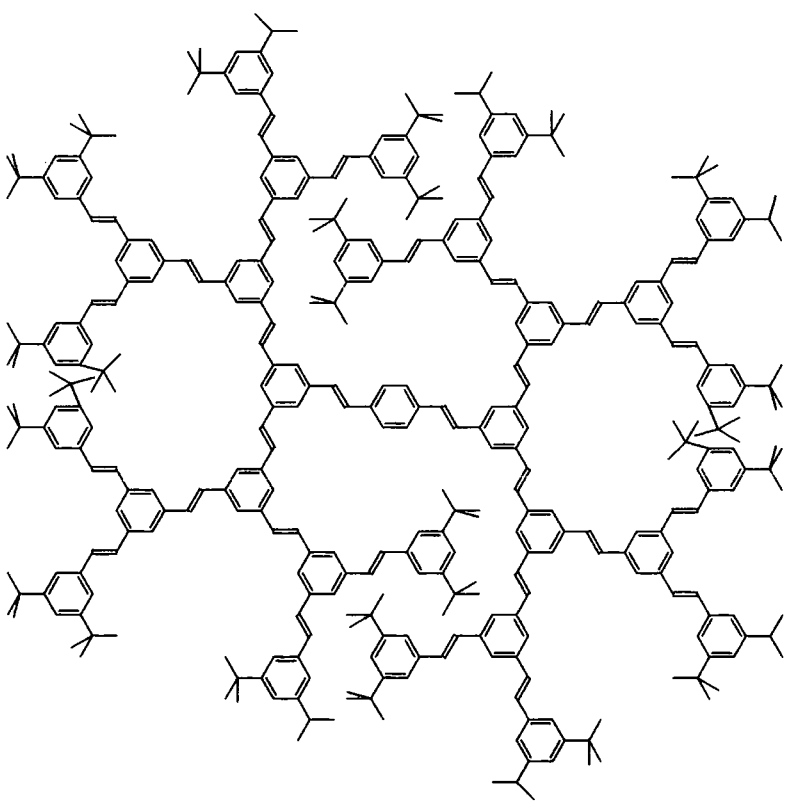

FIG. 4.23 *Chemical structure of second (2-DSB) and third (3-DSB) generation DSB-dendrimers.*

Again, due to the functional surface groups in these molecules (tertiary butyls), the dendrimers were soluble in most organic solvents for each generation studied. Chloroform was used to make solutions of these dendrimers. The optical and PL spectra of the solutions are shown in figure 4.24. The absorption spectra have identical shapes, although the strength of absorption in the 360-400 nm range relative to the peak at 320 nm is greatest for 1-DSB, and decreases for higher generations. This can be explained by the idea that spectra rise from the absorption of the distyrylbenzene core and the stilbene branching units; the relative amount of distyrylbenzene core (responsible for the 360-400 nm absorption as explained in section 4.4.2) and stilbene dendrons (responsible for the main absorption band at 320 nm) is greatest for 1-DSB and decreases for higher generations.

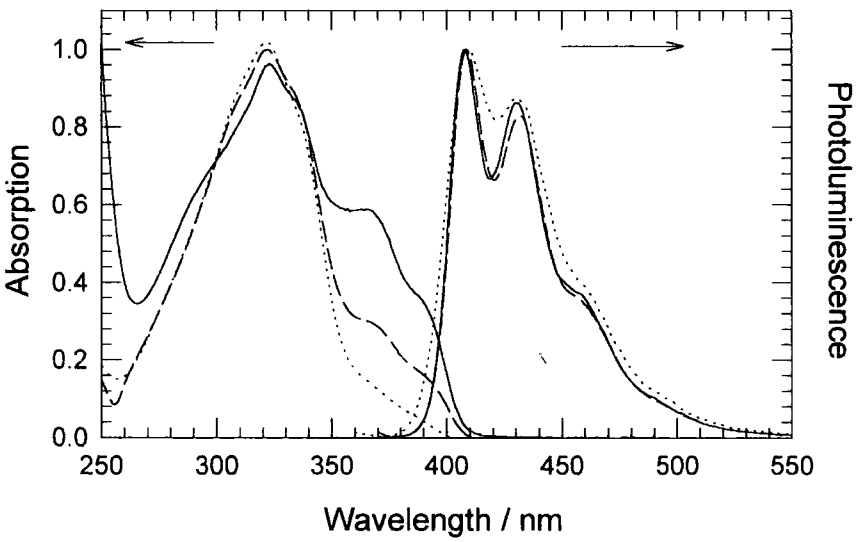

FIG. 4.24 *Normalised absorption and photoluminescence of first (continuous), second (dashed), and third (dotted) generation distyrylbenzene dendrimers in chloroform solution. All solutions were excited at 360 nm.*

The PL spectra of second and third generations were also independent of the excitation energy and, in contrast to the absorption spectra, consisted of emission exclusively from the distyrylbenzene core. Note that the spectra were very similar for all generations with two peaks at 410 and 440 nm. This means that the introduction of extra branching layers had no effect on the nature of the emitting species.

It was found that optical quality films of all generations can be prepared by spin coating directly from chloroform solution. The absorption spectra of these films are shown in figure 4.25. The absorption of films of all generations reflects the same scenario as in the solution case; the absorption of 1-DSB film consists of a superposition of the fragments (stilbene and distyryl benzene) absorption and is similar to 2-DSB and 3-DSB absorptions, although the ratio of the two species absorption is increasing with the generation number.

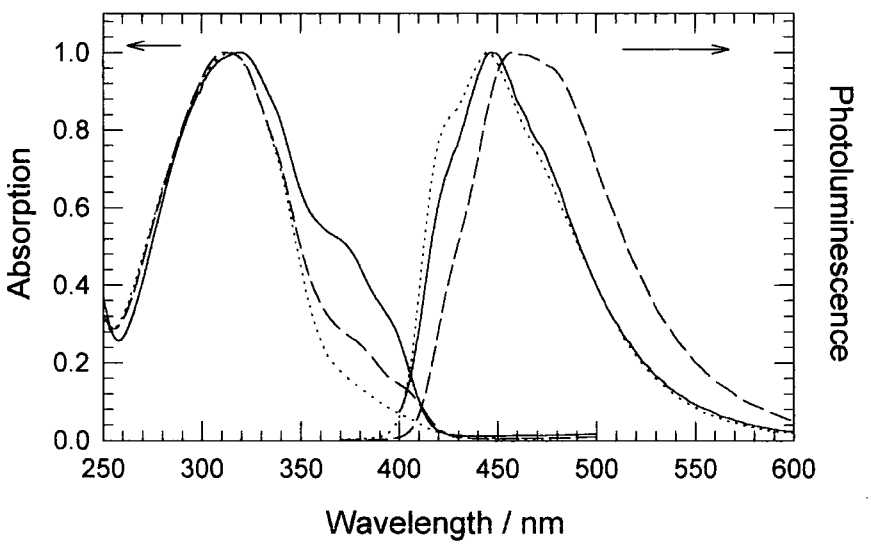

FIG. 4.25 *Normalised absorption and photoluminescence of 1-DSB (continuous), 2-DSB (dashed) and 3-DSB (dotted) spin coated films. All films were excited at 360 nm.*

The absorption of the films, when compared to the solution, is similar in shape but is more smooth particularly for the region where the stilbene absorbs. This is believed to be due to a distribution of conformations and/or broadening due to aggregation.

The PL of films of the three generations are also shown in figure 4.25. The PL of 1-DSB film is blue with a maximum emission at around 442 nm but red-shifted by approximately 50 nm with respect to the solution and with less structure. The red-shift in the emission profile in the solid state is also observed for some conjugated polymers and may be explained by the fact that in the solid state the molecules can

experience a wider distribution of conformations including a more planar state which would give rise to a lower HOMO-LUMO energy gap.

The PL spectra of the three dendrimer generations did not follow a trend. The emission profile of the second generation dendrimer (2-DSB) film was slightly red-shifted with respect to 1-DSB, with a maximum emission at around 458 nm. The red-shift observed in the case of 2-DSB is possibly due to increased electron delocalisation due to the extra 'layer' of stilbene units. Note that small differences in spectra between different batches of 2-DSB were observed; these appear to be correlated with the degree of heating at the end of the synthesis when the product is dried under vacuum to remove the solvent, but are not understood due to the difficulty in reproducing the same results.

A further red-shift might be expected for the third generation material (3-DSB) as a result of an extended π-electron delocalisation. This was not the case and instead a blue-shift of the PL spectrum was observed, which placed it at similar wavelength to that of 1-DSB (peak at 445 nm). A possible explanation of this behaviour is that the blue-shift in the in PL spectrum for 3-DSB is due to steric interaction between the dendrons of the dendrimer due to its crowded configuration. This leads to a twisting of the branches, and therefore a reduction of the electron delocalisation is expected.

This proposal is supported by J. Pillow's modelling of the dendrimer spatial configuration, which shows that for 1-DSB and 2-DSB the surface groups do not interact and that the cores are essentially planar as shown in figure 4.26. The dendrimers are also believed to be relatively planar. However, for 3-DSB, the surface groups are sterically crowded in a planar structure and cause the dendrimer to lose its planarity.

1-DSB

2-DSB

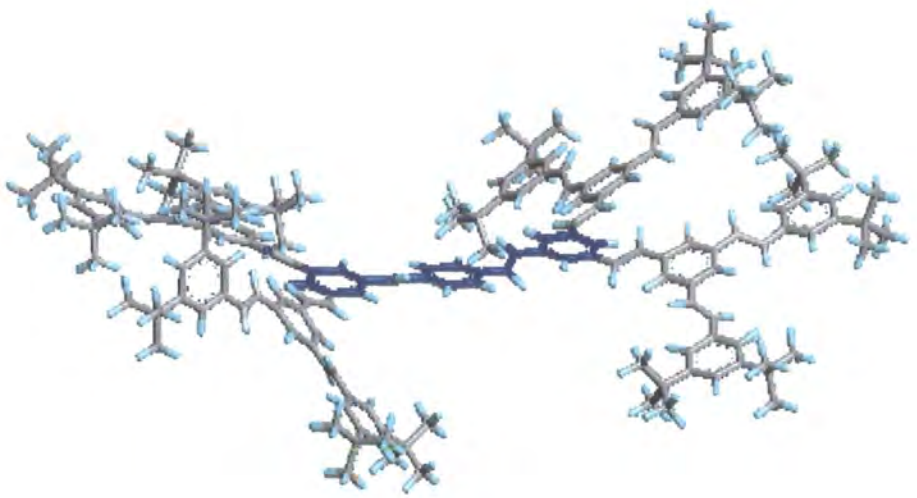

3-DSB

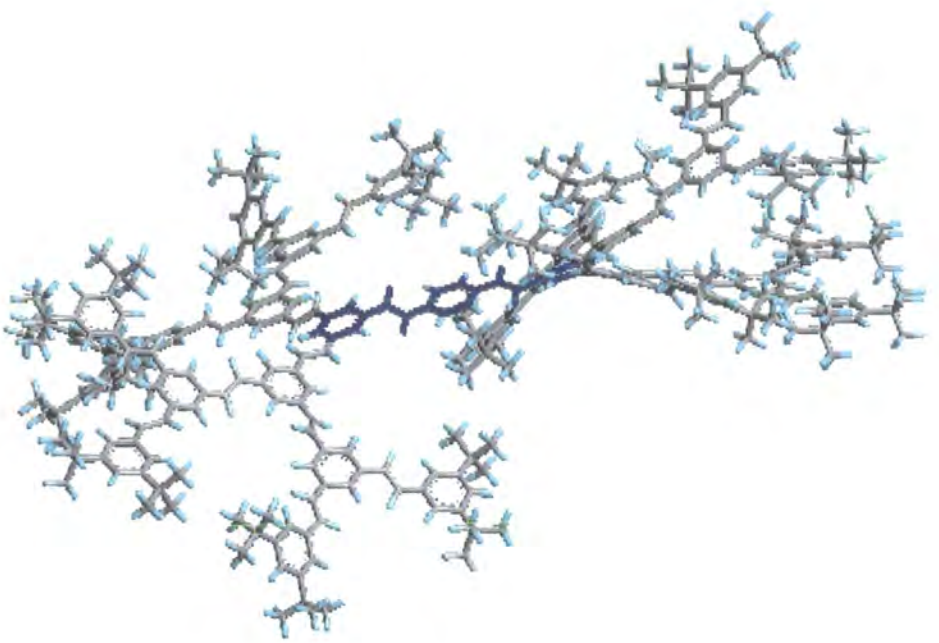

FIG. 4.26 *The optimised spatial configuration of the first (1-DSB), second (2-DSB), and third (3-DSB) generation distyrylbenzene-based dendrimers. In blue is the DSB core.*

The photoluminescence quantum yield, ϕ_{PL}, was measured for all films as described in section 3.5.2. The UV lines of the argon ion laser were used to excite the dendrimer films. The different quantum yields are listed in table 1.

Material	ϕ_{PL} (%)	± (%)
1-DSB	36	3
2-DSB	20	3
3-DSB	24	3
PPV (a)	27	2

a: taken from reference [28]

Table 4.1 *Photoluminescence quantum yield of 1-DSB, 2-DSB, 3-DSB, and PPV films.*

These values are relatively high for solid state films and are comparable to quantum yields reported for PPV derivatives [28,29]. This shows that these dendrimers are highly fluorescent and that concentration quenching effects which might be expected for the simple distyrylbenzene structure are substantially avoided by the dendritic molecular architecture. However the behaviour of ϕ_{PL} as a function of the generation number is not properly understood.

4.4.4 Electroluminescence in distyrylbenzene dendrimers

The three blue-emitting dendrimers were then incorporated into LED structures consisting of a single dendrimer layer sandwiched between ITO and metal electrodes as described in chapter 3. As these dendrimers have a large energy gap (~ 3 eV), a large energy barrier for electron injection was expected, and so calcium, which has a low workfunction, was used as the cathode. Measurements of current and light output as a function of applied voltage, as well as the EL emission spectra, were taken as described in chapter 3.

Given sufficient care in device preparation, LEDs of all generations of dendrimer were successfully made. Light-emission, which initially appeared blue to the eye, was observed from all three materials. Their EL spectra are shown in figure 4.27. Clearly the devices emit in the blue range of the visible spectrum. The 1-DSB EL spectrum was rather broad, featureless, and shifted towards lower energy with respect to its PL spectrum with a maximum at around 510 nm. It was also observed that there was an evolution of the colour of emission from blue to white on a time scale of seconds to minutes.

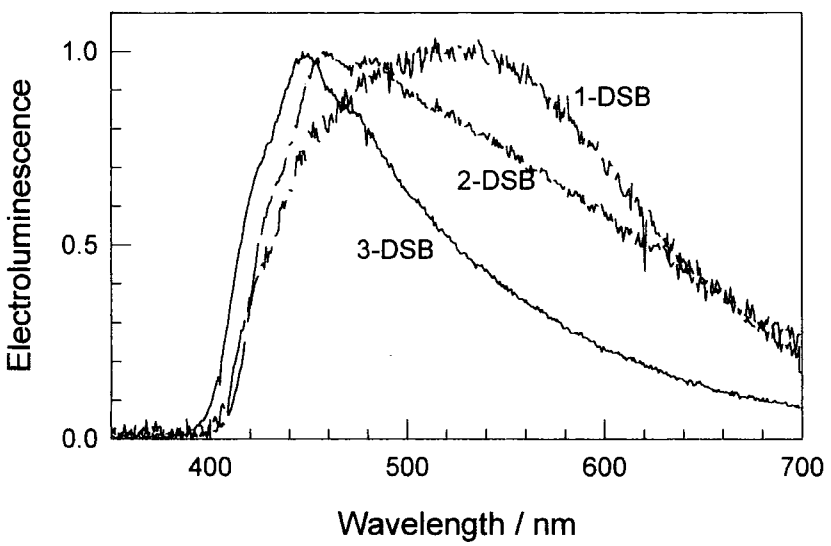

FIG. 4.27 *Electroluminescence spectra of dendrimer LEDs of first, second, and third generation.*

When the C.I.E. co-ordinates (see section 3.7) of the EL emission were plotted on a C.I.E. diagram, the corresponding colour was close to the achromatic point. Unfortunately in the case of 1-DSB, at the voltages required to produce sufficient emission to be observed under normal lighting conditions, the devices degraded rapidly, and hence it was difficult to measure the EL spectrum of 1-DSB while still in its initial form. The devices degraded also by sparking, these sparks gradually removed the calcium contacts while the device was exposed continuously to the electric field and led to the formation of dark spots, which were non-emissive and

tended to increase in area until the device stops emitting and no current was drawn through it. This was also observed in other organic and polymeric LEDs [30].

Devices prepared using 2-DSB and 3-DSB dendrimers were more stable and retained blue emission for longer which explains the difference in their EL spectra and those of 1-DSB. As shown in figure 4.28, the EL spectrum of the 2-DSB LED has a maximum at around 470 nm which coincides with the maximum of the PL. The EL spectrum also has some structure which is very similar to that seen in the PL spectrum. Overall the PL and EL of the 2-DSB dendrimer are very similar in the shorter wavelength region, which suggests that the same process is responsible for emission in the two regimes. This means that emission comes mainly from radiative decay of the dendrimer singlet excited states formed by the recombination of electron-hole pairs. Furthermore, the recombination process in the EL regime takes place in the central part of the molecule (core), as does PL, emitting photons with energy corresponding to the π-π^* transition energy.

The 3-DSB EL spectrum displayed similar behaviour as in the 2-DSB devices in that the EL spectrum was very similar to the PL spectrum with a visible vibronic structure. The maximum emission in EL also collides with the peak of the PL. The recombination of the opposite charges in the core is also valid in the third generation dendrimer.

This is an important property of these dendrimers which could be exploited to tune the emission wavelength in the visible spectrum simply by changing the electronic configuration of the dendrimer core. The application of this useful characteristic will be discussed in chapter 5.

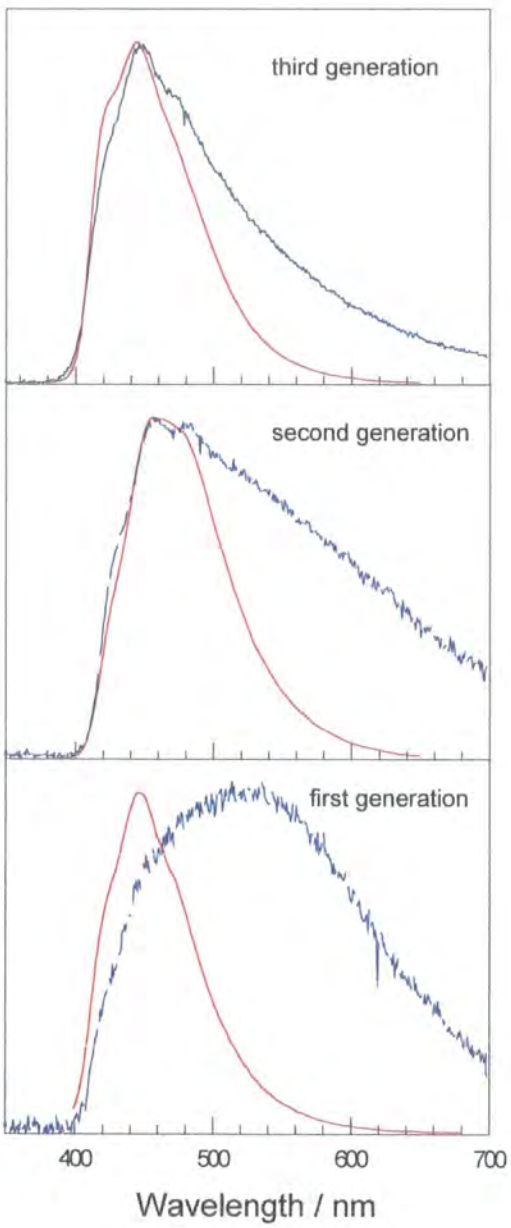

FIG. 4.28 *Comparison of photoluminescence (red) and electroluminescence (blue) of first, second, and third generation DSB dendrimers.*

Although similarities between the PL and EL process were very clear from their spectra, what was also clear is their differences which consist mainly in the longer wavelength region where an enhanced emission of the EL spectrum tail is observed. Since these dendrimers are believed to be good hole transporting layers, one could imagine that immediately after injecting holes and electrons into the dendrimer, the holes will travel directly to the cathode where they form an electron-hole pair that will possibly decay radiatively as illustrated in figure 4.29. Hence, the EL emission takes place at or in the vicinity of the metal-dendrimer interface which could be electronically different from the emission zone in the PL process which takes place in the 'pristine' bulk of the dendrimer, hence the difference between the PL and EL spectra.

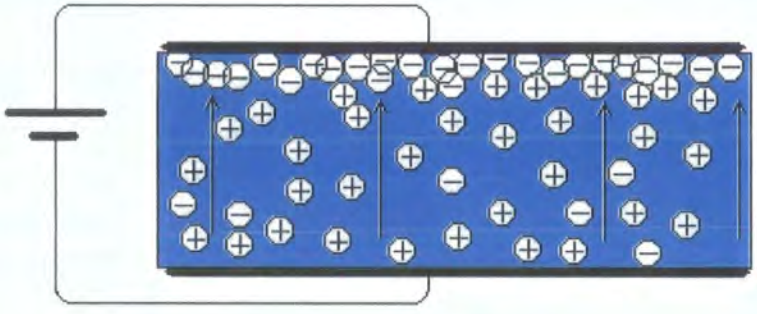

FIG. 4.29 *Illustration of a dendrimer LED, showing where charge recombination takes place.*

Another possible explanation of that enhanced tail emission is the structural changes the molecules could experience during device operation which will lead to the formation of lower energy sites that emit at longer wavelength. This low energy emission was noticed to increase with time as the EL turns from sharp blue to blue-white as seen in the 1-DSB EL spectrum. This will be investigated in section 4.4.5. Note that similar differences were observed in many other systems [31] and specifically in some macromolecules where X. Tao and co-workers have observed an enhanced tail emission from their hyperbranched polycarbazole structural defects which form a manifold of emitting trapped states and act as recombination centres

[32]. P. Wang and co-workers have also observed some differences between the PL and EL spectra in their anthracene dendrimers [33]. Instead of an enhanced tail emission, they have observed a substantial shift (~ 50 nm) of the EL spectrum towards higher energy with respect to the corresponding PL.

Dendrimer	x co-ordinate (EL)	y co-ordinate (EL)
1-DSB	0.34	0.38
2-DSB	0.29	0.32
3-DSB	0.23	0.24

Table 4.2 *CIE co-ordinates of electroluminescence in distyrylbenzene based dendrimers.*

The enhanced tail emission was also observed in 3-DSB devices (figure 4.33), with a similar evolution rate to 2-DSB, making the emitting devices appear whitish as shown in figure 4.33 (lower panel).

The current-voltage (*I-V*) and light output-current (*L-I*) characteristics of a typical ITO/2-DSB/Ca device are shown in figure 4.30 and 4.31. The *I-V* of 2-DSB is a typical diode-like behaviour showing a systematic increase of the current through the device and the emitted light after a certain threshold of the electric field (~ 1 MV/cm). Note that in organic LEDs the onset electric field is usually independent of the thickness of the active layer in the LED structure [34] which we have also observed in our distyrylbenzene based dendrimers. This suggests that the current in the device is injection limited. The onset of the luminance coincides with the onset of the current and reaches values of around 150 Cd/m^2. Note that these values were the best brightnesses achieved for this dendrimer. Although the typical values obtained for 2-DSB were in the range of 100 Cd/m^2, it was difficult to reproduce the best brightnesses, which is believed to be due to the difficulty in reproducing typical pressures in calcium evaporations.

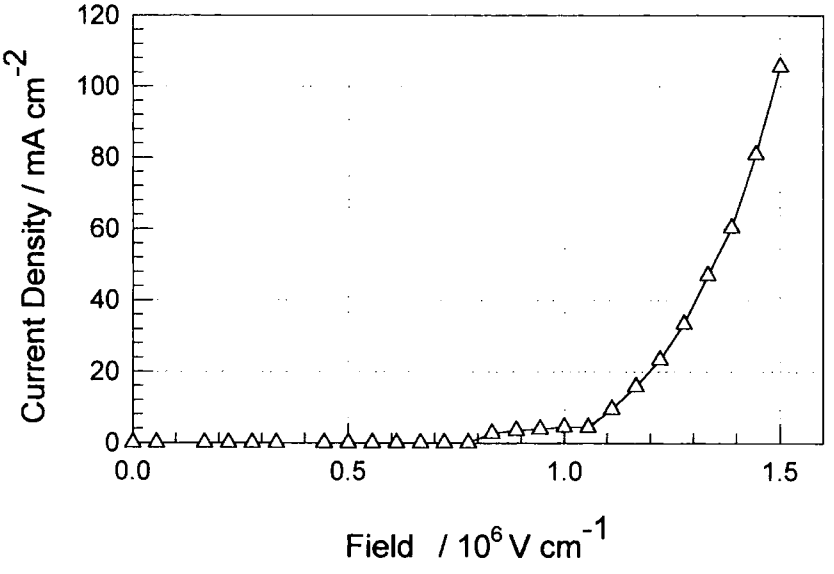

FIG. 4.30 *Current vs. voltage characteristics of a 2-DSB device with calcium electrodes.*

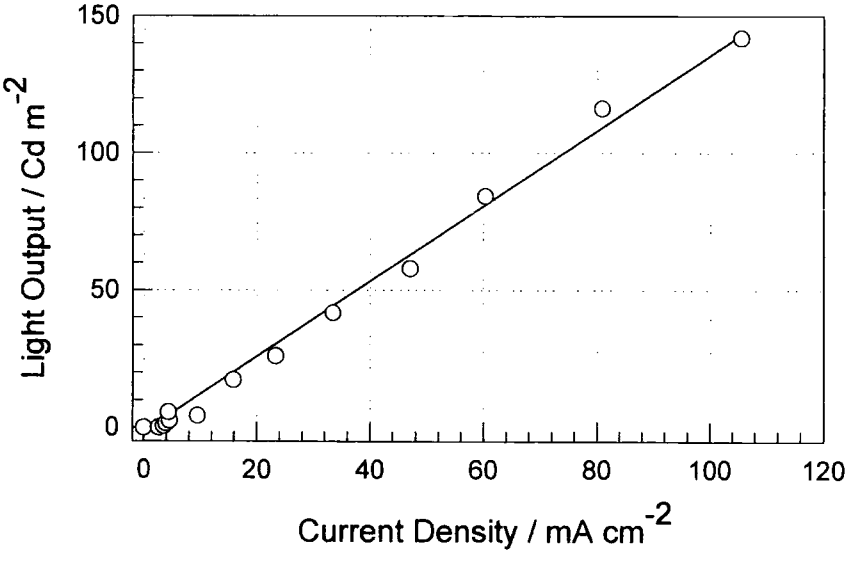

FIG. 4.31 *Light output vs. current characteristics of a 2-DSB device with calcium electrodes.*

This is believed to be crucial in device operation as it has been reported that the calcium, which is a very reactive metal, does have a major effect on device performance depending on the pressure used during the evaporation. W. R. Salaneck *et al* have reported that 'dirty' calcium, which is evaporated at pressures in the range of $1x10^{-6}$ mbar, results in devices with better performances compared to devices made using a 'clean' calcium evaporated at ultra high pressures (~ $1x10^{-12}$ mbar) [35].

Other dendrimers (1-DSB and 3-DSB) also manifest a typical rectifying diode behaviour. Some current anomalies (negative resistance) at low bias were observed in these dendrimers, mainly for the first generation which was also found to be very dependent on the calcium evaporation conditions.

The EL external quantum efficiencies of these dendrimer LEDs were deduced from their light output-current characteristics as described in chapter 3 and found to be 0.01 % for 1-DSB, 0.09 % for 2-DSB, and 0.03 % for 3-DSB. The efficiency of the second generation LED is rather good for blue-emitting single layer devices when compared to efficiencies reported for other blue LEDs such as m-LPP [36] and PBP [37]. These values are also in the same range or higher to the external quantum efficiencies of devices using the most conventional polymer, PPV, as the emissive layer in similar LED configuration (0.01 %) [38]. The other more important aspect of these efficiencies is an increase of almost an order of magnitude in going from the first to the second generation dendrimer. Unfortunately, going to a higher generation dendrimer (3-DSB) does not have the same effect on the EL efficiency which might be related to the spacing of the dendrimer molecules in higher generations. However we should not forget that these values are the first EL efficiencies, at the time, to be published on dendrimer light-emitting diodes.

4.4.5 Enhanced tail electroluminescence

It is of interest to understand the origin of that emission taking place at lower energy in the visible spectrum in the EL process (figure 4.33) with the aim of getting purer

emission, an emission that is identical to the PL profile, as well as enhancing the stability of these devices.

On first impressions, one might believe a possible explanation to this behaviour is the oxygen present in the bulk of the dendrimer. The core, distyrylbenzene, could easily react with the oxygen to result in new residuals as shown in figure 4.32, or what some researchers call complexes [39,40]. These complexes could be non-emitting. The excitons, to decay radiatively, are forced to migrate to lower energy sites which could be developed by the creation of those complexes.

However, if this was true one would expect to see the same changes in the PL spectra simply by recording the PL of an identical sample in air and investigating its behaviour with time. This was carried out on a sample deposited by spin coating from the same solution used to make LEDs, onto spectrosil glass discs. Using the same spinning parameters one would expect the samples to be identical.

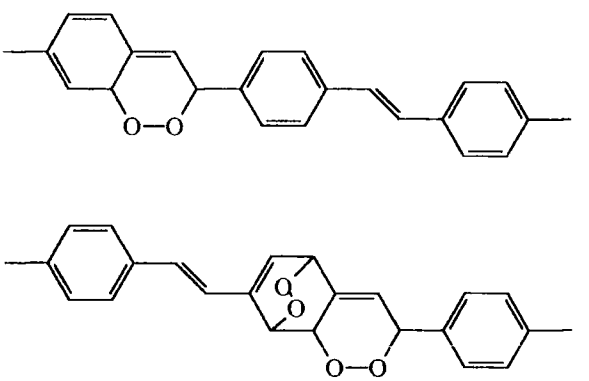

FIG. 4.32 *The possible products of a photo-oxidised DSB core.*

The excitation was provided with continuous illumination using the UV lines of an argon ion laser. The experiment was carried out in air for an accelerated photo-oxidation. Figure 4.34 shows the PL spectra of a 2-DSB film recorded using a CCD

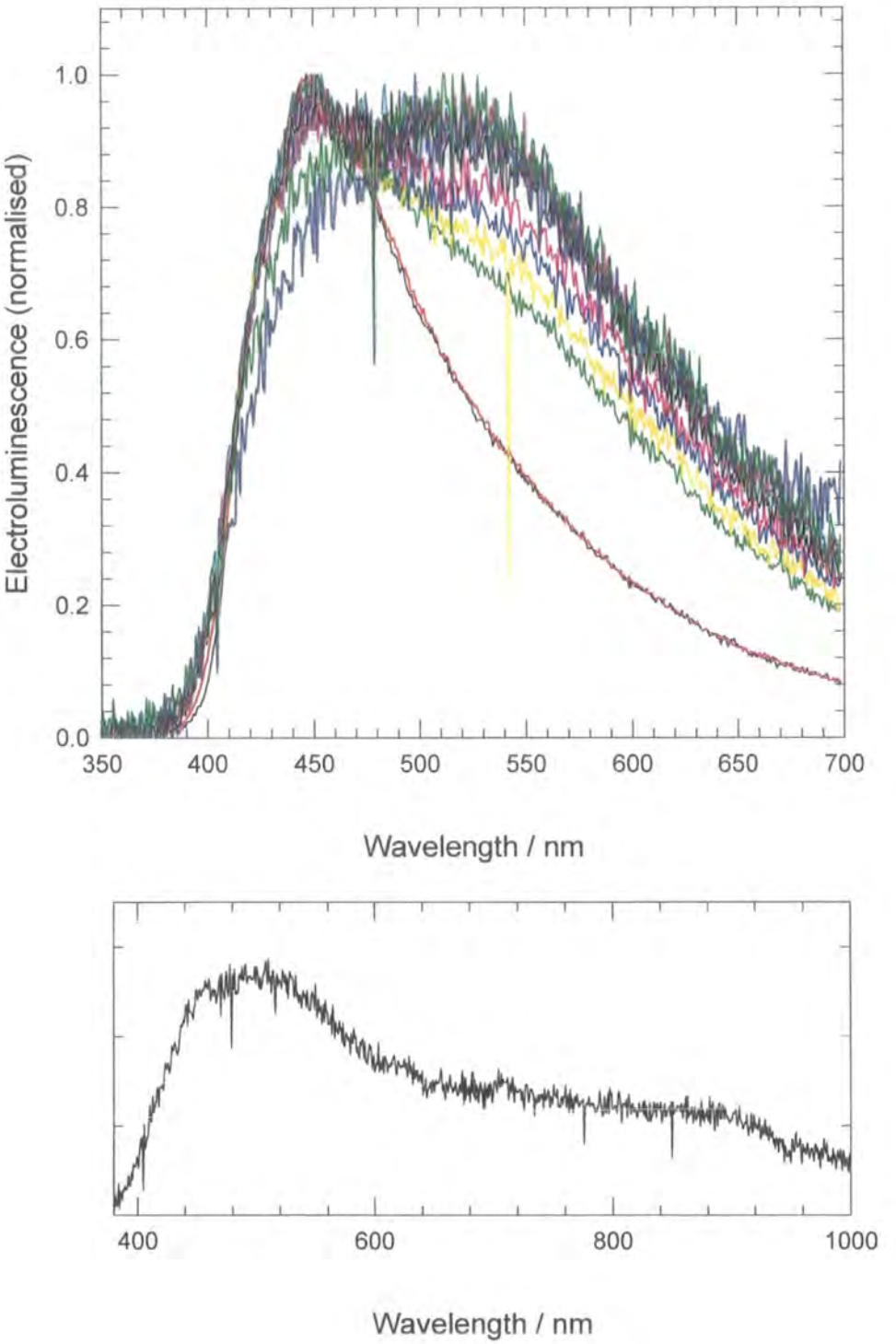

FIG. 4.33 ***Upper panel*** *Electroluminescence spectra of ITO/3-DSB/Ca/Al device. Spectra were taken every minute of a continuous LED operation.* ***Lower panel*** *The electroluminescence spectrum of 3-DSB after 20 minutes of continuous operation: the device appeared blue-white.*

spectrometer every 2 minutes with an integration time of 1 s. The spectra appears to be identical in shape with no evident intensity increase in the emission at longer wavelengths which confirms that the process responsible for that enhanced tail emission in the EL spectrum is probably not present in the PL regime and hence could be caused by the effect of the electric field across the device. Furthermore, the PL spectra decreases in intensity as the film was exposed to UV which is a sign of sample deterioration. This is possibly due to the dendrimer core reacting with the oxygen atoms to form some non-emitting complexes as explained earlier.

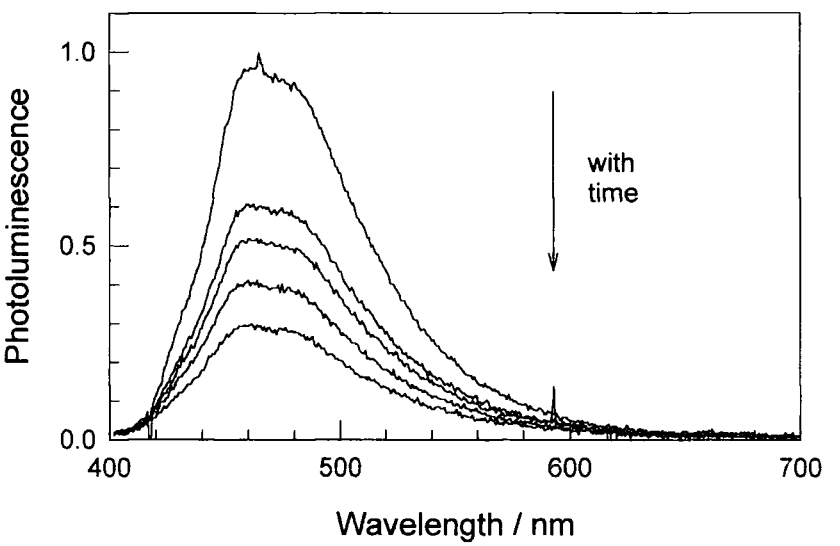

FIG. 4.34 *Photoluminescence of 2-DSB film excited continuously with the UV lines of an argon ion laser every 2 minutes.*

The other possible explanation is that since this phenomenon is observed in the EL regime, and after demonstrating that it is not the case in the PL process, one might think that it is related to device heating. This heating could affect the spatial arrangements of the molecules or cause a re-crystallisation of the dendrimer which, in either cases, will produce some ordering changes that will affect the electronic properties of the material and therefore result in a different emission. To investigate the effect of temperature on the luminescence properties of these materials, two spin

coated samples of first generation dendrimer were heated to 220 °C for 3 hours in a vacuum ($2.5x10^{-5}$ mbar). This is above the glass transition temperature (Tg) of 180 °C measured for the first generation dendrimer. The absorption and PL spectra of the treated and non-treated samples of 1-DSB are shown in figure 4.35. The spectra were measured with the films excited at 360 nm and appear to be similar, although there is a slight bump that appears at low energy in the treated samples emission profile. It is clear that this minor change could not account for the large time dependent difference between the PL and EL spectra of the same material.

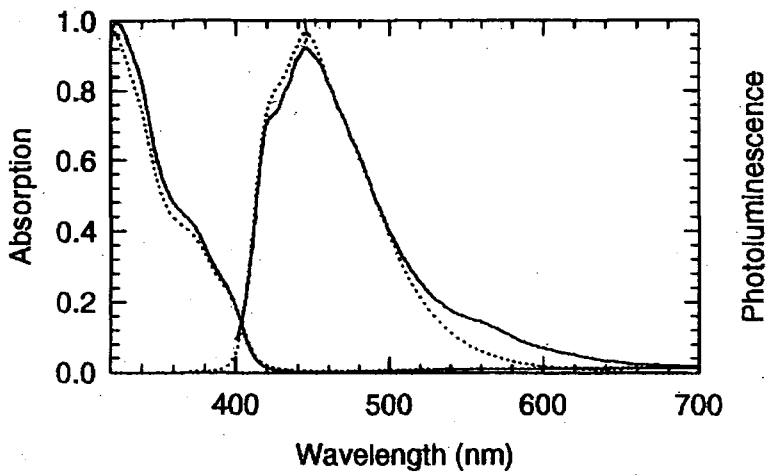

FIG. 4.35 *Absorption and photoluminescence of heated (continuous) and non-heated (dotted) 1-DSB films.*

Another explanation of what could affect the luminescence property in these dendrimer LEDs is the use of the unstable metal for the top electrode which could, under the influence of the electric field, migrate towards the dendrimer bulk and create some sort of different moiety or defective segments in the molecule, and most probably react with the dendrimer core.

4.5 Conclusion

A new concept has been used to develop new materials to be used as the emissive part in a monolayer LED structure. The concept consists of a core, branches and surface groups. Each of these segments has its own characteristic and an effect on the overall structure which can be tuned independently. These new dendrimers were conjugated and offered interesting properties such as tunnelling the charges towards the central core. The latter was found to behave as the chromophore in the dendrimer molecule and consequently controlled the luminescence characteristics of the molecule while the branches and the surface groups were controlling the charge transport properties and solubility respectively. The first generation was strongly luminescent in the blue range of the visible spectrum in both solution and solid state, although a red-shift of the film PL was observed which is attributed to the aggregation of the molecules due to their planar configuration. Higher generations of this dendrimer (second and third) were also investigated and show similar characteristics.

Dendrimer LEDs were successfully demonstrated using all generations of this dendrimer and gave blue light-emission. Efficiencies of these LEDs were also very promising for blue LEDs considering the difficulty to obtain such colour in the inorganic and polymer devices. The dendrimer generation number has a remarkable effect on the external quantum efficiencies as they seem to increase by almost an order of magnitude for the second generation. Slightly lower efficiencies, but purer colour, was observed for the third generation material. Higher generation materials appear to be more stable than the first generation as their EL retains purer emission.

References

1. J. H. Burroughes, D. D. C. Bradley, A. R. Brown, R. N. Marks, R. H. Friend, P. L. Burn and A. B. Holmes, *Nature,* **1990**, 347, 539.
2. R. H. Friend, D. Bradley and A. Holmes, *Physics World,* **1992**.
3. M. Gostick, *Electronic Engineering,* **1996**, 67.
4. A. R. Brown, N. C. Greenham, R. W. Gymer, K. Pichler, D. D. C. Bradley, R. H. Friend, P. L. Burn, A. Kraft and A. B. Holmes, *Proceeding of NATO ARW.*
5. P. L. Burn, A. B. Holmes, A. Kraft, D. D. C. Bradley, R. H. Friend and R. W. Gymer, *Nature,* **1992**, 356, 47.
6. C. Zhang, D. Braun and A. J. Heeger, *J. Appl. Phys.,* **1993**, 73, 5177.
7. P. L. Burn, A. B. Holmes, A. Kraft, D. D. C. Bradley, A. R. Brown and R. H. Friend, *J. Chem. Soc. Chem. Comm.,* **1992**, 32.
8. H. Vestweber, R. Sander, A. Greiner, H. Weitz, R. F. Mahrt and H. Bassler, *Synth. Met.,* **1994**, 64, 141.
9. J. Kido, K. Hongawa, K. Okuyama and K. Nagai, *Appl. Phys. Lett.,* **1994**, 64, 815.
10. A. J. Hudson, S. Tamura, M. B. Grieve, T. Richardson, J. E. Wong and D. W. Bruce, *J. Mater. Chem.,* **1995**, 5, 1867.
11. C. W. Tang and S. A. Vanslyke, *Appl. Phys. Lett.,* **1987**, 51, 913.
12. T. R. Hebner, C. C. Wu, D. Marcy, M. H. Lu and J. C. Strum, *Appl. Phys. Lett.,* **1998**, 72, 519.
13. J. M. J. Fréchet, *Science,* **1994**, 263, 1710.
14. J. Issberner, R. Moors and F. Vogtle, *Angew. Chem. Int. Ed. Engl,* **1994**, 33, 2413.
15. P. J. Dandliker, F. Diederich, M. Gross, C. B. Knobler, A. Louati and E. M. Sanford, *Angew. Chem. Int. Ed. Engl,* **1994**, 33, 1739.
16. A. Kraft, *J. Chem. Soc., Chem. Commun.,* **1996**, 77.
17. Y. Kuwabara, H. Ogawa, H. Inada, N. Noma and Y. Shirota, *Adv. Mater.,* **1994**, 6, 677.
18. P. Wang, Y. Liu, C. Devadoss, P. Bharathi and J. S. Moore, *Adv. Mater.,* **1996**, 8, 237.

19. L. L. Miller, R. G. Duan, D. C. Tully and D. A. Tomalia, *J. Am. chem. Soc,* **1997**, 119, 1005.

20. S. K. Deb, T. M. Maddux and L. Yu, *J. Am. Chem. Soc.,* **1997**, 119, 9079.

21. W. Tachelet, S. Jacobs, H. Ndayikengurukiye, H. J. Geise and J. Gruner, *Appl. Phys. Lett.,* **1994**, 64, 2364.

22. A. J. Hudson, S. Tamura, M. B. Grieve, T. Richardson, J. E. Wong and D. W. Bruce, *J. Mater. Chem.,* **1995**, 5, 1867.

23. See for example S. A. Jenekhe and J. A. Osaheni, *Science,* **1994**, 265, 765-768. J. F. Gruner and *et al.*, *Adv. Mater.,* **1994**, 6, 748. D. D. C. Bradley, M. Grell, X. Long, H. Mellor, A. Grice, M. Inbasekaran and E. P. Woo, *SPIE,* **1997**, 3145, 254.

24. R. Kopelman, M. Shortreed, Z.-Y. Shi, W. Tan, Z. Xu, J. S. Moore, A. B. Haim and J. Klafter, *Phys. Rev. Lett.,* **1997**, 78, 1239.

25. S. F. Swallen, Z.-Y. Shi, W. Tan, Z. Xu, J. S. Moore and R. Kopelman, *Journal of Luminescence,* **1998**, 76-77, 193.

26. A. Bar-Haim and J. Klafter, *Journal of Luminescence,* **1998**, 76-77, 197.

27. J. N. G. Pillow, M. Halim, I. D. W. Samuel and P. L. Burn, *Submitted to Macromolecules.*

28. N. C. Greenham, I. D. W. Samuel, G. R. Hayes, R. T. Phillips, Y. A. R. R. Kessner, S. C. Moratti, A. B. Holmes and R. H. Friend, *Chem. Phys. Lett.,* **1995**, 241, 89.

29. N. C. Greenham, S. E. Burns, I. D. W. Samuel, R. H. Friend, S. C. Moratti and A. B. Holmes, *J. Mol. Cryst. And Liq. Cryst.,* **1996**, 283, 51.

30. P. E. Burrows, V. Buloviv, S. R. Forrest, L. S. Sapochak, D. M. McCarthy and M. E. Thompson, *Appl. Phys. Lett.,* **1995**, 65, 2922.

31. E. I. Mal'tsev, M. A. Brusentseva, V. A. Kolesnikov, V. I. Berendyaev, B. V. Kotov and A. V. Vannikov, *Appl. Phys. Lett.,* **1997**, 71, 3480.

32. X. Tao, Y. Zhang, T. Wada, H. Sasabe, H. Suzuki, T. Watanabe and S. Miyata, *Adv. Mater.,* **1998**, 10, 226.

33. P. Wang, Y. Liu, C. Devadoss, P. Bharathi and J. S. Moore, *Adv. Mater.,* **1996**, 8, 237.

34. I. D. Parker, *J. Appl. Phys.,* **1994**, 75, 1656.

35. W. R. Salaneck and J. L. Bredas, *In Press.*

36. G. Leising, S. Tasch, F. Meghdadi, L. Athouel, G. Froyer and U. Scherf, *Synth. Met.*, **1996**, 81, 185.

37. A. Edwards, S. Blumstengel, I. Sokolik, R. Dorsinville, H. Yun, T. K. Kwei and Y. Okamoto, *Appl. Phys. Lett.*, **1997**, 70, 298.

38. S. Dailey, M. Halim, E. Rebourt, I. D. W Samuel and A. Monkman, *J. Phys. CM,* **1998**, 10, 5171.

39. K. Z. Xing, N. Johansson, G. Beamson, D. T. Clark, J. Bredas and W. R. Salaneck, *Adv. Mater.*, **1997**, 9, 1027.

40. See for example 28 section I in "Organic Photochemistry and Photobiology" **1995**, CRC Press, Inc.

Chapter 5

Control of Colour in Dendrimer Light-Emitting Diodes

5.1 Introduction

Improvements in materials have played a key role in the remarkable progress towards organic electroluminescent displays. Further progress is still desirable to improve areas such as the efficiency and lifetime of LEDs, control of colour and processibility. This chapter is devoted to the colour control in novel dendritic materials. The control of colour is an important property when developing new emissive materials for full colour flat panel display applications. Different colours are obtainable from different polymers: poly (*p*-phenylenevinylene) (PPV) [1] gives green-yellow luminescence while the poly(*p*-phenylene) (PPP) is a blue-light emitter [2]. Orange is obtainable by adding alkoxy side-groups to the polymer backbone as is the case in MEH-PPV [3]. In small molecules there is also a good library of materials emitting in different

regions of the visible spectrum such as *trans*-distyrylbenzene for blue [4] and Alq_3 (figure 5.1) for green [5].

In this chapter I will describe the concept of demonstrating colour control using a strategy that consists of selecting suitable cores in a novel family of conjugated dendrimers. The dendrimer concept, as described in chapter 4, involves molecules with a conjugated core, conjugated dendrons, and functional surface groups, which are believed to be responsible for different properties of the dendrimer.

I will first discuss the photophysical study which was carried out on first and second generation anthracene-based dendrimers where both generations emitted strongly in the green-yellow region. These dendrimers were also emitting in the same region when used in a monolayer LED structure.

I will then discuss the optical measurement carried out on another new conjugated dendrimer where the core was a porphyrin (figure 5.8). First and second generation porphyrin dendrimers were studied and compared to the core model compound, which gave important results on the arrangement of the dendrimer molecules in the solid state. The electroluminescence characteristics of the different porphyrin dendrimers will also be discussed.

Finally the possibility of tuning further the red emission was investigated in order to obtain specific colours, or perhaps to maximise the gamut range (see section 3.7).

5.2 The Anthracene Derivative

5.2.1 Introduction

In the previous chapter I have shown the results of the study carried out on a distyrylbenzene based dendrimer. Emission was believed to be originating from the

1-ANT

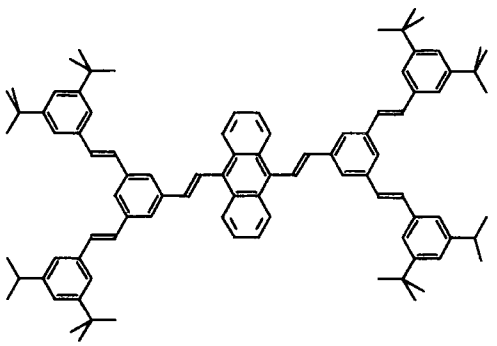

2-ANT

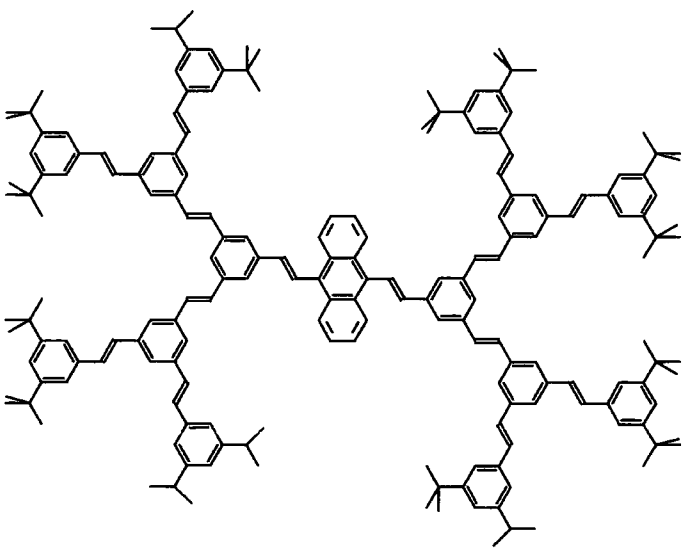

Alq_3

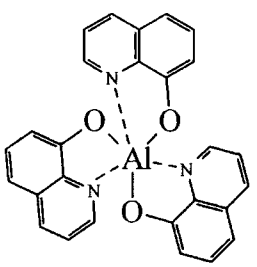

FIG. 5.1 *Chemical structure of first (1-ANT) and second (2-ANT) generation anthracene dendrimers. The structure of Alq_3 is also shown.*

central core. Thus the possibility of controlling the colour in conjugated dendrimers is investigated here.

The first target in this part of my project was to obtain a green dendrimer LED. The core chosen for this task was an anthracene derivative. The structures of the first (1-ANT) and second (2-ANT) generation anthracene dendrimers studied are shown in figure 5.1. The surface groups in these molecules are the same as the ones used in the DSB dendrimers in order to preserve the same processing properties. The branching units were also preserved in order to keep similar transporting properties and were attached to the core in a *meta* arrangement. This, as discussed in the previous chapter, is introduced to perturb the electron delocalisation along the core. As a result, both generations are soluble in most organic solvents.

5.2.2 Green-yellow emission

Solutions of 1-ANT and 2-ANT dendrimers were made using chloroform as a solvent (2 mg / 500 ml). Figure 5.2 compares the absorption and photoluminescence spectra of the two generations in solution. The solution absorption spectra have identical features at around 320 and 420 nm, although the absorption at high energies is more pronounced in the high generation dendrimer. A similar observation was discussed in the DSB-dendrimers where the absorption feature at high energy increased in intensity with the number of generation. The feature was attributed to the absorption of the branches. This is believed to be the reason behind that absorption (~ 320 nm) in the anthracene dendrimers. The feature at 420 nm is therefore a sign of the core absorption.

The PL spectra of the two generations were measured with excitation at 420 nm. The emission profiles were very similar, and peaked at around 580 nm. The emission is clearly independent of the generation number in solution state and most probably originates from the core of the dendrimer. This is based on a combination of two results: first the fact that no emission was observed from the branches in the DSB-dendrimers (chapter 4) and second is the independence of emission profile on the

generation number. Furthermore, the core is an anthracene derivative with extended electron delocalisation, hence the red-shift compared to the anthracene molecule which is known to emit in the blue range.

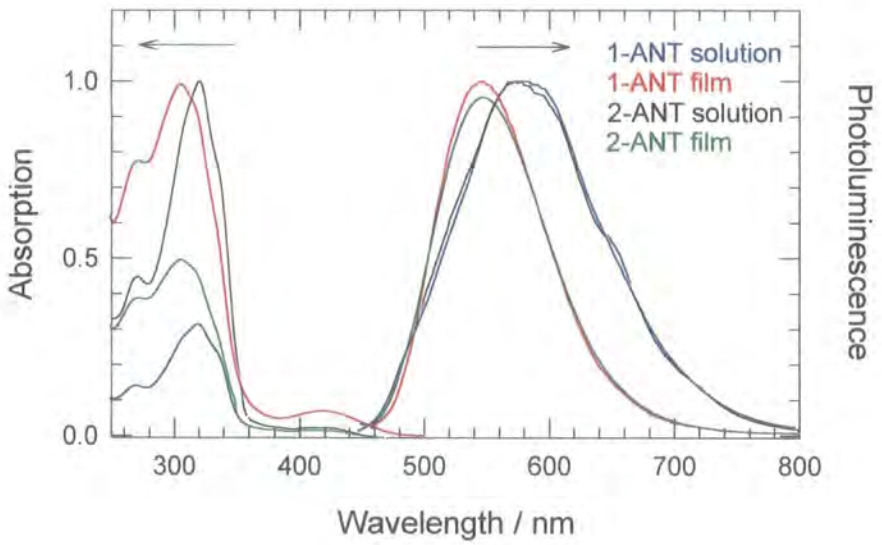

FIG. 5.2 *Absorption and photoluminescence of 1-ANT and 2-ANT dendrimer solutions and spin coated films. All samples were excited at 420 nm.*

It is worth mentioning that both solution PL spectra are quite broad with a FWHM in the range of 140 nm and are also featureless. This is unusual for solution fluorescence of conjugated polymers.

In conjugated molecules, physical dimers are new species associated with molecules being very close to each other in a special spatial configuration without creation of new chemical bonds. Note this is different from the photodimer where a chemical union of two identical molecules is created with new bonds that did not exist before. Figure 5.3 shows the difference between a photodimer and a physical dimer of the same anthracene molecule.

Excimers are another class of compound that differ from physical dimers in that they are only formed in the excited state. They exhibit the same optical absorption of the molecule but reveal a different emission profile, usually broad and structureless. The

excimer is formed when a molecule in its excited state participates in charge transfer with another similar molecule in its ground state.

$$M^* + M \rightarrow E^*$$

where *M* represents the molecule in its ground state and *M** indicates the electronically excited species. *E** is the excimer state.

There are some conjugated polymers that display relatively planar geometries and have a preferential rearrangement that lead to chain packing in the solid state [6-8].

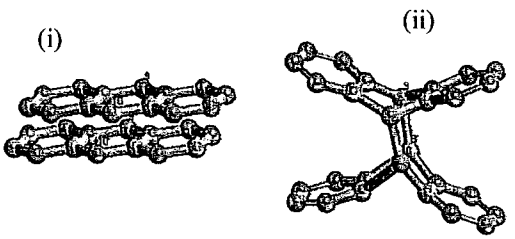

FIG. 5.3 *Structural diagrams of (i) the anthracene sandwich dimer (physical dimer) and (ii) the anthracene photodimer (taken from reference [9]).*

In solution the anthracene dendrimer (first and second generation) molecules are believed to occupy a planar configuration. This was calculated by J. Pillow [10] and a typical configuration of the molecules arrangement is shown in figure 5.5. The only part of the molecule that is not in the same plane is the anthracene-part of the core, although π-stacking of the molecule could still be possible. This could ease formation of excimers. The broadness and featureless characteristics of the solutions' PL is in agreement with excimer emission, although it remains difficult to explain exactly the nature of the emitting species.

Films were prepared by spin-coating from chloroform solutions of typical concentration 14 mg / ml. They were uniform and of good quality regardless of the generation number. Their absorption and photoluminescence are also shown in figure 5.2.

As discussed for the solution absorption, the films of the two generations have similar absorptions which consist of two components: the stilbene branches are absorbing at around 320 nm whereas the feature at lower energy is believed to be due to the anthracene derivative. The only difference in the absorption of the two generations is reflected by the more intense 320 nm absorption band, due to the presence of more branching units in the second generation dendrimer.

The films emitted in the green-yellow region of the visible spectrum when excited with a 420 nm excitation wavelength. The emission profile was similar for both generations which indicates that the increase of branching units does not upset the conjugation or the spatial configuration of dendrimer molecules. This also means that the emission in both dendrimers is due to the same singlet excited states. However, when compared to the corresponding solution emission spectra, the film photoluminescence is shifted towards higher energy. This behaviour is unusual for conjugated polymers as the excitonic species, created in the solid state, tend to migrate to lower energy sites resulting in a redder emission with respect to the solution fluorescence. A possible explanation for seeing the opposite of such behaviour could be due to the spatial arrangement of the molecules of the dendrimer in the solid state – the unusual shift could be due to the different packing of the dendrimer molecules in the solid state reducing the extent of electron delocalisation, hence the blue-shift.

The PL quantum yield was measured for 1-ANT and 2-ANT spin coated films using the integrating sphere technique and found to be 43 and 51 % respectively. The anthracene dendrimers are reasonably efficient when compared to other organic green emitters such as PPV (27 %) [14]. However, the quantum yield of 1-ANT and 2-ANT films decreases very sharply when measured in air (figure 5.4) suggesting a possible immediate photo-oxidation. This is slightly different from the behaviour of some conjugated polymers where the decay is observed to have a slower rate over a longer period of time (chapter 6). Interestingly, the sharp decrease was also observed at pressures of $1x10^{-1}$ mbar for 2-ANT film, although it remained stable at a value of 15 $\pm$ 3 % after the first 200 s .

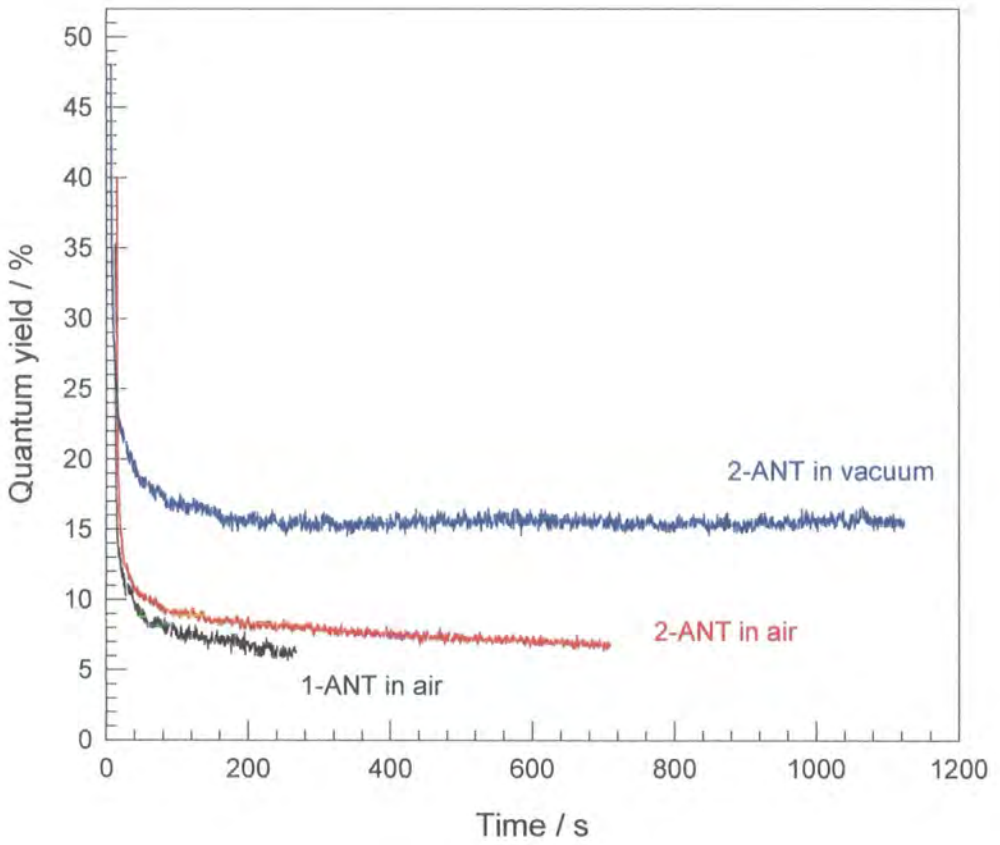

FIG. 5.4 *Photoluminescence quantum yield of first and second generation anthracene dendrimer as a function of time.*

1-ANT

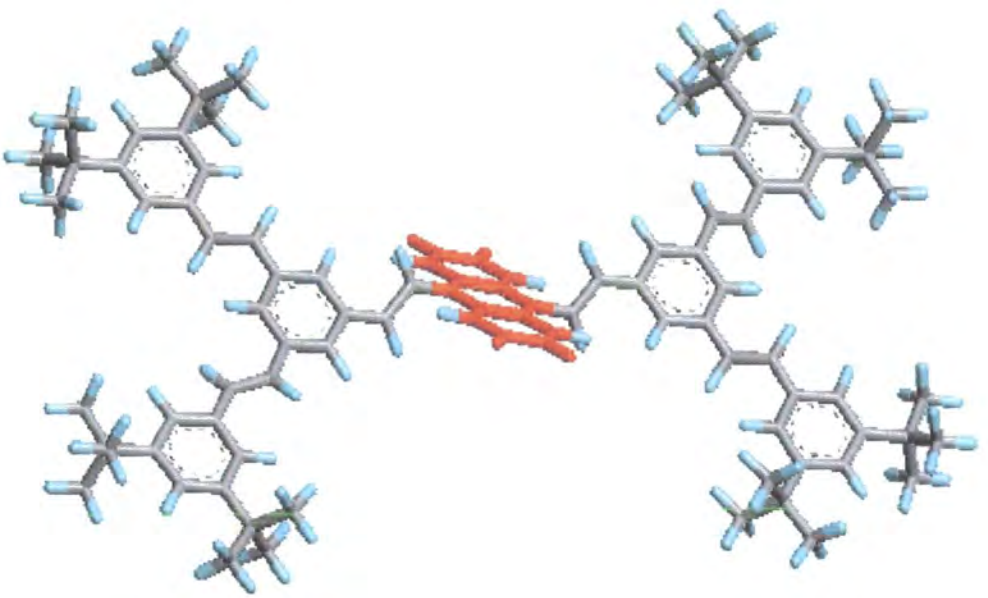

2-ANT

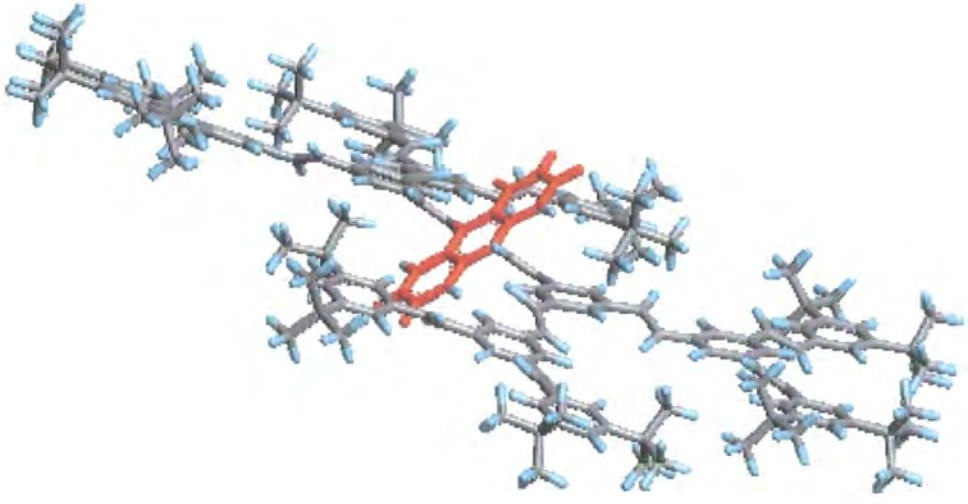

FIG. 5.5 *First (1-ANT) and second (2-ANT) generation anthracene spatial rearrangement. In red is the anthracene component marked for clarity.*

5.2.3 Anthracene dendrimer LEDs

The anthracene dendrimer (1-ANT or 2-ANT) was incorporated into single layer LEDs as described in chapter 3. Dendrimer layers were typically 100-130 nm thick. Different metals (Ca and Al) were used to inject electrons in the dendrimer. A large number of the devices made with calcium electrodes failed to emit any visible light. At sufficiently high voltages, some pixels emitted green-yellow light similar to that observed in PL. Unfortunately, at the voltages required to produce sufficient light for characterisation study, the devices degraded rapidly. Note that these measurements were carried out in a vacuum ($2.5x10^{-4}$ mbar). The fact that the failure of anthracene LEDs, with calcium electrodes, to emit light is probably due to calcium reacting with the dendrimer core. However, anthracene LEDs using aluminium as the top contact were found to be considerably more stable and were emitting green-yellow light when a bias was applied for longer periods. The EL spectrum of 1-ANT and 2-ANT in similar device configuration is shown in figure 5.6.

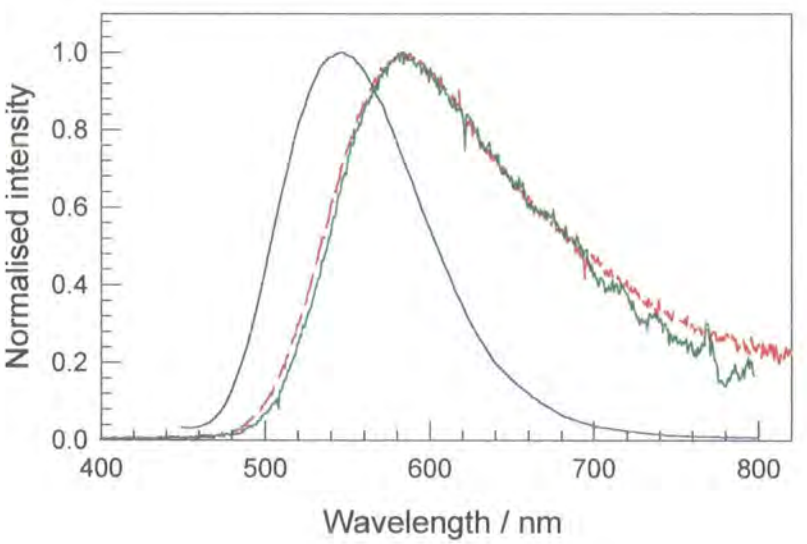

FIG. 5.6 *Electroluminescence spectrum of 1-ANT (red), and 2-ANT (green) LED. Photoluminescence spectrum of 1-ANT film (blue) measured at 420 nm excitation is shown for comparison.*

As shown in the figure above, the EL spectra of first and second generation anthracene dendrimers are broad and display no vibronic structures. They were both recorded for LEDs with the same configuration and using the same metal (Al) as the top electrode. Both spectra are identical to each other and similar to the PL spectra of corresponding generation dendrimers, suggesting emission from radiative decay of the same singlet excited state. However, the maximum emission wavelength of the EL spectrum is shifted towards the red end of the spectrum with respect to the PL spectrum's maximum emission. This shift between the EL and PL spectra, also seen in DSB-based dendrimers, is not unusual behaviour for conjugated molecules and has been reported for different polymer LEDs [12]. This shift is possibly due to the fact that the emission zone in the EL process could be slightly different from that in the PL process.

The current-voltage characteristic of an LED made using 1-ANT with aluminium as the cathode is shown in figure 5.7. The diode-like behaviour of the *I-V* characteristic is typical of an organic LED, although brightness was not very high. As can be seen from figure 5.10.a, the maximum brightness achieved in these devices was in the range of 17 Cd m^{-2}. From the light-output current density diode characteristics, the external quantum efficiencies were calculated and found to be 0.02 and 0.05 % for the first and second generation respectively. These results clearly agree with the results obtained on the distyrylbenzene based dendrimer, in chapter 4, showing an increase in the external quantum efficiency with the generation number, although the efficiency increased only by a factor of two. These efficiencies compare favourably with those of monolayer LEDs using PPV as the emissive layer [13]. The results obtained on this dendrimer are also reasonably good when compared to those obtained when similar emitting materials were used in monolayer LEDs. Wang and co-workers have used anthracene as the chromophore in a dendrimer structure using phenylacetylene as monodendrons [14]. They have observed an improvement of device performance and stability with high generation number (second or third), however the electroluminescence was weak, as no brightness nor efficiency were reported. This modest performance was believed to be due to solid state aggregation and self-quenching.

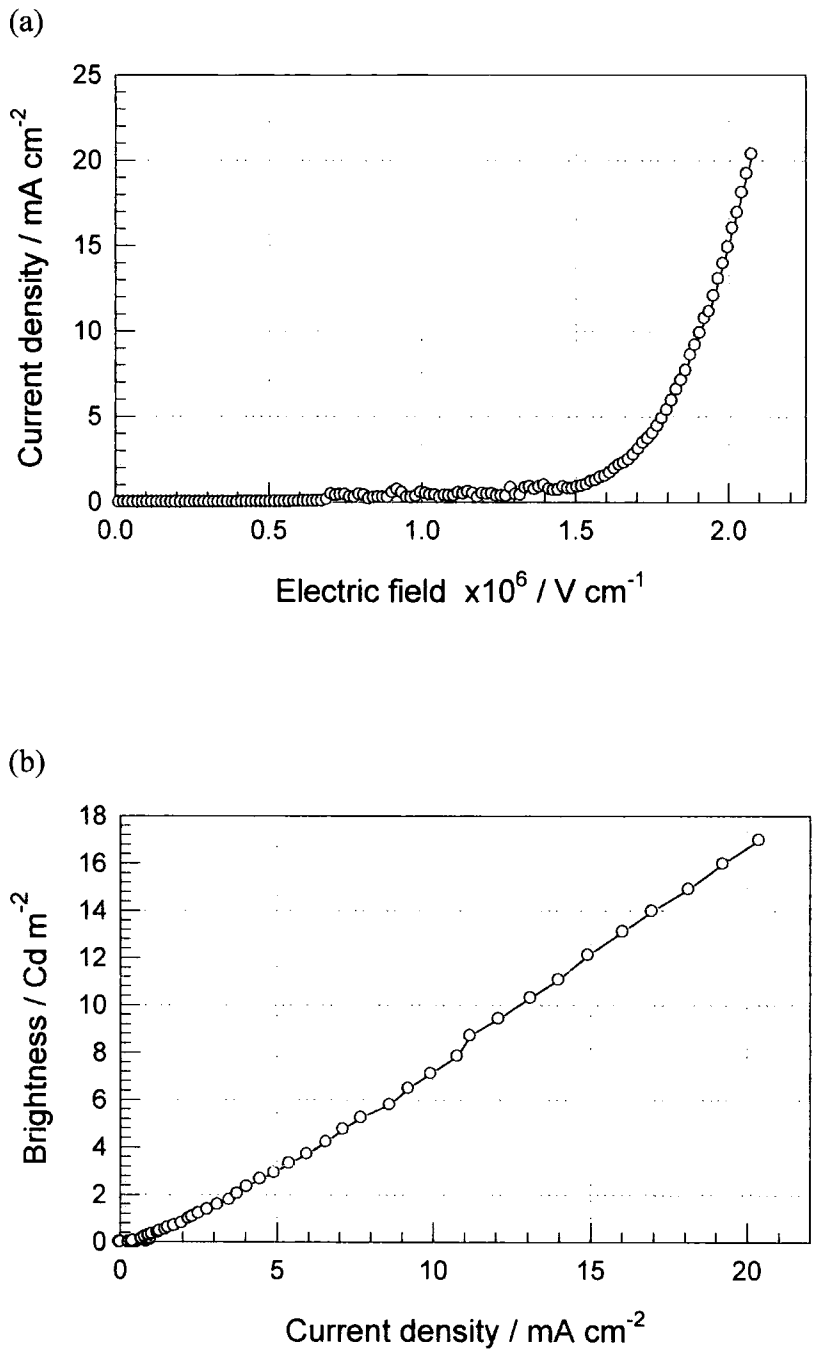

FIG. 5.7 *a) Current density vs. electric field characteristics and (b) brightness vs. current density of 1-ANT monolayer LED.*

5.3 The Red Dendrimer

5.3.1 Introduction

As far as multicolour display technology is concerned, red is a very interesting colour and as important as 'the blue'. This is because the primary colours are used to define the colour gamut that will be available for a given display. Furthermore, there is still a need for an efficient pure red for both polymer and small organic displays.

5.3.2 Porphyrin photoluminescence

For our project, a red chromophore is needed to be placed in the dendrimer centre to complete the colour range with a red emission. The porphyrin molecule was chosen for its electronic properties. The porphyrins [18] are an important class of compounds in biological systems. The basic structure of the porphyrin is shown in figure 5.8. It consists of four pyrrole rings, linked together through four extra carbon atoms in such a way as conjugation is preserved all over the molecule. This structure offers the porphyrin interesting optical properties such as red luminescence.

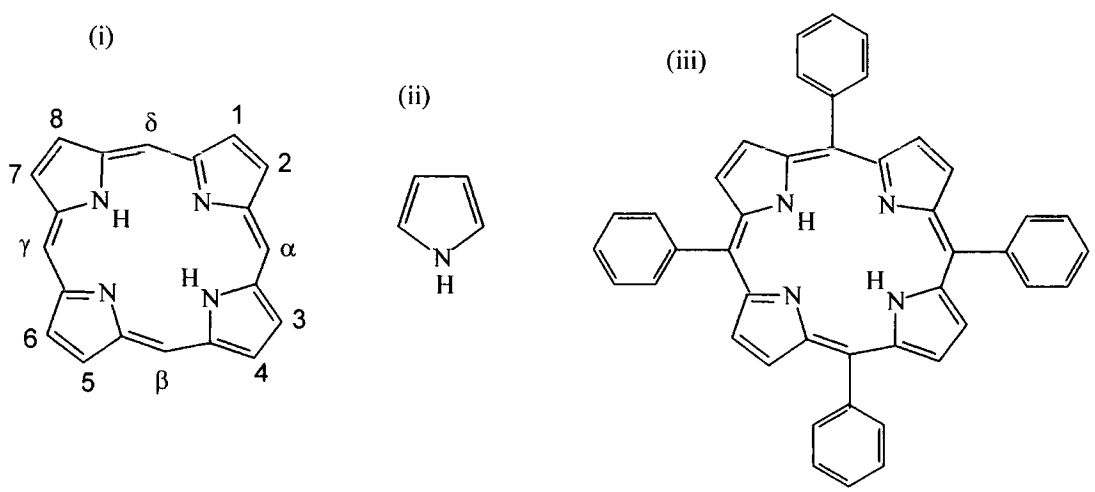

FIG. 5.8 *The chemical structure of the (i) porphyrin, (ii) pyrrole, and (iii) tetraphenylporphyrin molecule.*

At each position 1-8 and α-δ in the porphyrin molecule there is a single hydrogen. If there are two hydrogen atoms in the centre, then the molecule is called a free-base porphyrin (PH_2).

The porphyrin visible absorption spectrum shows intense absorption at around 400 nm; this absorption maximum is referred to as the 'Soret band'. The porphyrin absorption also shows a series of bands with less intensity at longer wavelengths. These bands are called the 'Q bands'. A typical free-base porphyrin absorption spectrum is shown below.

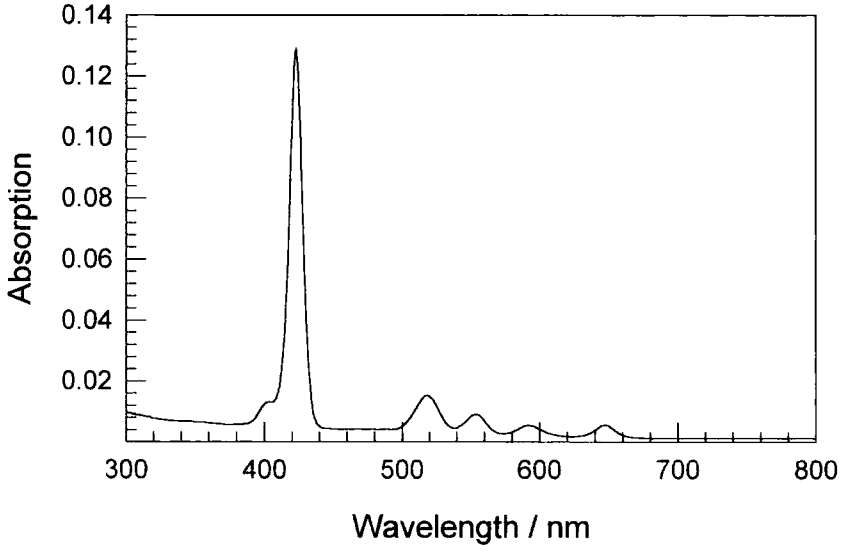

FIG. 5.9 Absorption spectrum of the free-base porphyrin.

An interesting property of the porphyrin is that the outer hydrogen atoms can be substituted by different groups and the molecules so derived, e.g. tetraphenylporphyrin in figure 5.8, could have different properties.

The porphyrin was used as the centre of the dendrimer with the aim of obtaining red emission. The branches and surface groups were the same as in previously studied dendrimers. The chemical structure of the first (1-POR) and second (2-POR) generation porphyrin dendrimers and the model compound used in the centre are shown in figure 5.11.

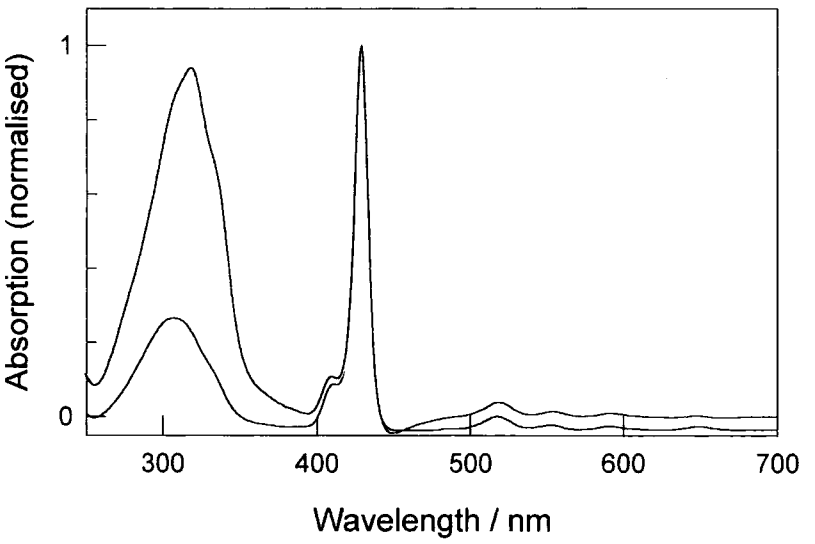

FIG. 5.10 *Absorption of 1-POR and 2-POR solutions.*

Both generations were readily soluble in most organic solvents and chloroform was used to prepare solutions of these compounds (~ 1 mg / l). The absorption spectra of first and second generations are shown in figure 5.10. The absorption of 1-POR consists of several features spread over the visible spectrum and could be divided into two parts. The first part is the band situated at around 420 nm and the bands, with relatively less intensity, at longer wavelengths. These are the same features seen in the second generation dendrimer and their model compound's absorption and hence could be attributed to the absorption of the dendrimer core. The other part is the absorption which lies at around 320 nm, and is present in both generations but not in the model compound's absorption (figure 5.9). This is due to the stilbene dendrons; it is more intense in the second generation dendrimer and is similar to the absorption observed in the distyrylbenzene and anthracene dendrimers, hence its stilbene origin. The solution PL was measured using an LS-50B fluorimeter with a 420 nm excitation wavelength.

1-POR

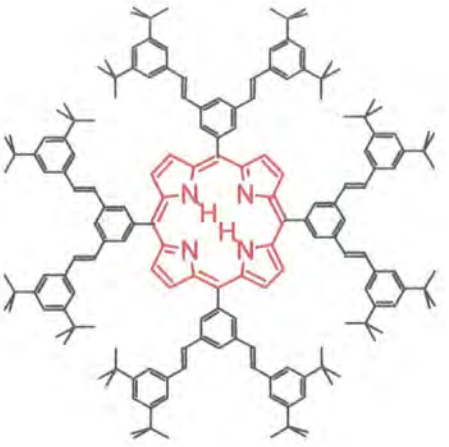

2-POR

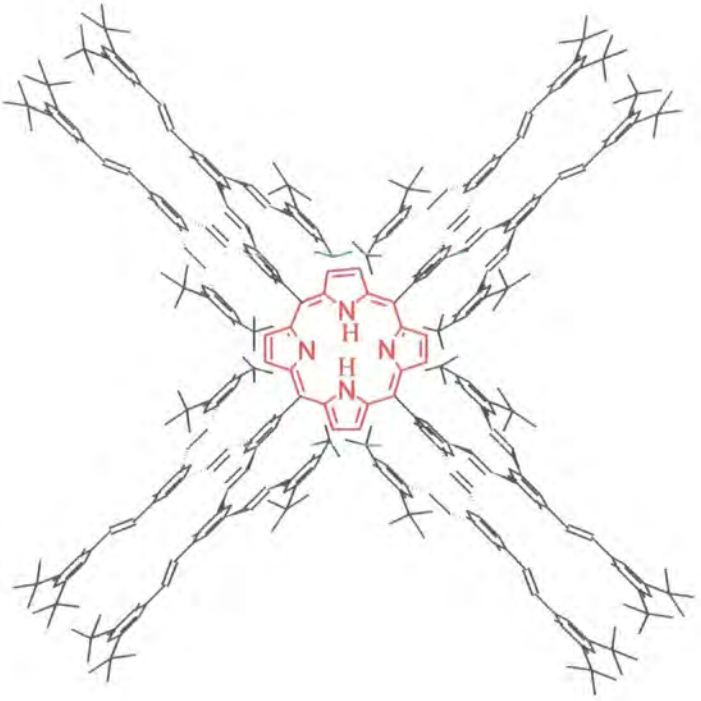

FIG. 5.11 *Chemical structure of first (1-POR) and second (2-POR) generation porphyrin dendrimers. In red is the chromophore, free-base porphyrin, used as the core of the dendrimer.*

Both dendrimers emitted red light. The PL spectrum of 1-POR, shown in figure 5.13, had two major peaks at 655 and 720 nm. This spectrum is relatively narrow, and when compared to the model compound porphyrin, the spectra are identical with no apparent shift of either spectra. This not only suggests that the luminescence of the porphyrin originates from the core of the molecule but also that there is little, if any, modification due to the stilbene dendrons. This is slightly different from the distyrylbenzene dendrimers where a small shift of the solution dendrimer PL with respect to the core PL was detected [17]. This was agreed to be a sign of extended electron delocalisation over the branches. Clearly this is not the case for the porphyrin dendrimer. Furthermore, the luminescence of the second generation dendrimer solution is almost identical to the first generation which indicates that the branching units have no effect on the nature of the emitting species in the porphyrin dendrimer.

As previously mentioned, because the branches and surface groups were the same as in other dendrimers previously studied in this thesis, the porphyrin dendrimer was expected to have similar processing properties e.g. solubility. In fact both porphyrins were soluble in chloroform, and spin-coating directly from chloroform solutions led to uniform thin films. The absorption of these films (data not shown) was identical to those of the corresponding solutions, showing the Soret and Q bands due to the absorption of the core. A sign of absorption of stilbenes could be seen as it was of different intensity in different generations. The PL spectra were measured, exciting the films at the maximum of their Soret band (420 nm), and are shown in figure 5.13. The 1-POR spectrum indicated a red luminescence with two bands of different intensities at 655 and 720 nm. The PL quantum yield was measured and found to be 11 ± 2 %. The PL spectrum of 2-POR also indicated a red luminescence with a very similar emission profile to that of 1-POR and an absolute quantum yield of the same range (11 %). The emission profiles of the two generations reflect the same results obtained from the solutions, in that increasing the number of the branching units has no effect on the luminescence of the two samples. More importantly, the spectra

1-POR

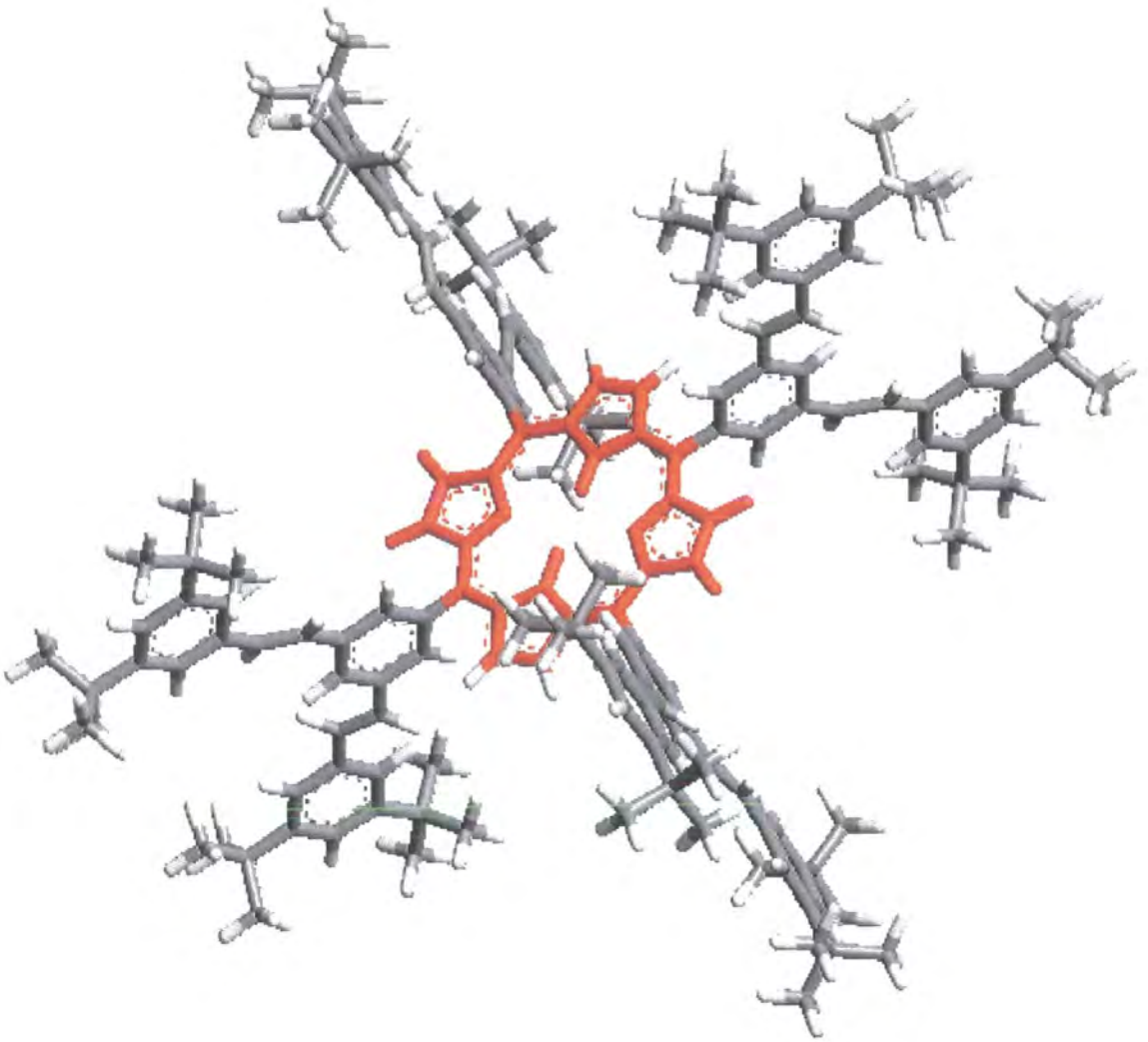

2-POR

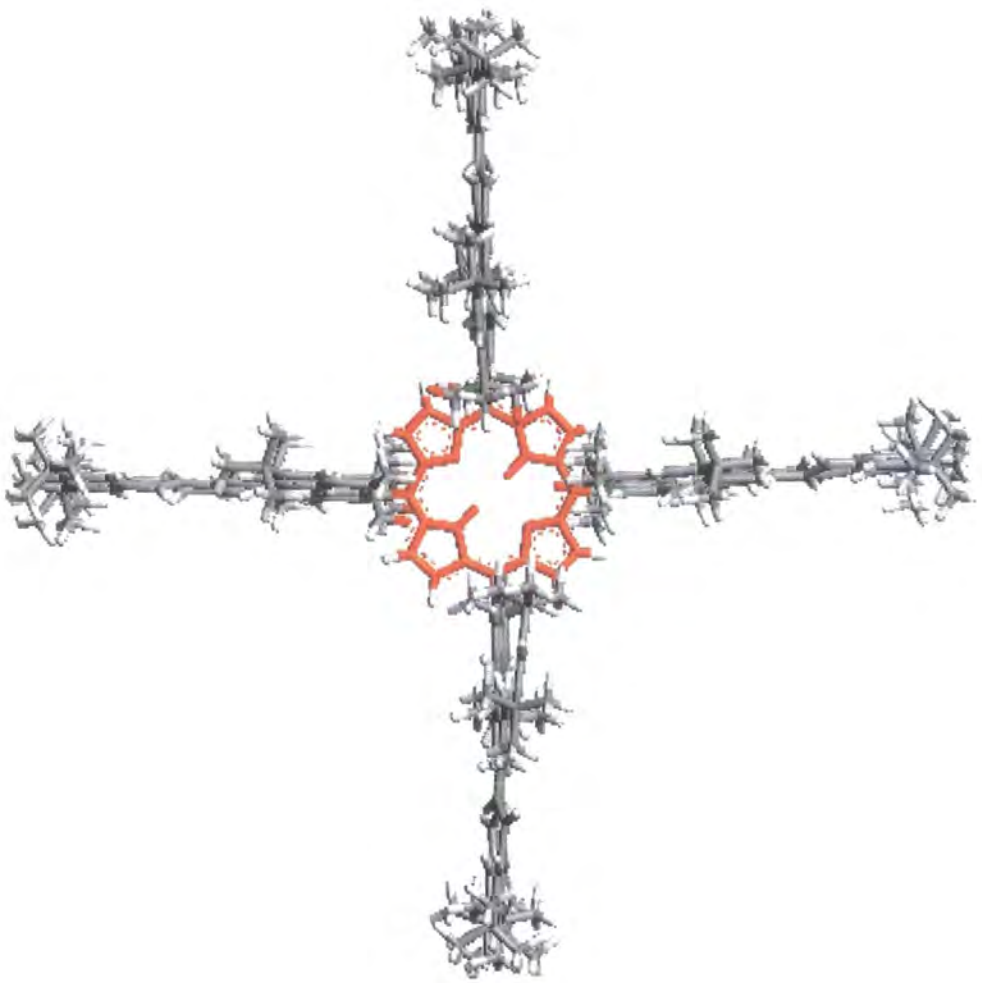

FIG. 5.12 *Computer generated molecular configuration of the first (1-POR)and second (2-POR) generation porphyrin dendrimers.*

appear identical to the corresponding solution with no apparent shift to either side of the visible spectrum. A possible explanation of this is that the molecules are of sufficient globular shape and of reasonable size to prevent their aggregation or the formation of inter-chain species. The computer generated spatial configuration of these two porphyrins, calculated by J. Pillow [10], gives us an idea of how these molecules occupy space (figure 5.12). In both generations the branches are occupying a different plane to that of the porphyrin core, and hence it is very unlikely for the dendrimer molecules to π-stack on each other. The spatial configurations also explain the similarity between the PL spectra of both dendrimers and core in solution. The planes of the core and branches are almost perpendicular so that there is no delocalisation of electrons from the core onto the dendrons. Unlike the distyrylbenzene or anthracene dendrimers the conjugation of the core is delocalised solely over the core, resulting in emission purely originating from the central core of the dendrimer.

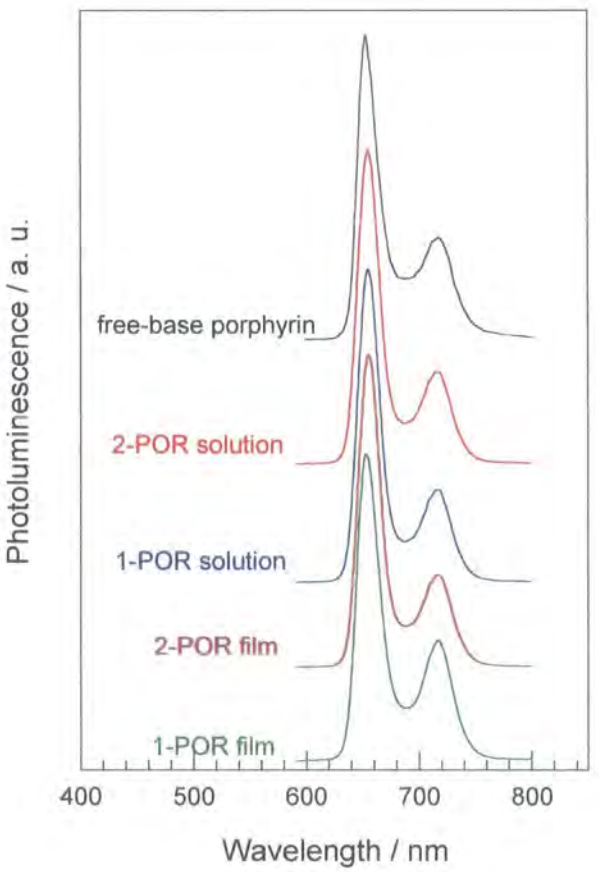

FIG. 5.13 *Porphyrin photoluminescence. The spectra have been re-scaled for clarity.*

5.3.3 Porphyrin electroluminescence

The two generations of the porphyrin dendrimer were then each used as the active layer in a mono-layer LED structure. Al or Ca were used to inject electrons while ITO was the hole-injector. The LED characteristics and EL spectra were measured as described in chapter 3.

The current-voltage (*I-V*) and light output-current (*L-I*) characteristics of a typical 2-POR LED are shown in figure 5.15. The *I-V* and *L-I* of 1-POR and 2-POR devices were characteristic of a typical organic LED. The current increased significantly at a certain turn-on voltage which corresponds to the same voltage where the LED starts emitting light. The EL external quantum efficiencies of 1-POR and 2-POR were calculated, and for devices using calcium contacts, found to be in the range of 0.017 and 0.035 % respectively. This is a respectable value compared to other red organic emitting diodes [18]. It is worth mentioning that the use of calcium as the top contact did not cause any particular problems as was the case with the anthracene devices. Using the same LED structure and similar preparation parameters 1-POR devices were made using a high workfunction metal (Al) and the devices emitted red light. Interestingly though, the external quantum efficiencies were in the same range as those of LEDs using calcium electrodes. This is rather unusual for conjugated materials as the use of a low workfunction metal tends to increase the external quantum efficiency compared to those with a higher workfunction [19,20]. This is probably because with red-emitters (low energy gap) the injection from high workfunction metals does not cause any problems as is the case with large band gap materials (see figure 5.14). Here it is very likely that hole-injection is the limiting factor and therefore electron-hole recombination is more or less insensitive to electron injection.

Note that a similar exception was observed for CN-PPV [20] where such behaviour could not clearly be explained. N. C. Greenham *et al* suggested that the formation of interfacial states and barrier layers could be an explanation in CN-PPV, although with different metals, one would expect different properties for such layers using different

materials. It is also hard to explain the origin of such similarity, especially when there is a barrier for electron injection when using aluminium while there is no barrier when calcium is used. The brightness of the porphyrin devices were also deduced from the diode characteristics and found to be around ~ 6 Cd m^{-2} for both generations.

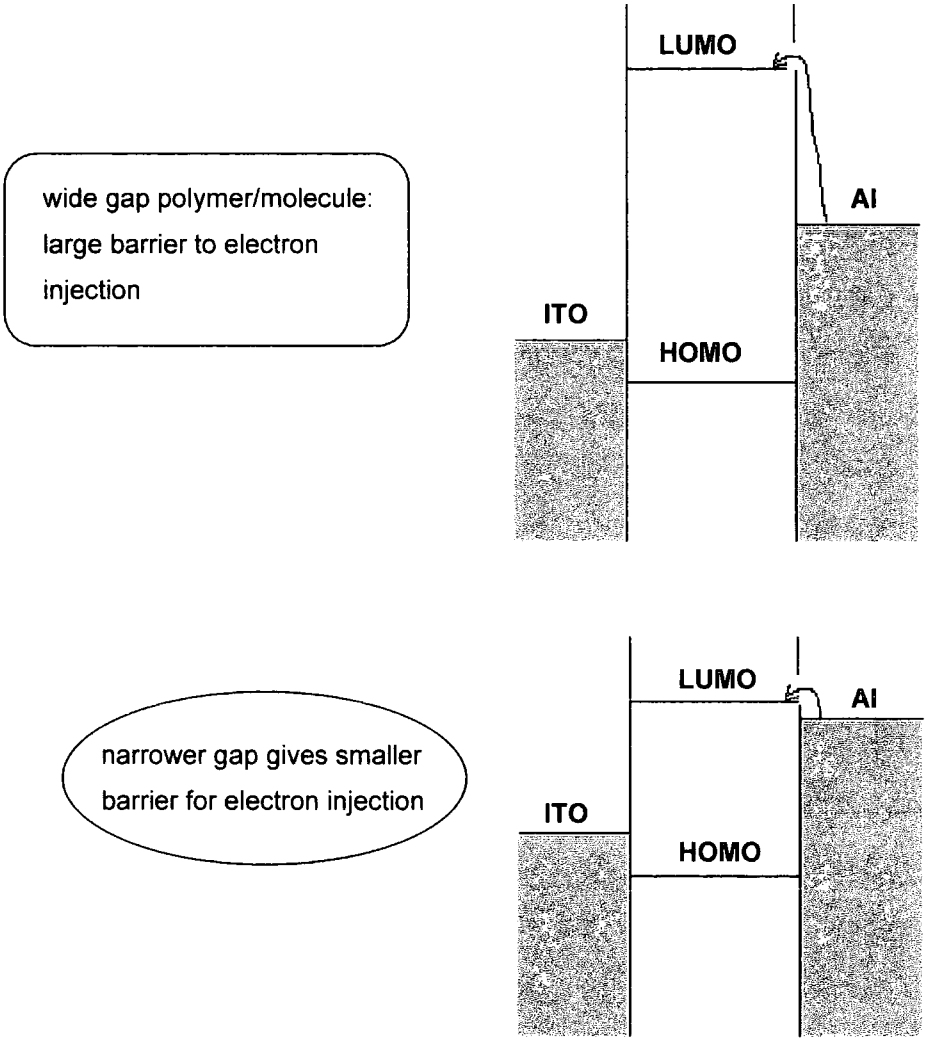

FIG. 5.14 *Schematic diagram illustrating the difference in electron injection between wide and narrow gap materials.*

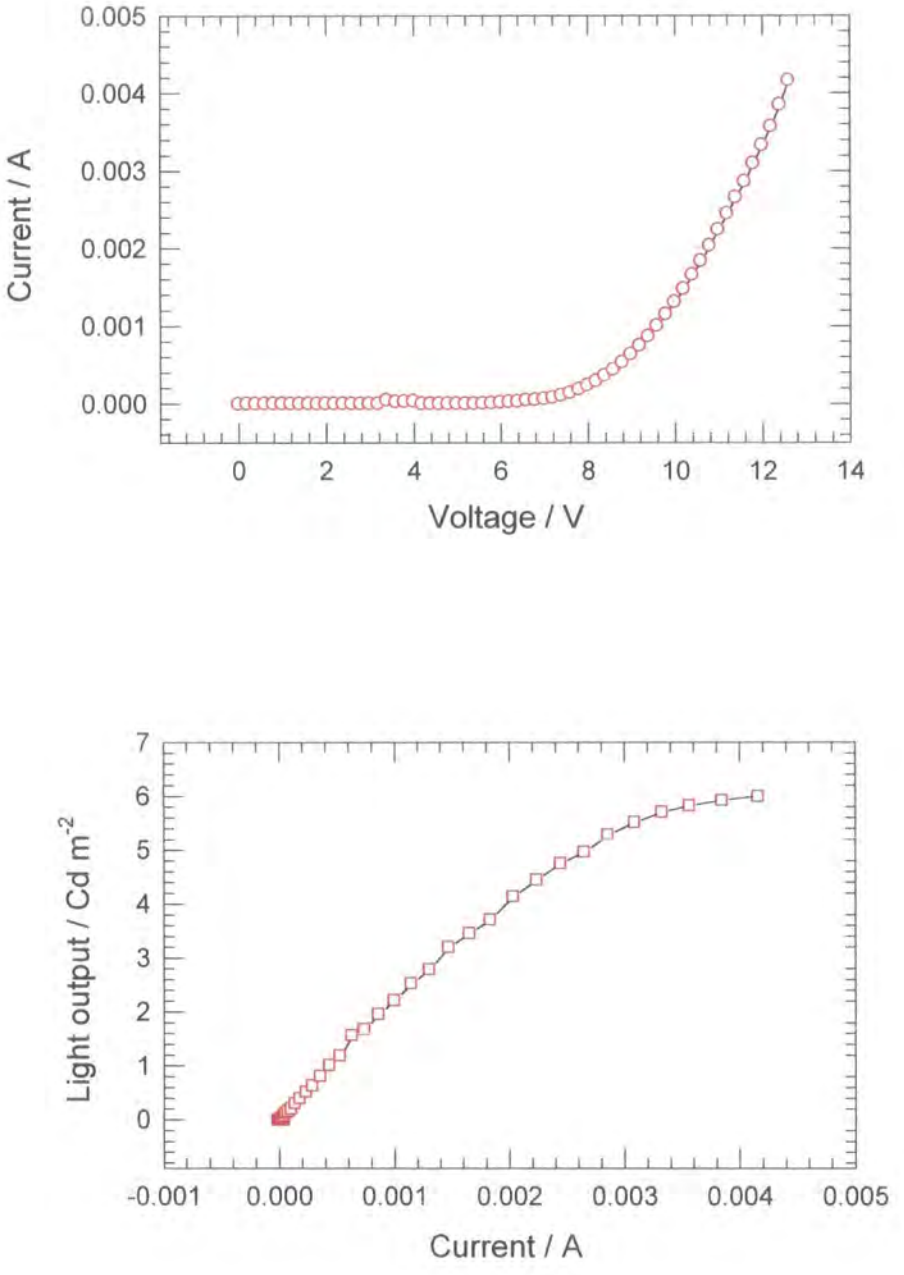

FIG. 5.15 *Current-voltage (upper panel) and light output-current characteristics (lower panel) of a ITO/2-POR/Ca device.*

Figure 5.16 shows the EL spectra of similar devices fabricated using either first or second generation porphyrin dendrimers. It can be seen that the emission from the single layer devices in both generations is identical. For both devices the EL spectra are similar to the PL of either generation. This latter point suggests that the same excited species is responsible for emission in both processes. Moreover there was not a significant difference between the EL and PL spectra, in contrast to other dendrimers. This might be a further sign of how the molecules arrange themselves in the solid state, avoiding aggregation and offering a further protection to the core, which is consistent with the size of these molecules.

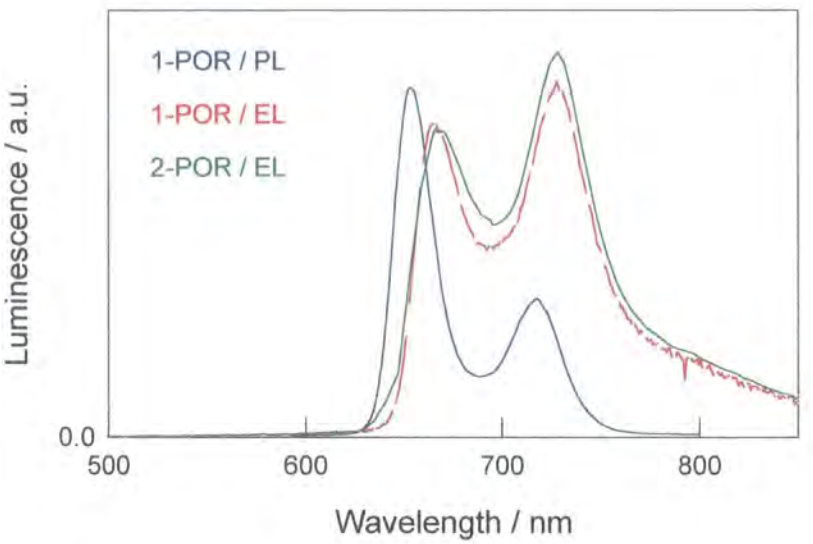

FIG. 5.16 *EL spectra of 1-POR and 2-POR LEDs. The PL spectrum of 1-POR is shown for comparison and was measured with an excitation of 420 nm.*

The only major difference between the EL and PL spectra is the ratio of the two peaks and it is possibly due to the difference between emission zones in the two emission processes and/or to migration of singlet excited states to low energy sites. These sites are believed to be present in the PL process but the singlet excited states are short lived, and therefore can not migrate to them.

5.4 C.I.E. Co-ordinates

The chromaticity co-ordinates for the distyrylbenzene, anthracene, and porphyrin dendrimer EL, with respectively blue, green, and red emission, have been calculated as described in section 3.3 and are listed in table 5.1. The co-ordinates have also been placed in the C.I.E. colour diagram shown below.

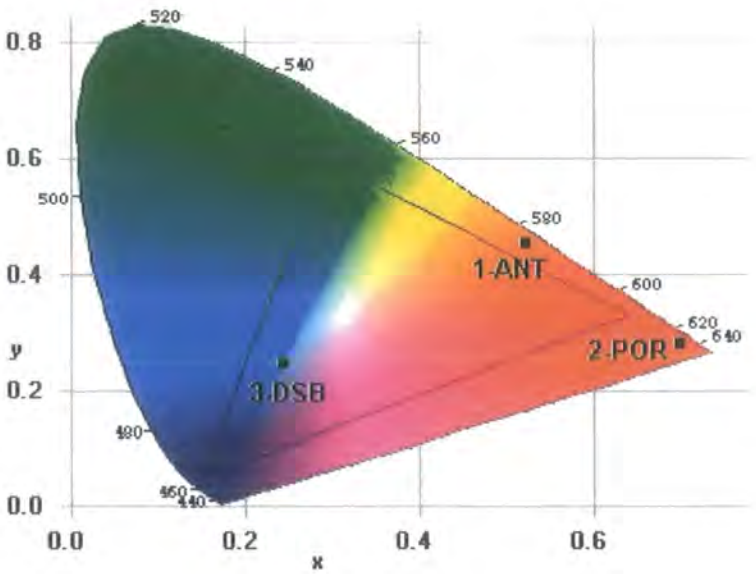

FIG. 5.17 *C.I.E. diagram showing the co-ordinates of the different dendrimer EL.*

It can be seen that the co-ordinates of 1-DSB and 2-DSB EL lie in the blue region very near to the achromatic point (white light). This reflects the whitish appearance of the emission and hence the impurity of the blue colour which was calculated and found to be 0.2 and 0.18. This is a result of the broad EL spectrum which reduces their effective y-co-ordinate and therefore restricts the gamut of colours available. The co-ordinates of the anthracene dendrimer placed the emission in the orange region while the red colour emitted by the porphyrin dendrimers was very close to a primary colour which gives it a rather high purity of 0.93. This is a desirable feature for colour displays and is believed to be the result of a narrow spectrum.

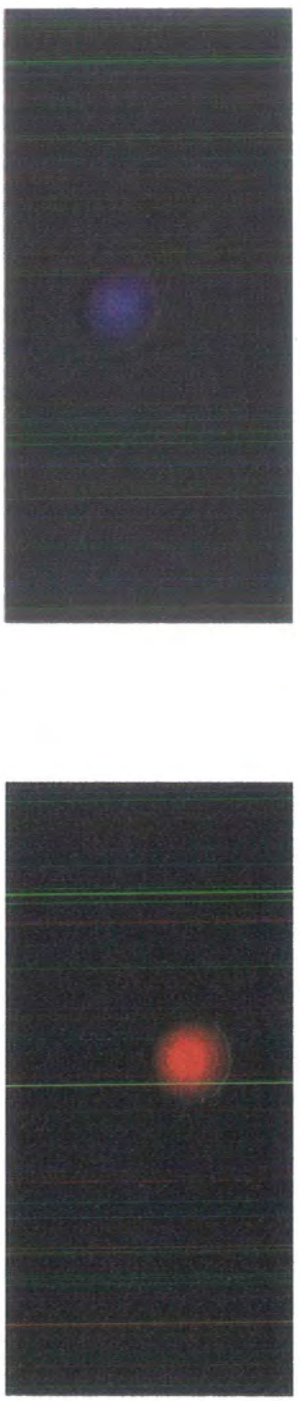

Photograph 5.1 *Blue (2-DSB) and Red (2-POR) dendrimer LED.*

Material	(x, y)
1-DSB ♦	(0.34, 0.38)
2-DSB ♦	(0.29, 0.32)
3-DSB ♦	(0.23,0.24)
1-ANT ♦	(0.52, 0.46)
2-ANT ♦	(0.52,0.46)
1-POR ◈	(0.69, 0.30)
2-POR ◇	(0.68,0.29)

Table 5.1 *Dendrimer electroluminescence chromaticities.*

5.4.1 Fine tuning the red emission

It is of interest to be able to obtain the maximum gamut of colours available for colour display application. The red colour obtained in the porphyrin dendrimer is pure and desirable for future applications, and therefore, is interesting to be able to obtain 'different reds' or more technically a pure red emission with different co-ordinates and consequently different dominant wavelengths. Since the emission in the dendrimer systems studied so far has been found to be primarily dictated by the core, clearly, in order to change the nature of the emission, changes have to be carried out on the core. The porphyrins are known for their characteristic of being able to donate the two protons linked to the nitrogen atoms and bond with metals to form what is known as metalloporphyrins (see figure 5.21). These compounds and their derivatives are well known for their optical properties as well as for their biological applications [16].

The free-base porphyrin was metalled with Cu, Mg, or Zn, and the resulting compounds will be referred to as Cu-P, Mg-P, and Zn-P respectively. The metalloporphyrins were dissolved in chloroform and the absorption and PL spectra were measured.

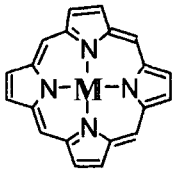

M: metal

FIG. 5.18 *The structure of a metalloporphyrin.*

The absorption of the solutions is shown in figure 5.19-a and compared to the free-base porphyrin absorption. The metal does have an effect on both Soret bands (~ 420 nm) and Q bands (> 500 nm) in the absorption spectra. There is a slight red-shift of the Soret band for Zn-P and Mg-P with respect to PH_2. Interestingly, the Q bands showed more dramatic changes. The shifts of the first two bands are shifted towards longer wavelengths while the other two have disappeared. This should reduce the self-absorption of emission which could be an advantage for light-emitting diodes.

The other attractive feature of these metalloporphyrins is their PL spectra. Shown in figure 5.19-b, are the emission profiles of the metalloporphyrins in solution following excitations in the range 430-440 nm. All the solutions displayed red emission, however, the PL spectra were slightly different. The Cu-P PL was similar to the free-base porphyrin PL, although the luminescence was less intense. The Mg-P emission has conserved the shape and intensity of the PL spectrum, but was blue-shifted with respect to the PH_2 spectrum. The Zn-P emission profile was also blue-shifted, but a reasonable change in the shape of the PL spectrum was observed; the two peaks in the PL spectrum are of the same intensity in the Zn-P emission profile.

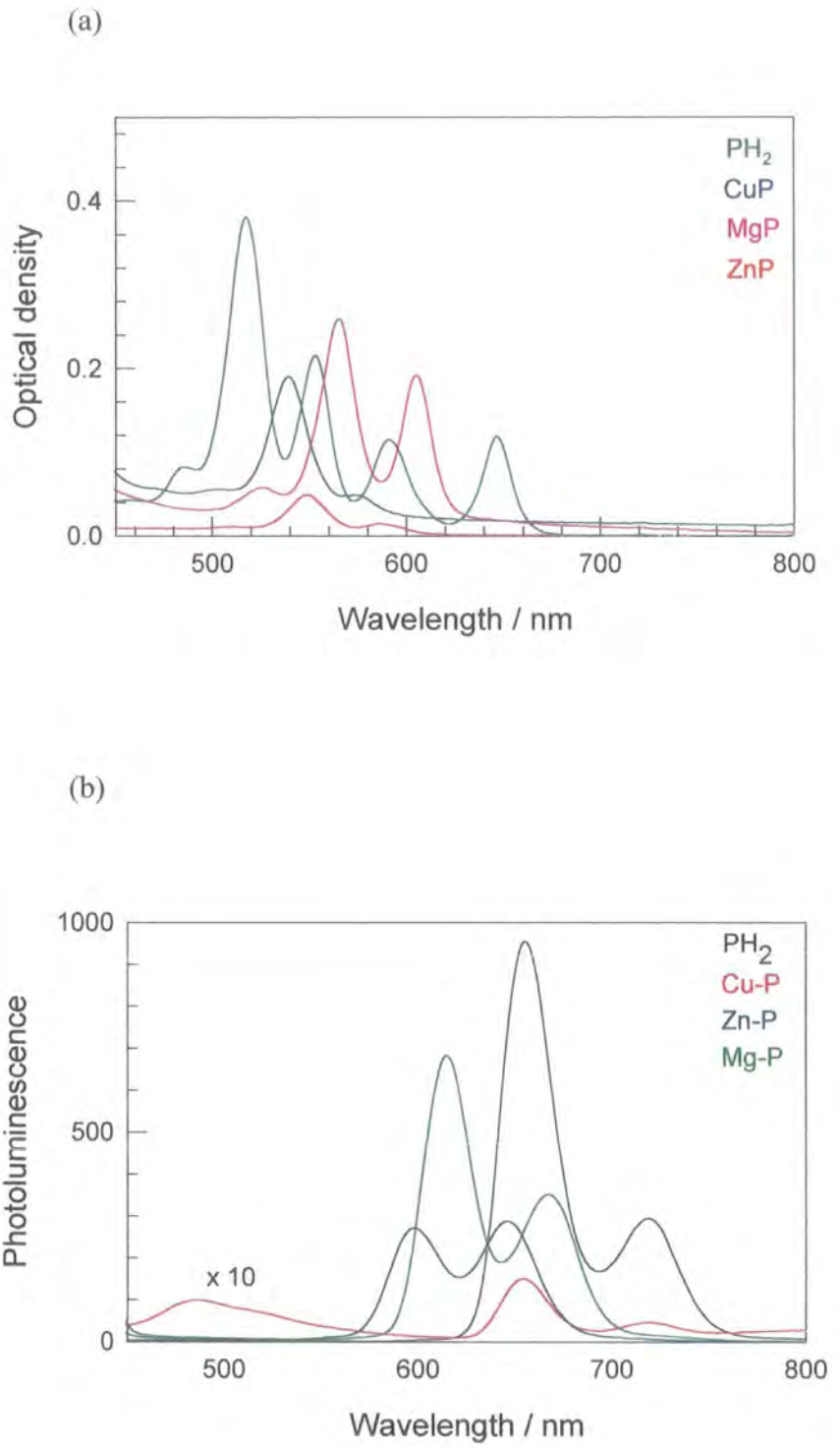

FIG. 5.19 *Absorption (a) and photoluminescence (b) of different porphyrins.*

The C.I.E. co-ordinates of the PL spectra were calculated to show the effect of this chemical tuning on possible applications. As can be seen from the figure below, the Zn-P and Mg-P have conserved the purity of the light emitted, as well as offering a different colour, with a different dominant wavelength. This, with other primary colours can offer a different gamut of colours.

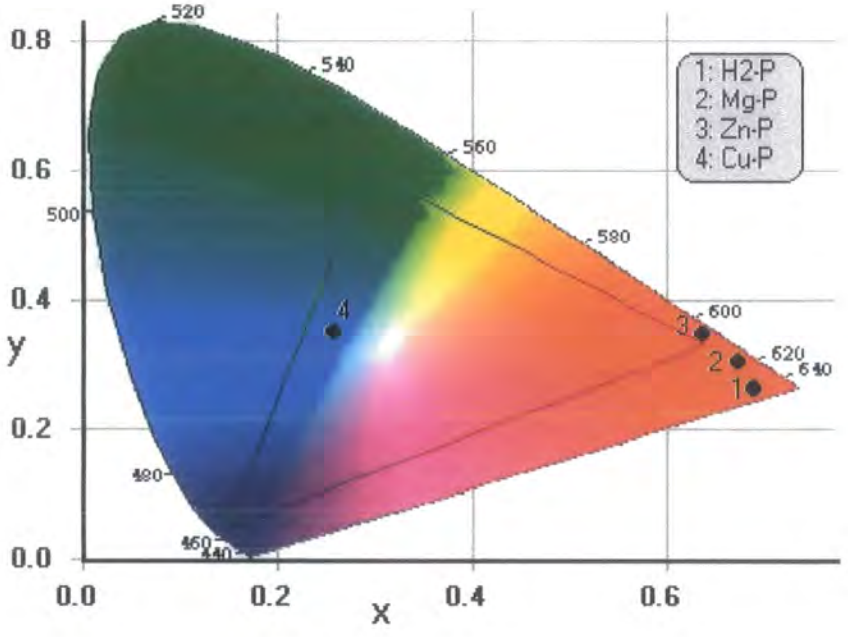

FIG. 5.20 *The chromaticities of the metalloporphyrins photoluminescence.*

The Mg-P was chosen to be used as the core in a dendrimer structure identical to 2-POR but with Mg-P in the central core instead of PH_2. The photoluminescence of the dendrimer was identical to the core which is understood to be a result of no aggregation due to the size of the molecule. The dendrimer was also incorporated into LEDs, however, the Mg-P dendrimer appeared red immediately after spinning the film and turned to a dark green film after evaporating the metal contacts. This is still unexplained as further experiments are needed to understand if it is an instability characteristic of the molecule in air or is directly related to the preparation conditions of the LEDs.

5.5 Conclusion

Having established that the luminescence of the dendrimers, developed in this project, is arising from the central core of the dendrimer, it was possible to obtain different colours throughout the visible spectrum simply by changing the cores; distyrylbenzene gave characteristic blue emission to the dendrimer, while anthracene and porphyrin made the dendrimer emit green-yellow and red respectively. All dendrimers were successfully integrated into monolayer LEDs and were emitting a similar colour to their PL.

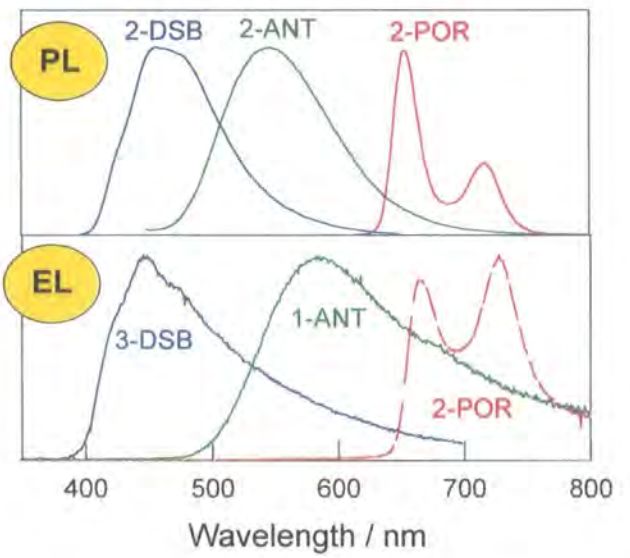

FIG. 5.21 *Control of colour demonstrated in both PL and EL.*

A further advantage of the dendrimer concept was the possibility of tuning the colour at the same time as keeping other electronic and processing properties constant. In other words, the electronic and processing properties can be tuned independently and hence optimising and accessing new efficient materials will be more effective. This was demonstrated in a number of dendrimers in both PL and EL.

These dendrimers offer an other important property which could prove very useful in colour display technology. In fact, the emission in the blue and green-yellow dendrimer in the solid state was shifted towards the red and blue region of the visible

spectrum respectively and slightly different from the PL of solutions. This was believed to be reflecting the aggregation of the molecules, which is a usual phenomenon in conjugated polymers, due to the planar configuration they adopt. This was avoided by the use of more globular cores occupying a larger space which was the case of the porphyrin dendrimer. Choosing cores with similar structures or size could give the high purity to the colours emitted.

It is therefore clear that the dendritic molecular architecture provides an efficient way of making chromophores solution processible so that different studies and applications can be made. The dendritic structure also offers a way of controlling aggregation in solid state and therefore offering pure emission.

Having demonstrated the dendrimer concept, one can extend the choice of chromophores to be used in LEDs.

References

1. J. H. Burroughes, D. D. C. Bradley, A. R. Brown, R. N. Marks, R. H. Friend, P. L. Burns and A. B. Holmes, *Nature,* **1990**, 347, 539.
2. G. Grem and G. Leising, *Synth. Met.,* **1993**, 55-57, 4105. Y. Yang, Q. Pei and A. J. Heeger, *J. Appl. Phys.,* **1996**, 79, 934.
3. D. Braun and A. J. Heeger, *Appl. Phys. Lett.,* **1991**, 58, 1982.
4. N. F. Colaneri, D. D. C. Bradely, R. H. Friend, P. L. Burn, A. B. Holmes and C. W. Spangler, *Phys. Rev. B,* **1990**, 42, 11670.
5. See for example C. W. Tang and S. A. Vanslyke, *Appl. Phys. Lett.,* **1987**, 51, 913. C. W. Tang, S. A. Vanslyke and C. H. Chen, *J. Appl. Phys.,* **1989**, 65, 3610.
6. T. Yamamoto, H. Suganuma, Y. Saitoh, T. Maruyama and T. Inoue, *Appl. Phys. Lett.,* **1996**, 35, L1142.
7. S. A. Jenekhe and J. A. Osaheni, *Science,* **1994**, 265, 765.
8. J. Bisberg, W. J. Cumming, R. A. Gaudiana, K. D. Hutchinson, R. T. Ingwall, E. S. Kolb, P. G. Mehta, R. A. Minns and C. P. Petersen, *Macromolecules,* **1995**, 28, 386.
9. M. Pope and C. E. Swenberg, "*Electronic Processes in Organic Crystals*" **1982**, Clarendon Press, Oxford.
10. J. N. G. Pillow, PhD thesis, **1998**, University of Oxford.
11. N. C. Greenham, I. D. W. Samuel, G. R. Hayes, R. T. Phillips, Y. A. R. R. Kessner, S. C. Moratti, A. B. Holmes and R. H. Friend, *Chem. Phys. Lett.,* **1995**, 241, 89.
12. J. Kalinowski, "Organic Electroluminescent Materials and Devices" 1997, OPA, Amsterdam.
13. S. Dailey, M. Halim, E. Rebourt, I. D. W. Samuel and A. Monkman, *J. Phys. CM,* **1998**, 10, 5171.
14. P. Wang, Y. Liu, C. Devadoss, P. Bharathi and J. S. Moore, *Adv. Mater.,* **1996**, 8, 237.
15. A. D. Adler "The Chemical and Physical Behaviour of Porphyrin Compounds and Related Structures" **1973**, V. 206, New York Academy of Sciences.

16. J. D. Koyle, R. R. Hill, and D. R. Roberts, "Light, Chemical Change and Life"

17. M. Halim, J. N. G. Pillow, P. L. Burn, I. D. W. Samuel, *in Press*.

18. R. A. Campos, I. P. Kovalev, Y. Uo, N. Wakili and T. Skotheim, *J. Appl. Phys.*, **1996**, 80, 7144.

19. D. Braun and J. Heeger, *Appl. Phys. Lett.*, **1991**, 58, 1982.

20. N. C. Greenham, S. C. Moratti, D. D. C. Bradley, R. H. Friend and A. B. Holmes, *Nature*, **1993**, 365, 628.

Chapter 6

Light-Emission in Conjugated Polymers: Poly(*p*-pyridine) and Poly(*p*-phenylenevinylene) derivatives

6.1 Introduction

A large number of the published work in the field of conjugated polymers for light-emitting diodes has been dedicated mainly to emission characteristics, such as spectral range and luminescence efficiency [1-5]. However, there is still the need to develop more photo-stable materials in order to reach the industry recommended life-time for plastic LEDs. Encapsulation of the active layer is known to be a possible way to enhance the photo-stability of the luminescent polymer and hence a longer life time can be achieved. Another possible technique resides with the material itself – a slight modification of the chemical structure could enhance the oxidative stability of conjugated polymers.

For example, poly(*p*-phenylene) (PPP), shown in figure 6.1, is a well known conjugated polymer which emits in the blue region of the visible spectrum and has been used successfully by different research groups as an active layer in polymer LEDs [4,6,7], but it is easily photo-oxidised like most conjugated polymers. However, the introduction of a nitrogen heteroatom into the π system, whilst retaining the conjugation, does have an affect on the photo-stability of the resulting polymer PPY (see figure 6.1) as well as on other properties as will be discussed in this chapter. In fact T. Yamamoto and co-workers have studied PPY and found that not only is it luminescent, but that it is not possible to oxidise the polymer, even electrochemically under severe conditions [8]. This is an indication of a promising new generation of photo-stable polymers for LEDs.

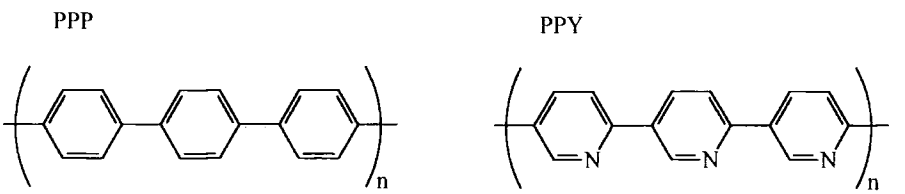

FIG. 6.1 *Chemical structure of poly(p-phenylene)(PPP) and poly (p-pyridine)(PPY).*

In this chapter, I shall present the luminescence properties of PPY both in solution and in solid state in order to answer the questions on the nature of the singlet excited states in PPY, which are responsible for the polymers distinctive characteristics such as the large red-shift between solution and solid state PL. The study includes the absorption, photoluminescence (PL) and the quantum yield (ϕ_{PL}). Further results obtained on PPY luminescence as a function of temperature, blending concentration and protonation will also be discussed.

Modifications to the polymer backbone are also investigated in a different polymer. In poly(*p*-phenylenevinylene) (PPV) the introduction of alkoxide side groups is known to alter the properties of the original polymer such as its processibility and π-π* transition energy and so various alkoxide substituted PPVs were studied.

6.2 Photoluminescence in PPY

J. W. Blatchford and co-workers at the Ohio State University have studied different PPY-based polymers [9]. Their polymers, including PPY, were strongly photoluminescent in solution state while the solid state films displayed a strongly red-shifted luminescence with respect to solution PL and low quantum yields. They have suggested that the red-shift of the film PL is a result of the formation of low energy aggregate sites due to strong inter-chain interactions.

The PPY prepared in Durham (by E. Rebourt and L. E. Horsburgh) was synthesised using a modified version of the route published by T. Yamamoto *et al* [8]. The polymer is not soluble in most organic solvents, with the exception of formic acid. This is a desirable feature for the fabrication of multilayer LEDs as deposition of multilayers is not affected by the solubility of the materials in similar solvents. Thin solid films were then spin coated directly from formic acid solution (~ 14 mg / ml) onto spectrosil substrates.

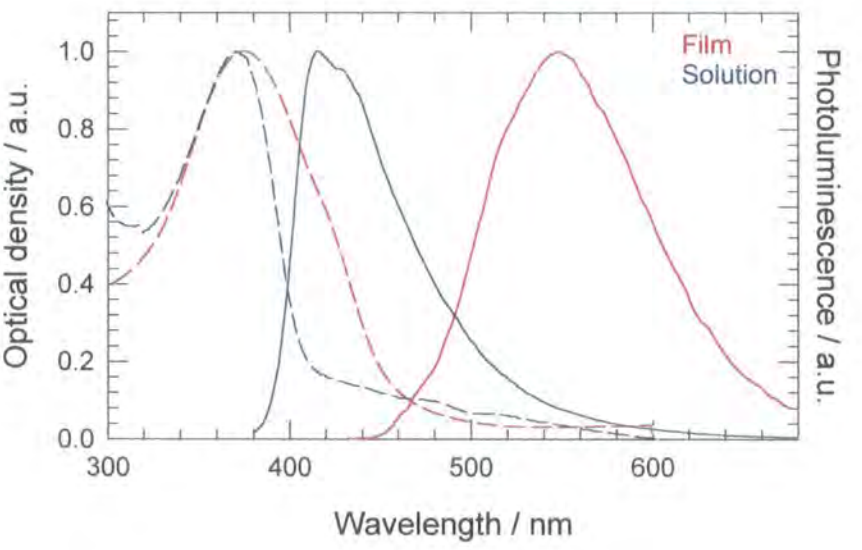

FIG. 6.2 *Absorption (dashed) and photoluminescence (continuous) of PPY solution and spin coated film.*

The absorption and PL spectra of PPY in solution and solid state are shown in figure 6.2. The absorption of the solution and solid state are very similar, although the vibronic structure is less resolved in the solution state absorption. A. P. Monkman *et al* have reported that there is little solvent induced shift to the absorption band over a wide range of dilutions (10^{-1} to 10^{-6} M repeat units of PPY in formic acid) [10]. The difference between the solution and solid state becomes more pronounced in the PL process – the solution emits in the blue region with a maximum emission around 416 nm. In the solid state, however, the PL spectrum is substantially red-shifted (~ 130 nm) with respect to the solution emission profile, to have a maximum emission wavelength at around 548 nm. The spectrum is not broadened, but the structure present in the solid sate spectrum is poorly defined in the solutions' PL. These results are slightly different from those previously published by other research groups [8,9] where no structure is observed in the solid state PL. The red-shift between solution and solid state PL is a frequent characteristic of conjugated polymers and is observed for different systems such as PPV [11], MEH-PPV [12] and other PPV derivatives [13]. This shift has been attributed to the migration of excited states (excitons) to lower energy sites of the polymer chains which correspond to the longest conjugated segments. The increase in the conjugation length in the solid state is believed to be a result of an improved ordering of the polymer chains. The red-shift was also observed by H. S. Woo *et al* when going from the solution phase to the solid state phase in some phenylenevinylene oligomers [14]. They attributed the shift to the reduction of the torsion angle of the phenylene rings, as a result of the preferred planar configuration adopted by the molecules in the solid state.

J. W. Blatchford *et al* has suggested that aggregation or excimer formation is a possible explanation to the red-shift in PPY PL spectrum. However A. P. Monkman and co-workers have found that the PL spectrum of PPY solution remains approximately unchanged between concentrations of 1M and 10^{-7} M (figure 6.3), which suggests that aggregation of the polymer chains is unlikely to be the cause of such a shift. Note that the slight change in the PL spectrum in the concentrated solution is probably due to self-absorption. The unchanged spectrum is also an

indication of non-excimer formation, as it is known that features due to excimer emission should appear spontaneously after a certain concentration threshold [15-17].

Note that the nitrogen p_z orbitals are not delocalised into the π-conjugation and stick out of the ring, though still in the same plane as the conjugation. Light scattering and crystallinity studies have revealed that PPY is a rigid rod polymer [18] and therefore would prefer to stack cofacially in the solid state form. The nitrogen lone pair will then orient between the chains. The rigid rod nature of the PPY chains is also reported by T. Yamamoto *et al* [8]. Theoretical calculations yield a minimum energy chain geometry for PPY with a 30° inter-ring twist torsion angle between neighbouring pyridyl rings [19]. Therefore in the solid state, inter-chain interactions are believed to force the polymer backbone into the most planar configuration, i.e. lowest ring torsion angle geometry. The more planar the chains the more delocalised the π-cloud which will be reflected in a low energy gap.

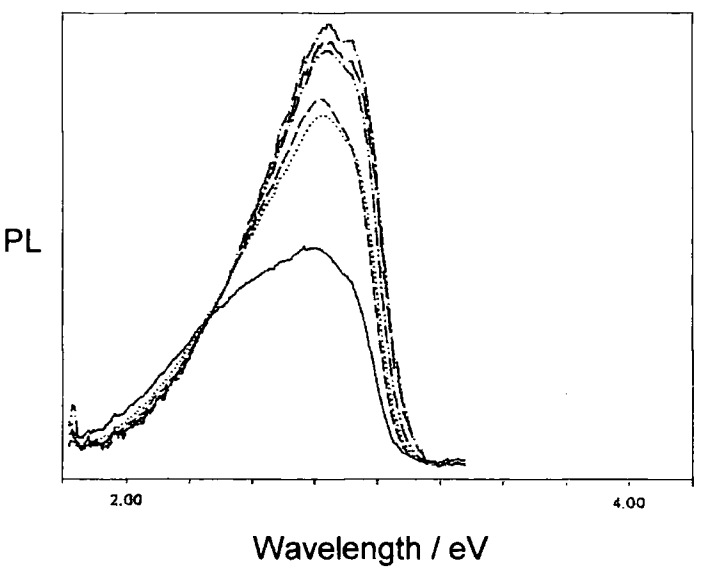

FIG. 6.3 *Photoluminescence dependence of polypyridine solution on concentration (from 1M to 10^{-7} M). Data taken from reference [10].*

The PL quantum yield, ϕ_{PL}, of PPY in solution and solid state was measured as described in chapter 3. The films, when excited with the UV lines of an argon ion

laser, were strongly luminescent in the green region of the visible spectrum. In fact their ϕ_{PL} was in the range of 30 ± 3 %, much higher than the values reported by A. J. Epstein *et al* [20] and compares favourably with other well known conjugated polymers, which emit in the same wavelength range [21]. Our material shows higher ϕ_{PL} compared to values reported by other groups and this is perhaps due to purity and modifications introduced to the synthesis of PPY. In fact, the integrating sphere technique served as a good way for assessing the synthesis of PPY. The synthesis was modified further by Dr L. Horsburgh to achieve a PL quantum yield of around 37 ± 3 % [22]. Interestingly the PL quantum yield in formic acid solution (10^{-6} M) was found to be 17 ± 3 %. This is in contrast to most conjugated polymers where the solution ϕ_{PL} is higher compared to that in the solid state. The reason for such a contrast in PPY is believed to be the quenching of luminescence in solution due to intersystem crossing (ISC). J. W. Blatchford *et al* have reported that the ISC increases with increasing torsion angle [23], and so one would expect the quenching to be more efficient in solution. Another possible explanation for the relatively low ϕ_{PL} in solution is solvent quenching, although this was found not to be the case as will be discussed in the next section.

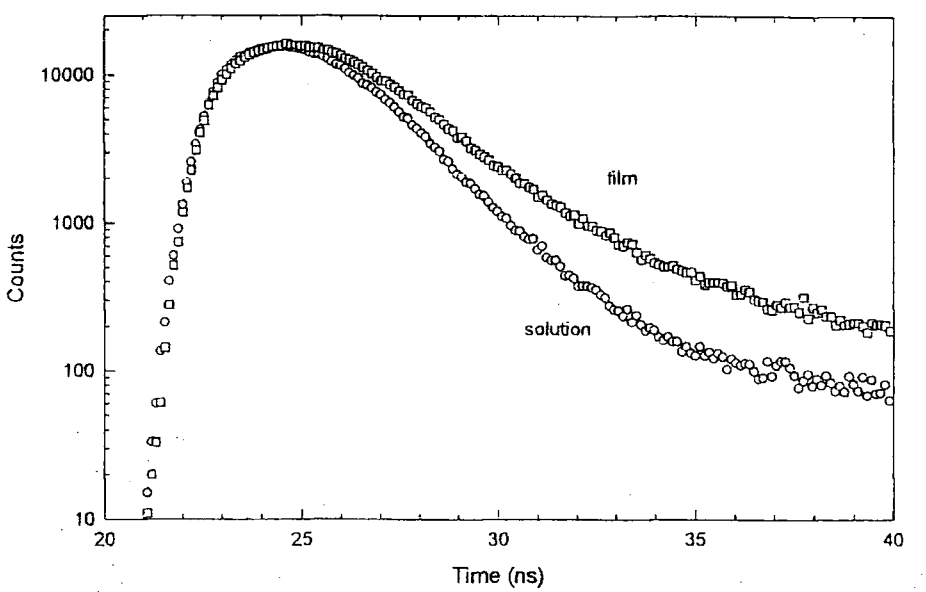

FIG. 6.4 *Luminescence decay in PPY solution and solid state.*

The luminescence decay (fig. 6.4) in PPY films was measured by M. Sluch using the time-correlated single photon counting technique and found to have two components (fitted to double exponential) of time constant 1.2 ± 0.1 ns and 5.3 ± 0.1 ns, irrespective of the excitation wavelength over the absorption band range [10]. The fitted time constant for PPY solution was 1 ± 0.1 ns. It is clear that in the solid state the excited species are longer lived than those in solution which could be an indication of inter-chain interactions [24]. This is in contrast with other conjugated polymers [25,26] as the opposite was observed in comparisons of solution and solid state luminescence kinetics. Longer lived PL in film than in solution was reported by Samuel *et al* for CN-PPV [24].

6.3 Stability in PPY

The time dependence of the photoluminescence quantum yield was also measured for thin films of PPY. The experiment was first carried out in air and the results are shown in figure 6.5.

Immediately after striking the sample with the laser beam in air the PL intensity drops slightly, but remains unchanged afterwards (over several hours). The experiment was repeated in different atmospheres, first with a continuous flow of nitrogen into the integrating sphere and secondly in a vacuum (~ 10^{-1} mbar). The results, also shown in figure 6.5, are curiously unexpected. In nitrogen, the intensity of the emitted light began to decrease immediately after starting to excite the sample. After the first 500 seconds, the rate of decrease of intensity of the emitted light slows considerably. When the experiment was repeated in a vacuum of 10^{-1} mbar the luminescence decreased rapidly with a higher rate than in the nitrogen case. The temporal dependence of the PL quantum yield in vacuum started also with a much faster decay for the first 10 minutes, followed by a slower decay.

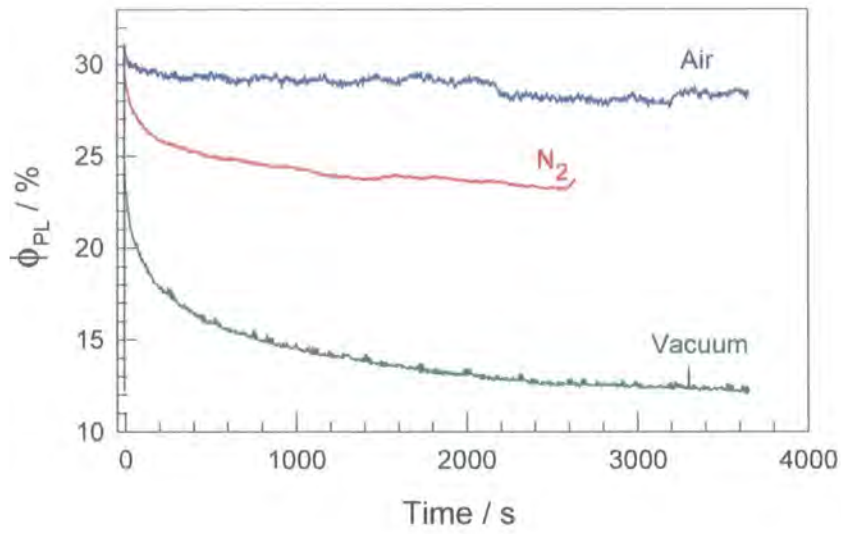

FIG. 6.5 *Temporal behaviour of photoluminescence quantum yield of PPY films in different atmospheres.*

Clearly the vacuum had an effect on the luminescence of the PPY films and so it is of interest to determine whether both light and vacuum are responsible for the drastic decay of the PL quantum yield in vacuum. Therefore, an experiment was carried out in which the PPY film was illuminated, in the same vacuum, for only 3 seconds in each minute, rather than continuously. The results are shown in figure 6.6. The decay of the luminescence was similar in shape to that of continuous illumination in that the luminescence starts to decrease sharply for the first 10 minutes, although it seemed to remain constant for the remaining time of the experiment. However, after a certain time (region A) the sample was excited continuously to see if the light has a further combined effect on the luminescence. In fact the luminescence does decay further on continuous illumination.

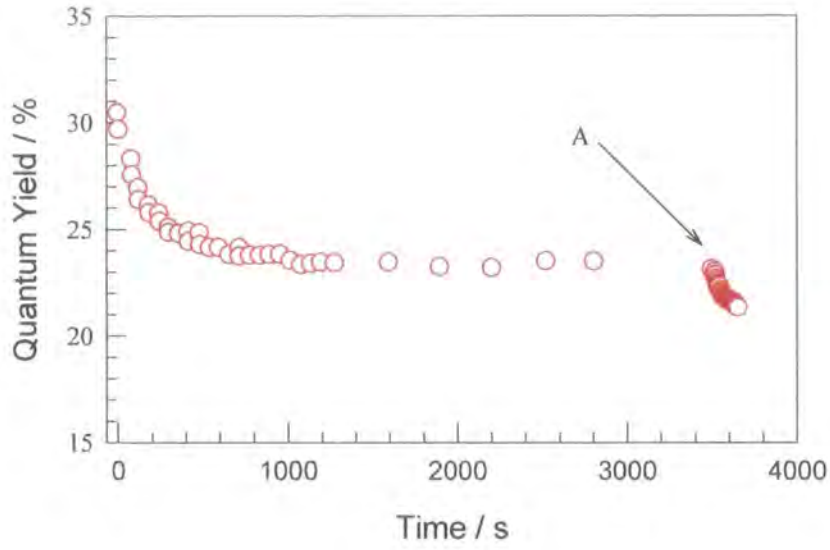

FIG. 6.6 *Quantum yield time dependence of PPY film under vacuum. The sample was illuminated for 3 seconds in each minute. Region A: the sample was illuminated continuously.*

These results clearly show that the vacuum has the effect of reducing the PL quantum yield of PPY. This is not the only factor responsible for the decay, as the continuous illumination (light) also plays a role in the decay, a role that is more effective in the vacuum. Interestingly though, the PPY films appear to be stable in air but, astonishingly, not under vacuum. However, the behaviour of PPY luminescence quantum yield in air and vacuum is contrary to what one would expect from most conjugated polymers. The stability of the PPY in air is in agreement with the fact that PPY is stable to chemical and electrochemical oxidation and is believed to be due to the fact that the pyridyl rings are electron deficient hence difficult to oxidise. Nevertheless the behaviour in vacuum is difficult to explain. Removal of the solvent (formic acid) can not be responsible for the luminescence decay in vacuum because the opposite effect – in solution the PL quantum yield is lower – was observed in solution. However a plausible explanation could be that oxygen is interacting with nitrogen lone pair electrons and blocking intersystem crossing.

A comparative study was carried out on a spin coated PPV film, which emits in a similar region of the spectrum (see figure 6.7), to illustrate the common behaviour of conjugated polymers in the presence/absence of oxygen.

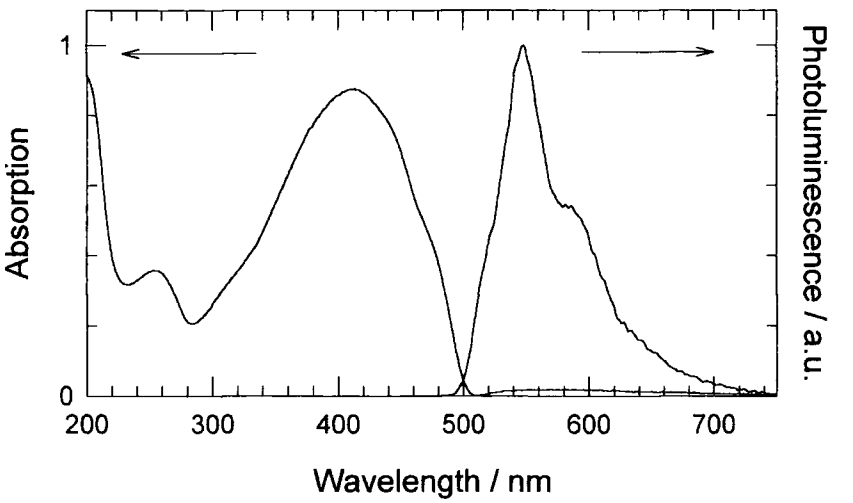

FIG. 6.7 *Absorption and photoluminescence spectra of a PPV film.*

The ϕ_{PL} was first measured in air on a spin coated PPV film. Then the film was excited continuously with the same excitation wavelength (488 nm) in air. The experiment was repeated in a vacuum ($1x10^{-1}$ mbar).

The quantum yield of PPV, when measured in air, decreases very rapidly for the first ten minutes followed by a smoother decay in the remaining time of the experiment. After an hour, the film is weakly luminescent with a quantum yield in the range of a few percent. The experiment was repeated using a fresh sample which was expected to have the same quantum yield. This was verified by measuring the quantum yield in air. The laser beam was then blocked while the integrating sphere was being pumped down until a pressure of around $1x10^{-1}$ mbar was reached. At this stage the sample was excited continuously. The quantum yield, as shown in figure 6.8, has shown no major change in the duration of the experiment (one hour), although a slight increase in the quantum yield was observed at the start of the experiment.

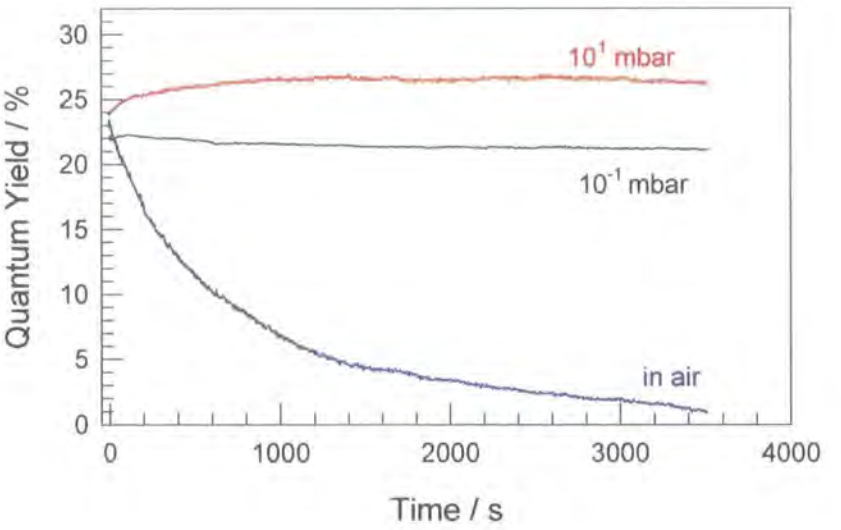

FIG. 6.8 *The temporal dependence of the photoluminescence quantum yield of a PPV film in different atmospheres. The samples were both excited with 454 nm wavelength.*

A similar experiment was carried out on another identical sample, although this time more oxygen (air) was allowed to remain in the integrating sphere by controlling the vacuum at around $1x10^{1}$ mbar inside the sphere. Similar behaviour was observed as in the previous experiment (with better vacuum) in that the quantum yield remains constant during the continuous pumping. Note that a slight decrease of about 2-3 percent was observed in the first hundreds of seconds. The behaviour of the ϕ_{PL} in PPV is due to the effect of photo-oxidation. Once the sample is exposed to air, new products such as carbonyls are expected to be generated in the polymer backbone, as a result of oxygen interacting with the phenylene ring, and act as quenching centres for singlet excitons [27]. This is also consistent with results reported by K. Z. Xing and co-workers using XPS data [28]. K. Z. Xing has also reported that the formation of these new complexes is more pronounced at longer exposures of light, which is in agreement with time dependence of the photoluminescence quantum yield shown in figure 6.8.

In a vacuum, completely different behaviour is observed, as was expected. The quantum yield remains constant throughout the experiment which is in agreement with luminescence quenching due to photo-oxidation.

6.4 PPY Blends

Further experiments were needed to understand the nature of the excited species in PPY and to explain the substantial red-shift in the solid state PL with respect to the solution emission profile. The study was carried out on PPY films but this time PPY was blended in PMMA, in an attempt to produce isolated PPY chains, and consequently explore the possibility of controlling the inter-chain interactions.

PPY was dissolved in formic acid, to which was added various ratios of PMMA ranging from 1:1 to $1:10^4$, PPY:PMMA by weight. Films were either spun onto spectrosil substrates or cast onto silicon wafers and will be referred to as 'blends'. The dilution in the blends shows no major effect on the PPY absorption as one would expect considering the solution and solid state have similar absorption. On the other hand, the emission profiles of the blends as a function of concentration shown in figure 6.9 were different. In fact the PL spectra of blends of concentrations ranging from 1:1 to $1:10^2$ were very similar in shape. Moreover they were similar to the emission profile of a pristine PPY film PL spectrum. At $1:10^3$, the emission starts developing a band at higher energy around 440 nm which corresponds to a blue emission, similar to that in the solution state. Diluting the PPY further ($1:10^4$) made the 440 nm band even more pronounced. In fact it dominated the PL spectrum, with the green emission being transformed to a shoulder spreading along low energy.

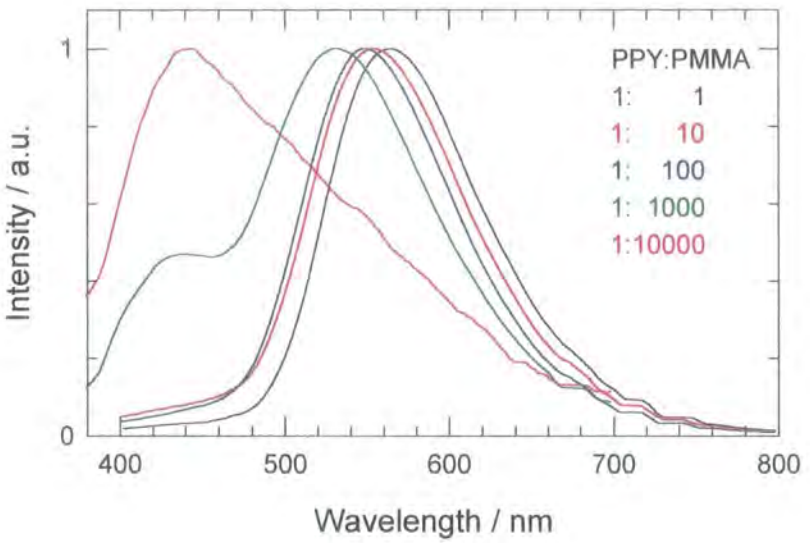

FIG. 6.9 *PPY emission as a function of dilution in PMMA.*

This data clearly shows that the changes in the PL spectra are an indication of different excited species responsible for the radiative decay in these blends. The emission in the blue range only appears at a reasonable degree of dilution, hence the characteristic green emission of a PPY film is a result of the polymer chains being very close to each other. This, as mentioned earlier, is in agreement with the theoretical calculations which shows that there is a 30° inter-ring twist between neighbouring pyridyl rings in solution [19]. Hence one can imagine, bearing in mind that in the solid state the polymer chains tend towards planarity, that as the concentration of the PPY in the blends decreases, there will be less interchain interactions and the pyridyl rings will become free to rotate. This will be the case until a concentration threshold is reached, where there will be no low energy chain segments which is reflected by the emission originating in shorter segments as it the case for PPY solution.

The luminescence intensity was also observed to be concentration dependent. The blends became less emissive as the concentration of the PPY decreased in the blends, which is another indication of separation of the chains in the solid state creating a

solution-like environment where intersystem crossing is expected to be more efficient, hence the low luminescence quantum yield. This is further supported by the measurement of the photoluminescence excitation spectra of the diluted blend where the emission profile consisted in a green and blue band. The spectra, shown in figure 6.10, were measured with emission wavelength at 450 and 530 nm and are slightly different. Moreover the spectrum measured at 450 nm is similar to the absorption of PPY solution whereas the excitation profile, measured on the same sample but at 530 nm, is similar to the absorption of PPY in the solid state. This clearly shows the modification of the polymer environment by separation of the chains which is believed to allow the pyridyl rings to rotate and lead to a solution-like environment.

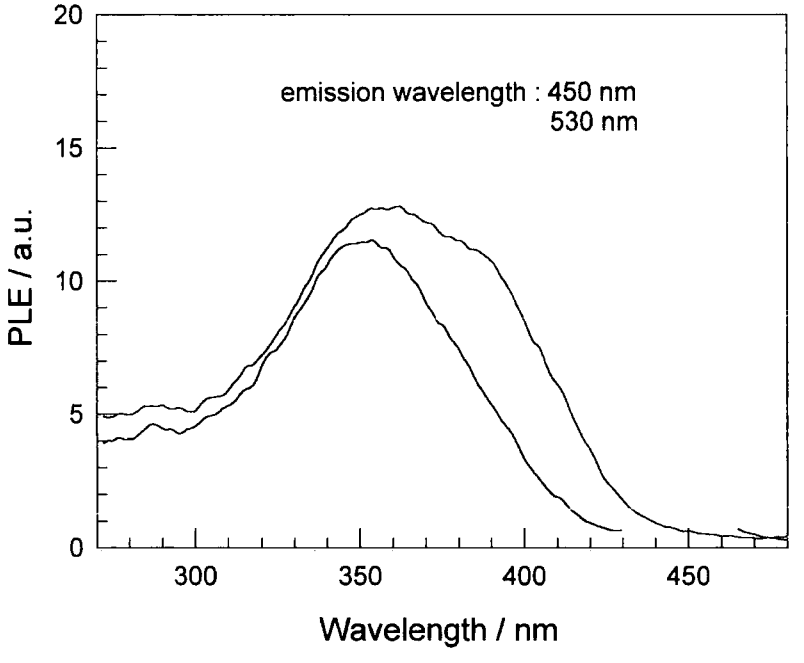

FIG. 6.10 *Photoluminescence excitation of PPY:PMMA blend (1:1000). The emission wavelength was monitored at 450 and 530 nm.*

Note that it was possible to form free standing flexible films of PPY:PMMA blends with the same emissive properties as the corresponding spin coated films which is a desirable feature.

6.5 PPY Protonation

From the results obtained so far, it is very likely that the planar configuration of PPY in the solid state is responsible for the difference between emission in solution and solid state, although further evidence is required to support the inter-chain effects on the PPY luminescence.

Using polyaniline (PANI) as a model, it is known that functionalised sulphonic acids provide very different properties to the polymer as compared to inorganic Brönsted acids [29,31]. One main influence is the hydrogen bonding of the counter ion which dictates crystal structure and many physical properties of PANI [31,32]. Their strong acidic nature in weak organic acid solvents means they can be used in the PPY system.

A range of functionalised and non-functionalised acids (figure 6.11), which are soluble in formic acid, were used to protonate PPY in solution. These solutions were used to spin coat thin films of the 'doped' PPY. Both strong and weak acids remain in the polymer bulk and in some cases protonation of the PPY nitrogen sites could be clearly seen from the XPS data [33]. In the case of PPY, the intention of using molecules is to be able to alter the spacing between adjacent rigid rod PPY chains and thus break or alter any inter-chain interactions that could occur in the solid state. The doping acids were camphorsulphonic acid (CSA), 2-acrylamido-2-methyl-1-propanesulphonic acid (AMPSA), dichloroacitic acid (DCA), and *meta*-cresol (*m*-cresol) and their structures are shown in figure 6.11. The acids were added in molar ratios to PPY monomer units such that doping levels of 25, 50, 75, and 100 % were nominally achieved.

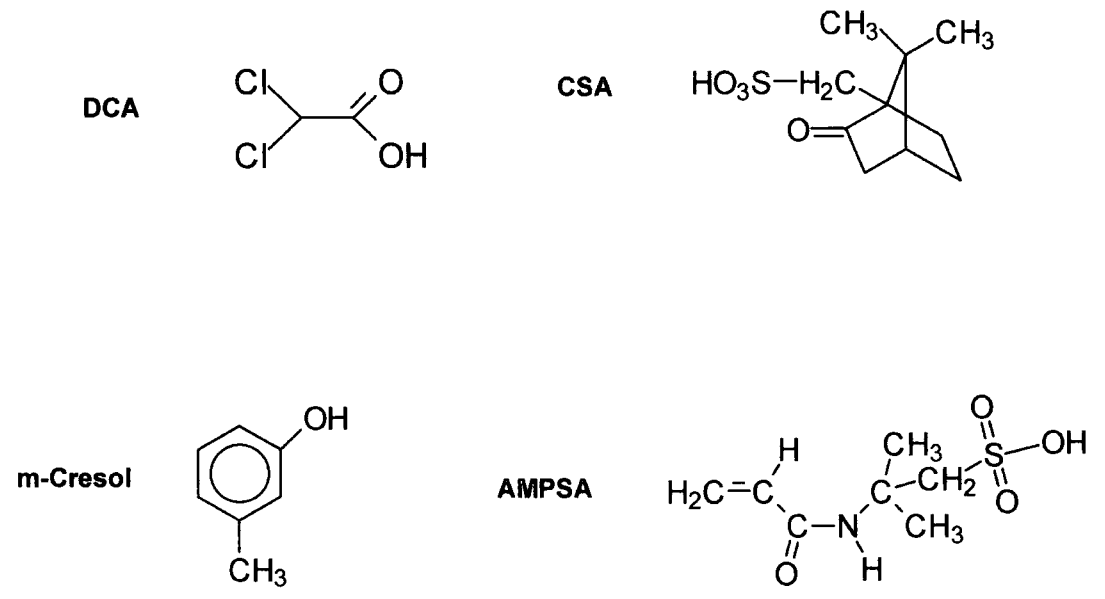

FIG. 6.11 *Chemical structures of dichloroacitic acid (DCA), meta-cresol (m-Cresol), camphorsulphonic acid (CSA), and 2-acrylamido-2-methyl-1-propanesulphonic acid (AMPSA).*

For example, in PANI, 50 % doping implies that one acid molecule was added for every two PANI repeat units i.e. theoretically half of the nitrogens present in the polymer, in an ideal configuration, should be protonated [34]. This is also applicable to PPY.

The absorption spectra of PPY films doped with CSA are shown in figure 6.12 together with the absorption of a pristine PPY film for comparison. As mentioned earlier, the absorption of PPY films consist of a major absorption band at 380 nm, a shoulder which is observed around 413 nm, and a high energy knee at 365 nm. These features will be referred to here and thereafter as MAB, LES, and HEK respectively. Upon initial protonation with CSA (25 %) the entire absorption band broadens slightly and shifts towards lower energy with respect to the pristine PPY's absorption.

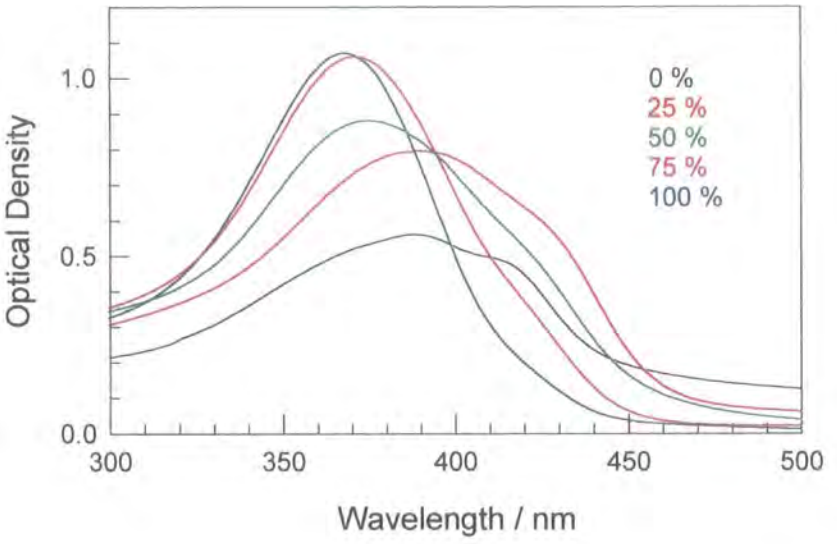

FIG. 6.12 *Absorption spectra of PPY as a function of CSA doping level.*

Increasing the CSA doping level causes a monotonic decrease in the intensity of the of the LES. At high acid concentration, e.g.100 %, the HES has disappeared from the spectrum. The MAB shifts towards a shorter wavelength as the doping increases. Note also that at high acid concentrations, the absorption spectrum is featureless and is very similar to the absorption of PPY in formic acid solution.

The PL spectra was measured for identical samples (25-100 %) and the results are shown in figure 6.13. The 25 and 50 % doped samples have similar profiles with only a small red-shift with respect to the pristine PPY spectrum (0 %). However at higher doping levels, 75 and 100 %, a new feature appears at around 470 nm. It is more pronounced in the 100 % sample and is situated in the blue region of the visible spectrum. This is very similar to the emission in PPY solution and could also be of the same origin as the new emission seen in PPY blends. The PL quantum yield, ϕ_{PL}, of the doped samples was measured with the integrating sphere and are shown in figure 6.15. Again the 25 and 50 % doped films had quantum yields in the same range as PPY (37 %), however, the 75 and 100 % films had lower quantum yields in the range of 22 %. This value is in the same range as the PPY solution ϕ_{PL} (17 %). It is still a

respectable quantum yield as it compares favourably with other conjugated polymer efficiencies [21].

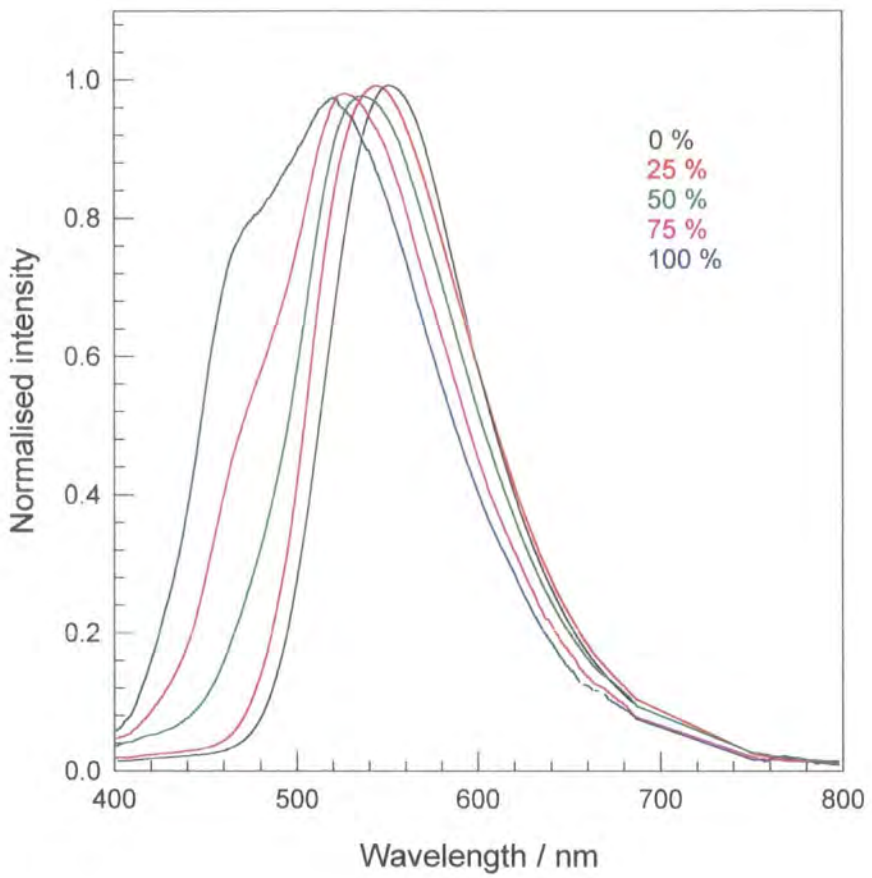

FIG. 6.13 *Photoluminescence of PPY as a function of CSA doping.*

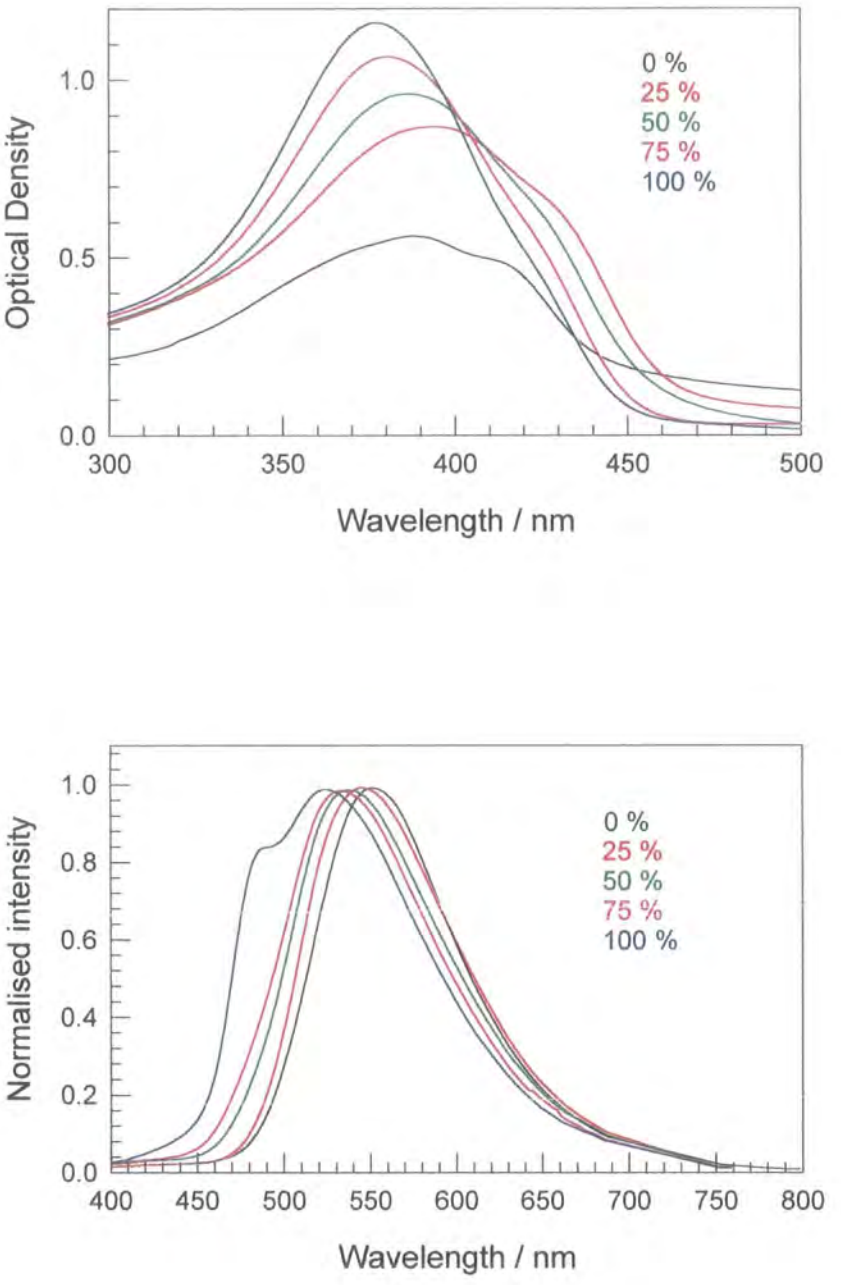

FIG. 6.14 *Absorption (upper panel) and photoluminescence (lower panel) of AMPSA doped PPY films.*

The absorption of AMPSA doped PPY is shown in figure 6.14 together with their PL spectra. Very similar behaviour to CSA is observed in the absorption of AMPSA-PPY films, except at 100 % doping level where the LES has not completely disappeared. The MAB has not blue-shifted as far as in the CSA case. The samples also show the same PL dependence on concentration: at low doping level, the PL spectra are only slightly red-shifted with respect to the non-doped film. However, a new feature appeared, only in the 100 % doping at around 486 nm and is slightly red-shifted with respect to the similar feature seen in 100 % CSA doped films (~ 467 nm).

The behaviour of ϕ_{PL} is very different from that of the CSA films – the quantum yield decreased to a value of 20 % for the AMPSA-25 % film. Increasing the doping level had the opposite effect as the quantum yield increased to reach a value of 28 % for the AMPSA-100 % doped films.

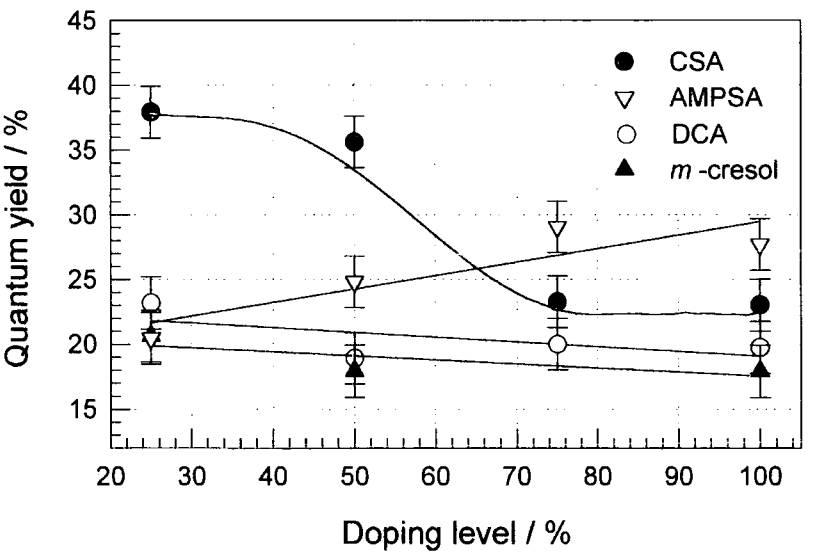

FIG. 6.15 *Poly(p-pyridine) photoluminescence quantum yield as a function of acid doping level for different acids. The lines are a guide to the eye.*

The DCA doping effect on the PPY absorption consisted in a blue-shift of the MAB which becomes featureless. The LES disappears at high doping levels. On the other hand, DCA had little affect on the PPY emission compared to the other previous acids

(CSA and AMPSA). The PL spectra are slightly red-shifted as the concentration of DCA increased. The emission remained green while the quantum yield has been reduced to approximately 20 %. This was independent of the protonation level (fig 6.15).

Finally, the *m*-cresol doped films showed different changes to both absorption and PL profiles. The absorption, shown in figure 6.17, appears to shift towards higher energy as the acid level increases. However, the real change consists in the reverse in intensity ratio between the MAB and HEK. At 100 % it is quite clear that the HEK is the most pronounced feature in the absorption spectrum. The PL of the *m*-cresol doped films was reflecting different changes to those seen in CSA and AMPSA. In fact, there was not a considerable shift observed as the acid doping level increases. Instead, the spectra developed some structure, at early acid concentration (25 %), that was independent of the doping level. Again the ϕ_{PL} was independent of the acid concentration but has been reduced to a value of around 20 % as was the case for DCA doped films.

It was also found, after XPS study, that both CSA and AMPSA protonate PPY films whereas DCA and *m*-cresol do not [33]. Moreover two doping induced features were observed in the N1s XPS spectra. This tentatively ascribed to evidence of hydrogen bonding between the protonated nitrogen sites and the carbonyl moieties on the acid counter ions [33]. Using DCA and *m*-cresol as dopents had little effect on the emission profile of the different doped PPY films. However, the PL quantum yield drops clearly to a much lower value (~ 20 %) where it remains independent of dopent concentration. Self absorption is clearly not responsible for the behaviour of ϕ_{PL} as the emission spectra of DCA or *m*-cresol doped films are far from their absorption edge. The ϕ_{PL} decrease could be a result of solvent quenching.

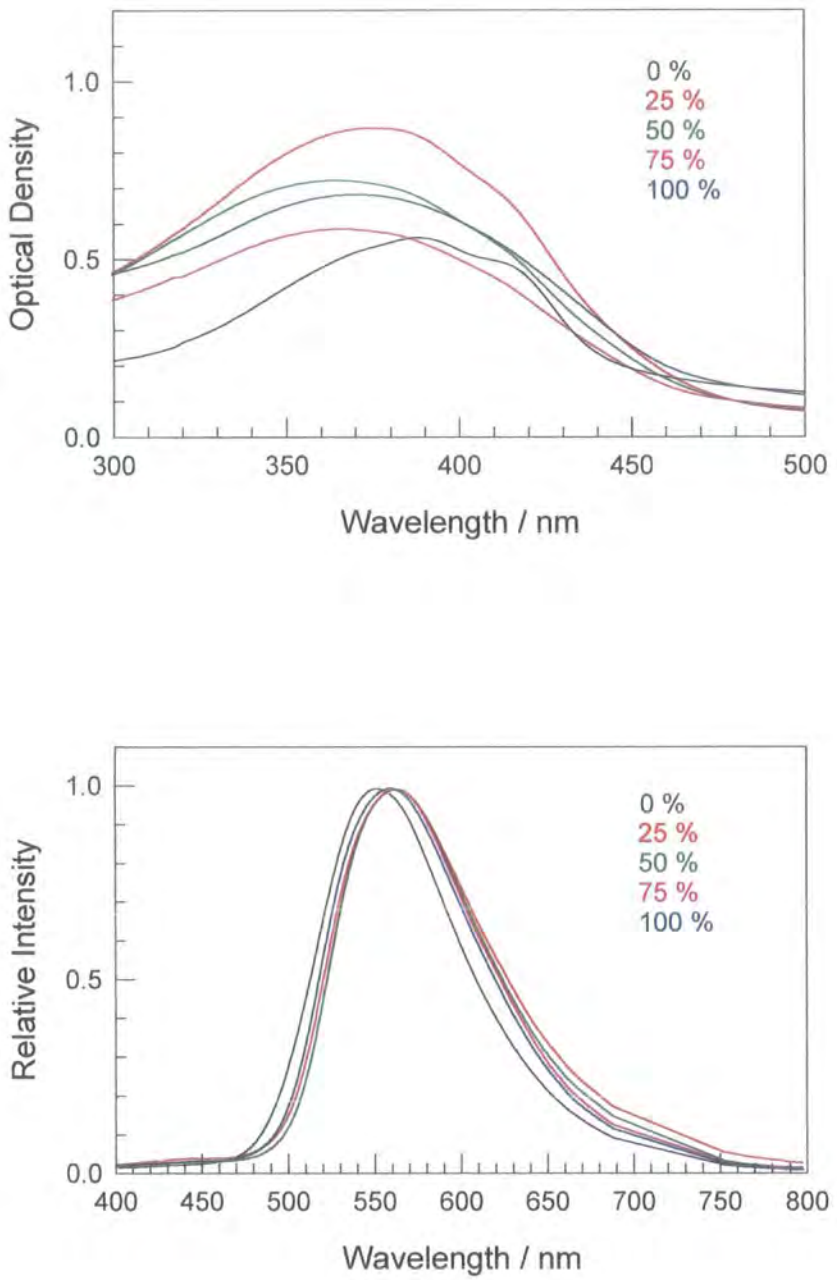

FIG. 6.16 *Absorption (upper panel) and photoluminescence (lower panel) of DCA doped PPY films.*

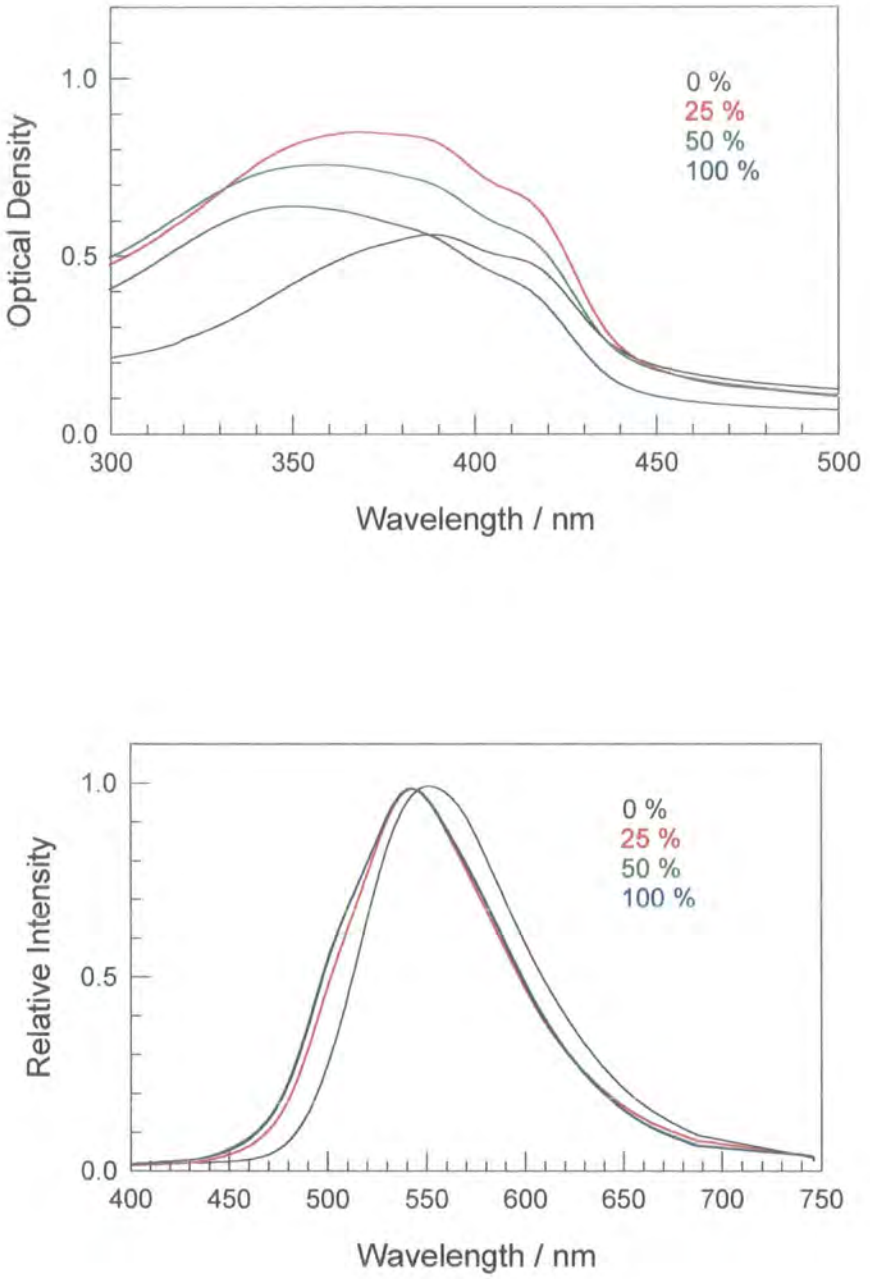

FIG. 6.17 *Absorption (upper panel) and photoluminescence (lower panel) of m-cresol doped PPY films.*

Upon addition of CSA and APMSA the inter-chain interactions, especially at higher doping levels, are expected to be reduced. This is achieved by increasing separation distance between chains by breaking PPY:PPY interactions which will then allow the pyridine rings to revert back to a more twisted geometry which corresponds to a lower energy. The excitons, after being created, will always migrate to low energy sites, which corresponds to the longer conjugated segments in the chain, and then decay radiatively, hence the green emission. The density of such low energy sites has to be considerably reduced before exciton migration to those sites is limited to such a level that not all excitons can find the low energy segments where they would recombine, but instead they are trapped in high energy segments where they could recombine radiatively by emitting blue light. As shown experimentally, this only occurs at high doping levels for the PL whereas a monotonic change, in the absorption spectrum as a function of acid concentration, is observed as one would expect. This indicates the continuous effect of chain separation on PPY geometry.

The absorption of CSA and AMPSA doped samples also show some changes in intensity as a function of doping. This was assigned to the difference in the thickness of the samples. In fact the 25 and 50 % CSA doped films were of roughly the same thickness and about a 100 nm thinner than the 75 % doped sample. This could be due to changes in solution viscosity possibly due to the doping acid. The 100 % doped film was found to be too soft to measure with the α-step profilometer which could be a further indication of the reduction of the inter-chain interactions in the solid state.

The difference between CSA and AMPSA in the quantum yield behaviour could be assigned to the hydrogen bonding that, according to A. P. Monkman's XPS study [33], will occur alongside protonation. AMPSA is a complex acid containing an amide moiety that will give rise to weaker hydrogen bonding than in CSA.

6.6 Effect of Temperature in PPY

The PL spectrum of PPY was measured as a function of temperature (9 – 280 K). The spin coated film was mounted in a closed loop helium displex cryostat while the excitation was provided by the UV lines of an argon ion laser and the light emitted was collected with a quartz fibre connected to a CCD spectrometer. The structure observed in the room temperature (figure 6.18) sample was also present in the spectra measured at low temperatures, but was more pronounced. The sharpening of the structure in the PL spectrum was also observed in the absorption spectrum. Interestingly, though, there was no substantial shift of the emission profile as the temperature decreases. This is unusual for conjugated polymers as they tend to red-shift with decreasing temperature [35].

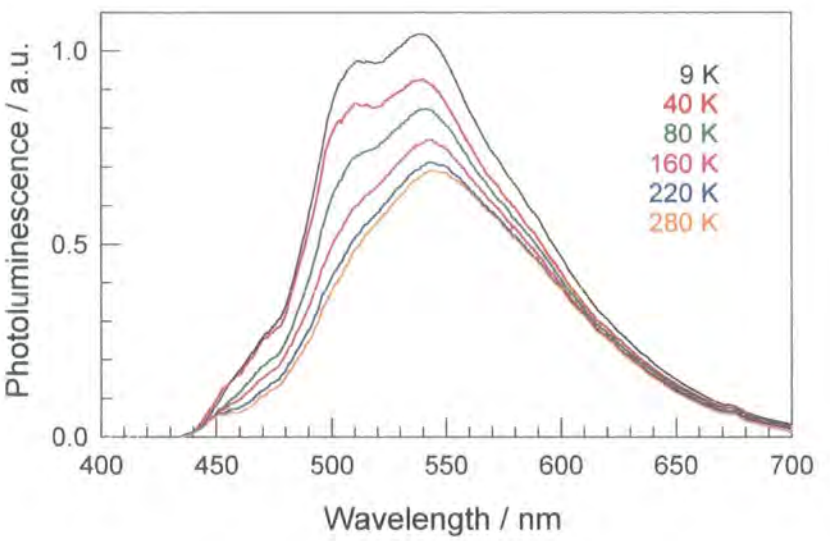

FIG. 6.18 *Photoluminescence spectra of PPY film throughout 9 – 280 K temperature range.*

For example, in PPV the emission profile exhibits a shift towards lower energy as the temperature decreases. This is believed to be a result of freezing out torsional modes between phenylene rings in the polymer chain at low temperatures. This will give the polymer chain a more planar configuration which will increase the effective

conjugation length and hence the low energy emission. A similar, but larger, red-shift was also observed in CN-PPV and could be explained by the same phenomenon.

The absence of the shift in the PPY films spectra could be an indication of the planar geometrical configuration that the molecules adopt at room temperature. This agrees with results obtained on blends and doped PPY.

The relative photoluminescence quantum yield was measured as a function of temperature simply by integrating the area under each emission profile. By assigning a 30 % quantum yield, which was measured on a similar sample with the integrating sphere, to the room temperature spectrum, the other relative quantum yields were then simply deduced from the corresponding spectra. The temperature dependence of the luminescence efficiency of PPY films is shown in figure 6.19.

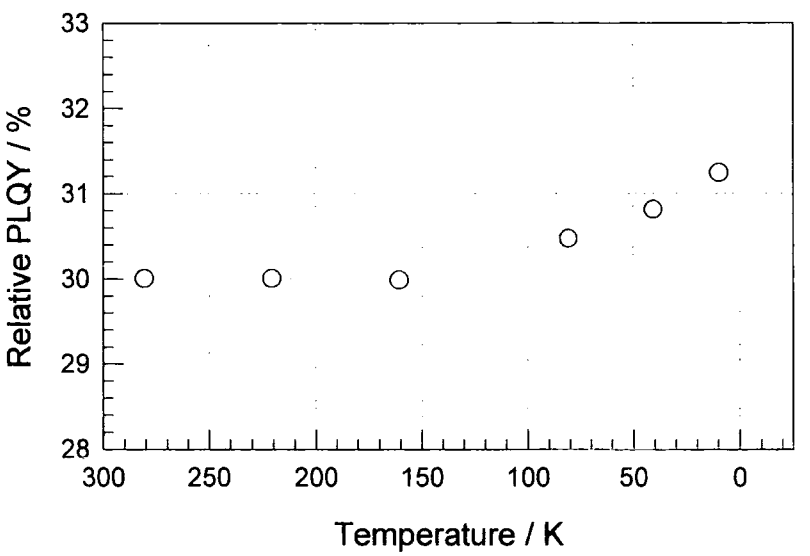

FIG. 6.19 *The relative PL quantum yield of PPY film as a function of temperature.*

The luminescence efficiency of PPY films clearly increases at low temperature, although it is in the same range as the error in the ϕ_{PL} measurement (3 %) and therefore could be considered negligible. Again, this behaviour is not totally consistent with other conjugated polymers. In PPV, for example, the PL efficiency is enhanced at low temperatures particularly on the range up to about 120 K [36]. The

increase in the luminescence efficiency with low temperatures is usually assigned to the suppression of thermally-activated diffusion of excitons to quenching sites. A similar explanation, for PPY behaviour, is possible here, although the reason for the negligible change in intensity is not very clear. A possible reason for such a behaviour could be that at the room temperature, the quantum yield is reasonably high compared, for example, to PPY solution, because of the suppression of some non-radiative decays due to its planar configuration.

6.7 Alkoxide Substituted PPVs

Since previous work of different research groups on PPV and its derivatives has revealed the possibility of optical and electronic tuning of the PPV properties, simply by attaching side chains on the monomer units, alkoxy-substituted PPVs seem very useful in terms of studying the effect of side chains on the PPV properties. This has the purpose of tuning the colour over a large range in the visible spectrum and to study the effect of side-chains on intermolecular interactions.

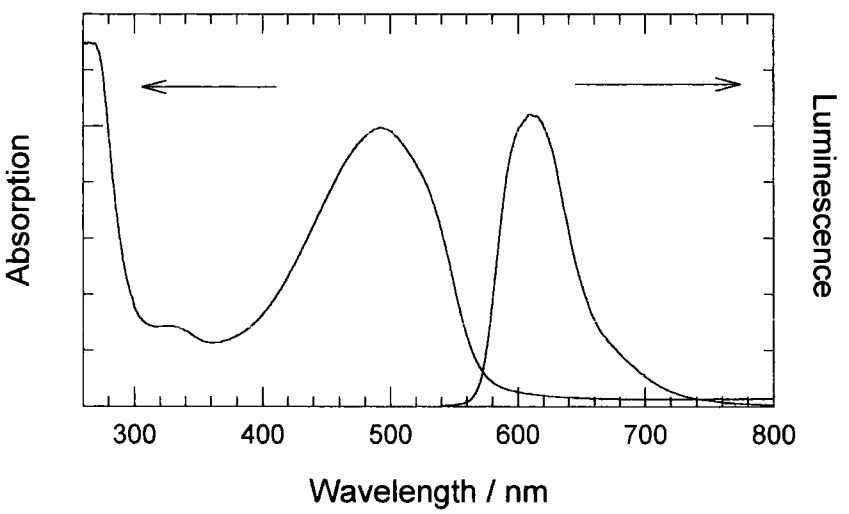

Fig. 6.20 *Absorption and emission spectra of MEH-PPV film (λ_{ex} = 500 nm).*

MEH-PPV, which is a 2,5 asymmetrically substituted PPV (see figure 6.22) has undergone simple chemical modification. This has affected the polymer properties in many ways. Solubility is one important change as MEH-PPV is soluble in most

organic solvents, although the more desirable feature is the different range of light-emission. In fact MEH-PPV has a narrower energy gap resulting in a luminescence which is shifted towards longer wavelengths. The spin coated films emit orange light with a maximum wavelength at around 600 nm. Figure 6.20 shows the absorption and emission spectra of spin coated films from chlorobenzene solution.

The quantum yield of the spin coated film was measured and found to be around 15±2 %. This is in the same range as values reported by other groups [37] and is clearly lower than values measured for solution (35±5 %) [38]. The emission is believed to be a result of intra-chain excitons decaying radiatively although possibilities of inter-chain species are also considered. It is worth mentioning that the emission spectrum of MEH-PPV was found to be dependent on the solvent used for solution preparation. For example, when chloroform was used instead of chlorobenzene, the spin coated films had slightly different emission profiles to that seen in figure 6.20. This is believed to be related to the fact that emission is morphology dependent. Some solvents could be considered as 'bad' while others could be 'good' solvents – in solution the polymer chains will adapt different conformations, possibly 'curlier' in a good solvent and 'straighter' in a bad solvent. Consequently, the situation could also be transmitted to the solid state, hence the small difference in the emission spectra.

The alkoxide substituted polymers used in the rest of this chapter were synthesised by P. C. Marr and J. A. Crayston [13]. The symmetrical and unsymmetrical monomers were first synthesised by a modified Williamson synthesis and from the *p*-methoxyphenol starting material respectively. The polymerisation reaction (figure 6.21) was then carried out by the method reported by Swatos and Gordon [39].

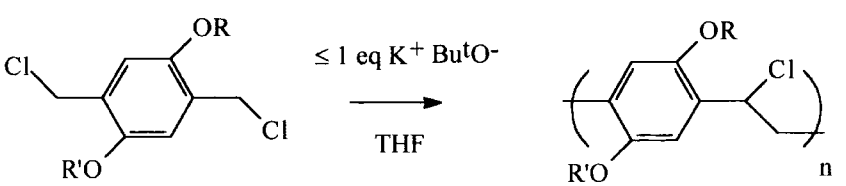

FIG. 6.21 *Polymerisation reaction of the precursor polymers.*

Polymer	Chemical structure
PPV	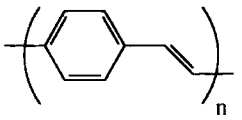
MEH-PPV	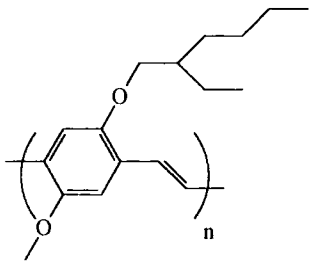
Polymer **1**	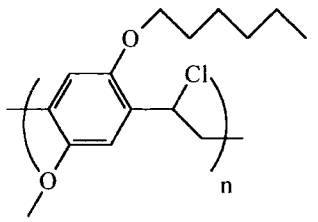
Polymer **2**	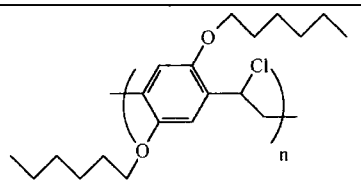
Polymer **3**	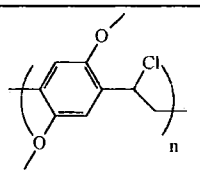
Polymer **4**	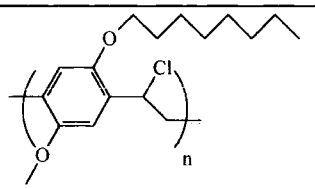
Polymer **5**	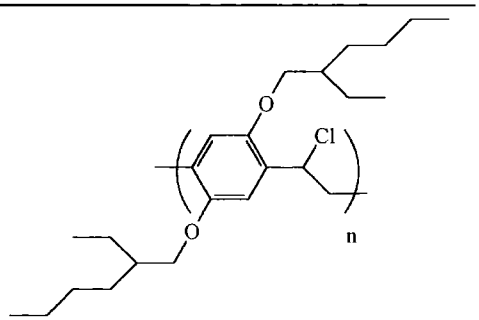

Table 6.1 *Chemical structure of different PPV based polymers.*

The precursor polymers were soluble in the following solvents in decreasing order: chlorobenzene, DMF, THF, benzene, toluene, and chloroform. The chemical structures of the alkoxide-substituted polymers are shown in table 6.1.

It should be noted that the NMR study, carried out on the precursor polymers (non-conjugated) by P. Marr *et al* [13], allowed to estimate the degree of conjugation. The results are summarised in the table below.

Polymer	Conjugation / %
1	39
2	23
3	25
4	38
5	< 5 (a)

(a) indicates that no aromatic peaks were apparent.

Table 6.2 *Estimates of the degree of conjugation from ^1H NMR data.*

It is clear from the values above that the polymers that are the most conjugated are **1** and **4**. Polymer **5** seems to be the least conjugated, and thus is believed to remain in its precursor form.

The absorption profile is another way of investigating the degree of conversion in this type of polymer [40,41] and so the absorption measurement was carried out on solutions to investigate the conversion and conjugation and also to study the effect of side chains on the polymers' optical properties.

Thin films were prepared by spin coating from 10 % w/v solutions of the polymers in chlorobenzene, except for polymer **2** films which were spin coated from chloroform. Spin speeds were in the range of 700-1200 rpm / 60 s. The absorption spectra of the polymer solutions and spin-coated films are shown in figure 6.22. The polymers seem to be divided into two groups. Polymers **1**, **2**, and **4** display a strong absorption in the

visible spectrum, peaking at around 450-500 nm. This indicates the presence of long conjugated segments in the polymer backbone. The other polymers, **3** and **5**, were weakly absorbing in the visible range with spectra dominated by features in the near-UV which indicates the dominance of non-conjugated segments.

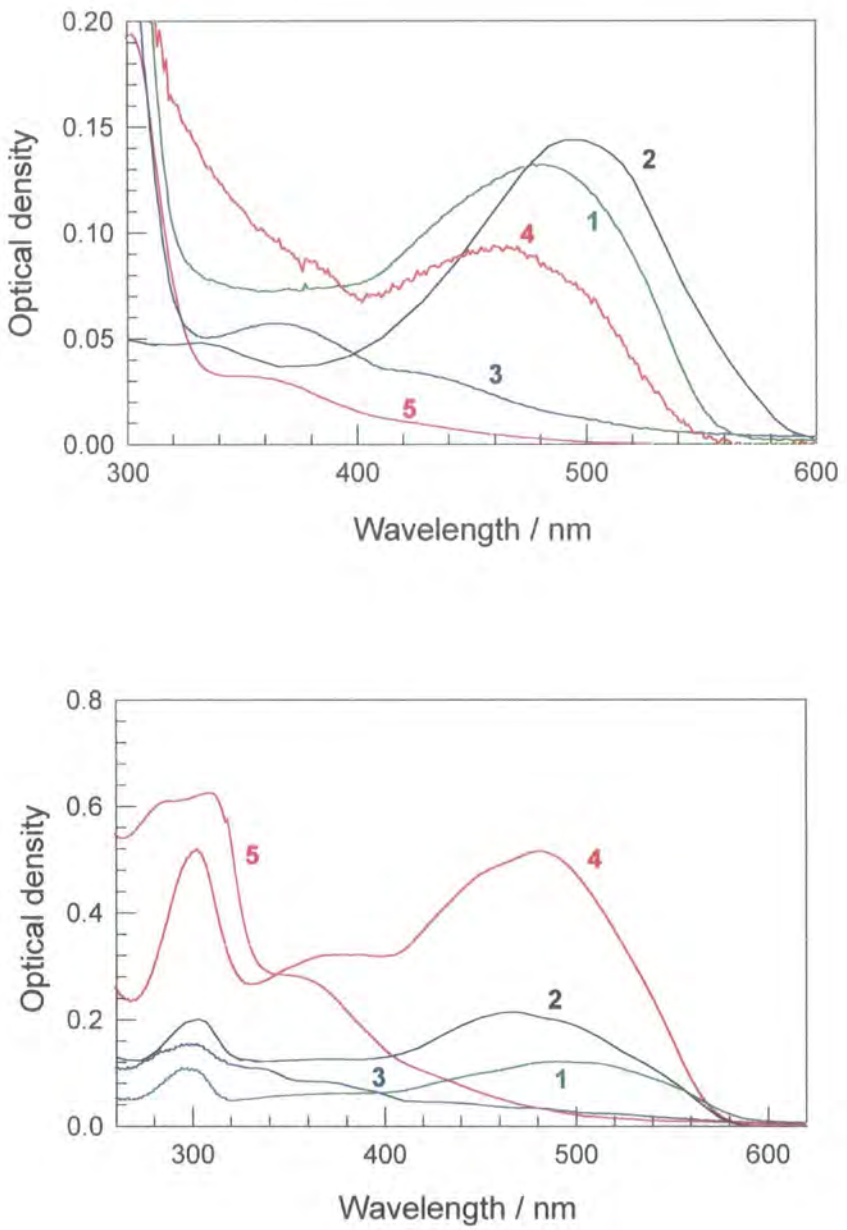

FIG. 6.22 *Absorption of PPV derivatives in solution (upper panel) and spin coated films (lower panel).*

The contrast observed in the absorption of these polymers can be related to several factors: inductive effects, degree of conversion or conjugation length, steric effects, and solubility. The inductive effect would explain the red-shift in the absorption of polymers **1**, **2**, and **4** with respect to the non-substituted PPV, however one would expect only a small inductive effect between the alkoxide substituted PPVs in their absorption spectra and therefore could not be responsible for the differences observed in the polymers' absorption.

The degree of conversion and the conjugation length could be a major factor in determining the difference between the absorption spectra of these polymers. This is in agreement with the NMR results which showed that polymers **1** and **4** have undergone a relatively high conversion, hence longer conjugation segments, whilst polymer **5** remains unconverted. Steric effects are also believed to have some influence on the conjugation in these polymers due to the twists and folds of the polymer chain causing a reduction in the extent of electron delocalisation. No evidence of such effects could be deduced form the absorption of polymers **1** - **4** . However, due to the bulky size of the side groups in polymer **5**, the steric hindrance is believed to be severe to such a degree it is preventing the elimination reaction, hence the non-conjugated precursor form of the polymer which is consistent with NMR and optical data. It is difficult to explain the different results obtained on polymer **2** and **3** despite their similar conversion ratios estimated by the NMR data.

H. Meier *et al* have studied dialkoxy-PPV oligomers where they considered the role of steric hindrance, inductive, and solubility effects on optical spectra [42]. They found that steric effects due to bulky side groups is demonstrable in molecular modelling calculations.

The PL measurement is another technique that could give valuable information on the conjugation of the polymer chain. Measurements were carried out on solution and spin coated films of polymer **1** - **5** and the spectra are shown in figure 6.23.

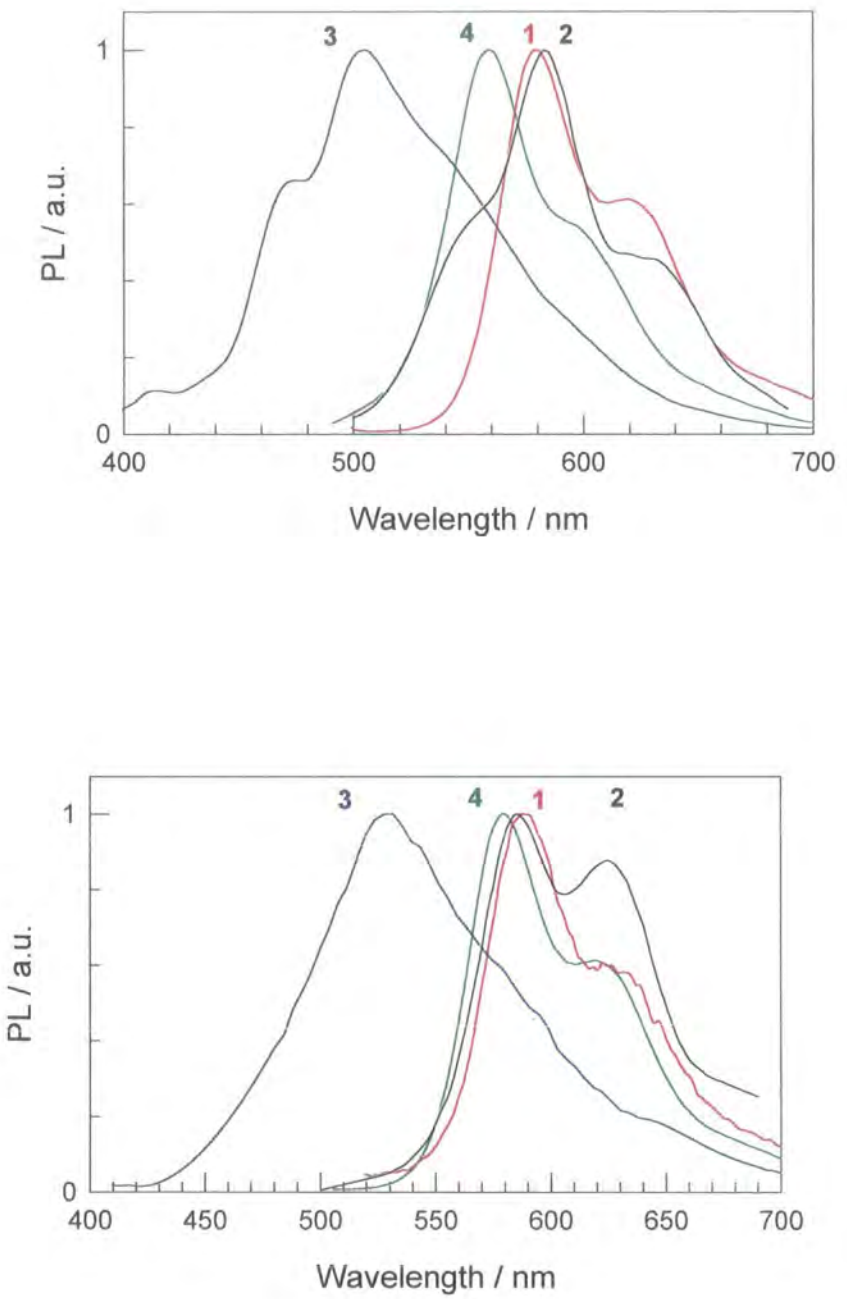

FIG. 6.23 *Photoluminescence of alkoxide PPVs in solution (upper panel) and spin coated films (lower panel).*

The photoluminescence spectrum of polymer **1** solution shows a defined vibronic structure with a maximum emission at around 580 nm. Note that the emission profile in polymer **1** is similar to MEH-PPV PL spectrum which is as expected, considering the similarity of their structures. Polymers **2** and **4** emit in the same range as **1** with similar spectra. Note that polymer **4** emits at slightly shorter wavelength with respect to **1** and **2**. The PL spectra of the corresponding spin coated films showed also the same solution results with the polymers emitting in the orange region of the visible spectrum and with similar spectra. Theses are the samples which were absorbing strongly in the visible region. PL spectra were also recorded for polymer **3** in solution and solid state and showed an unusual broad spectrum peaking at 506 and 530 nm respectively. Polymer **5** was found to be non-luminescent.

In conjugated polymers, it is believed that the polymer chains consist of a number of conjugated segments of varying length. This is reflected in the polymer absorption with a broad spectrum. However in the PL process, excitons, which are responsible for the luminescence, tend to migrate to lower energy segments before decaying radiatively, and therefore the emission in conjugated polymers occurs at longer conjugated parts of the polymer chain. Therefore the PL spectra of polymers **1**, **2**, and **4** indicates the well-conjugated environment particularly when compared to MEH-PPV. In polymer **3** the broadness of the spectrum could be an indication of emission that arises from a wide distribution of conjugation lengths caused by its intermediate conjugation estimated by NMR. The low concentration of well-conjugated segments is in agreement with the tail of the absorption of polymer **3** which spreads into the visible region.

P. Marr *et al* also reported the results TGA/DTA study [13]. The results showed that polymer **1** and **4** have undergone a similar degree of HCl elimination whereas polymer **5** shows a much lower amount. This is in contrast to the NMR data and is explained by the fact that polymers contains some cross-links which, although arising from HCl loss, do not lead to the formation of conjugated segments. Polymers **1**, **4**, and **5** are believed to have developed more cross-links than the other polymers due to easier elimination of HCl through formation of cross-links.

6.8 Conclusion

Poly(*p*-pyridine) has recently become one of the exciting members of the family of polymers for LEDs due to its interesting luminescence properties. In solution, PPY behaves much like the other luminescent conjugated polymers and is emitting in the blue range of the visible spectrum with a reasonable quantum yield in the range of 17 %. However, in the solid state the emission is more efficient (37 %) and substantially shifted towards longer wavelengths. The relatively low quantum yield in solution is attributed to efficient quenching due to formation of triplets by intersystem crossing, which is believed to increase with increased torsion angle (30° in solution). The red-shift is also related to the different environment in solution and solid state created by the twists in the pyridyl rings. PPY is a rigid rod polymer and so its chains are believed to adopt a planar configuration due to inter-chain interactions which reduces the torsion angle leading to extended electron delocalisation, hence the red-shift. Aggregates can be ruled out as dilution studies on PPY solution PL show no major differences in the emission profile. PL dilution studies on PPY films were carried out using PMMA as a host material. The results are in agreement with the previous work as they showed the appearance of a new emitting species in the blue range as the dilution decreased. The emission corresponds to the solution emission.

The proposed model of planarity of PPY chains in the solid state is further supported by the protonation study carried out on PPY using some strong functionalised studies. The solution-like emission was clearly seen together with the green (solid state) emission at higher doping levels. The blue emission was accompanied with a decrease in the absolute photoluminescence quantum yield which reflects the solution state.

Sample	Emission (nm)	ϕ_{PL} (%)
s_PPY	416	17
f_PPY	548	37
f_PPY$_{100CSA}$	520 - 470	22
f_PPY$_{100AMPSA}$	522 - 485	28
f_PPY$_{100DCA}$	560	20
f_PPY$_{100m\text{-}cresol}$	543	18

The prefix s_ and f_ stand for solution and solid state respectively and are used for the purpose of clarity.

Table 6.3 *Summary of the emission wavelengths and quantum yields of different PPYs.*

The effect of temperature on the emission and its intensity of PPY films is also in agreement with the model in that the configuration of the polymer chains are reasonably planar and hence the low temperature had little effect on the position of the emission and PL quantum yield.

Dialkoxy substituted PPVs were also studied to understand the effect of side chains on the polymers properties. NMR investigations on the precursor polymers revealed the partial conjugation in the polymers backbone, except for polymer **5**. This was verified using absorption and photoluminescence spectroscopy. The results agreed with the NMR data showing a different degree of conversion (conjugation) in the polymers. The difference in the optical spectra were related to the degree of conversion and other factors such as inductive effects, solubility, and steric hindrance. The low-temperature elimination of HCl was found to be affected by the large substituents. For example in polymer **5** the elimination of HCl is blocked due to large side groups affecting the backbone rotation necessary prior to elimination. Cross-linkage was also believed to be more favourable than formation of conjugated segments in the polymers with large side chains.

References

1. P. L. Burn, A. B. Holmes, A. Kraft, D. D. C. Bradley, A. R. Brown and R. H. Friend, *J. Chem. Soc. Chem. Comm.*, **1992**, 32.
2. S. Chung, K.-Y. Kwon, S.-W. Lee, J.-I. Jin, c. H. Lee, C. E. Lee and Y. Park, *Adv. Mater.*, **1998**, 10, 1112.
3. D. Hwang, S. T. Kim, H. Shim, A. B. Holmes, S. C. Moratti and R. H. Friend, *Synth. Met.*, **1997**, 84, 615.
4. Y. Yang, Q. Pei and A. J. .Heeger, *J. Appl. Phys*, **1996**, 79, 934.
5. F. Cacialli, R. H. Friend, N. Haylett, R. Daik, W. J. Feast, D. A. dos Santos and J. L. Bredas, *Appll. Phys. Lett.*, **1996**, 69, 3794.
6. G. Grem and G. Leising, *Synth. Met.*, **1993**, 55-57, 4105.
7. G. Leising, S. Tasch, F. Meghdadi, L. Athouel, G. Froyer and U. Scherf, *Synth. Met.*, **1996**, 81, 185.
8. T. Yamamoto et al, *J. Am. Chem. Soc.*, **1994**, 116, 4832.
9. J. W. Blatchford, S. W. Jessen, L.-B. Lin, T. L. Gustafson, D.-K. Fu, H.-L. Wang, T. M. Swager, A. G. MacDiarmid and A. J. Epstein, *Phys. Rev. B*, **1996**, 54, 9180.
10. A. P. Monkman, M. Halim, S. Dailey, I. D. W. Samuel, M. Sluch and L. E. Horsburgh, *SPIE*, **1997**, 3148, 82.
11. A. Brown, PhD thesis, **1992**, University of Cambridge.
12. C. L. Gettinger, A. J. Heeger, J. M. Drake and D. J. Pine, *J. Chem. Phys.*, **1994**, 101, 1673.
13. P. C. Marr, J. A. Crayston, M. Halim and I. D. W. Samuel, *Submitted to Macromolecules.*
14. H. S. Woo, O. Lhost, S. C. Graham, D. D. C. Bradley and R. H. Friend, *Synth. Met.*, **1993**, 59, 13.
15. S. A. Jenekhe and J. A. Osaheni, *Science*, **1994**, 265, 765.
16. D. D. C. Bradley, M. Grell, X. Long, H. Mellor, A. Grice, M. Inbasekaran and E. P. Woo, *SPIE*, **1997**, 3145, 254.
17. N. N. Barashkov, D. J. Guerrero, H. J. Olivos and J. P. Ferraris, *Synth. Met.*, **1995**, 75, 153.

18. A. P. Monkman *et al, to be published.*

19. G. Grezsinzki, N. Johanssen, A. P. Monkman and W. J. Salaneck, *in press.*

20. A. J. Epstein, Y. Wang, W. Jessen, J. W. Blatchford, D. Gebler, L. Lin and T. L. Gustafson, *Macromol. Symp.,* **1997**, 116, 27.

21. N. C. Greenham, I. D. W. Samuel, G. R. Hayes, R. T. Phillips, Y. A. R. R. Kessner, S. C. Moratti, A. B. Holmes and R. H. Friend, *Chem. Phys. Lett.,* **1995**, 241, 89.

22. A. P. Monkman, M. Halim, S. Dailey, I. D. W. Samuel, and L.E. Horsburgh, ISCM, **1998**, France.

23. J. W. Blatchford, T. L. Gustafson and A. J. Epstein, *J. Chem. Phys.,* **1996**, 105, 9214.

24. I. D. W. Samuel, G. Rumbles and C. J. Collison, *Phys. Rev. B,* **1995**, 52, R11573.

25. I. D. W. Samuel, B. Crystall, G. Rumbles, P. L. Burn, A. B. Holmes and R. H. Friend, *Chem. Phys. Lett.,* **1993**, 213, 472-478.

26. U. Lemmer, R. F. Mahrt, Y. Wada, A. Greiner, H. Bassler and E. O. Gobel, *Appl. Phys. Lett.,* **1993**, 62, 2827.

27. H. Antoniadis and e. al, *Phys. Rev. B,* **1994**, 50, 14911.

28. K. Z. Xing, N. Johansson, G. Beamson, D. T. Clark, J. Bredas and W. R. Salaneck, *Adv. Mater.,* **1997**, 9, 1027. K. Z. Xing, M. Fahlman, M. Logdlund, D. A. D. Santos, V. Parente, R. Lazzaroni, J. Bredas, R. W. Gymer and W. Salaneck, *Adv. Mater.,* **1996**, 8, 971.

29. Y. Cao and P. Smith, *Synth. Met.,* **1995**, 69, 187.

30. E. R. Holland, S. J. Pomfret, P. N. Adams and A. P. Monkman, *J. Phys. Cond. Matter,* **1996**, 8, 2991.

31. L. Abell, P. N. Adams and A. P. Monkman, *Polym. Comm.,* **1996**, 37, 5927.

32. O. T. Ikkala, L. Pietila, L. Ahjopalo, H. Osterholm and P. J. Passiniemi, *J. Chem. Phys.,* **1995**, 22, 9855.

33. A. P. Monkman, *to be published.*

34. P. Adams *et al, in Press.*

35. C. J. Collison, PhD Thesis, Imperial College of Science, London.

36. N. F. Colaneri, D. D. C. Bradley, R. H. Friend, P. L. Burn, A. B. Holmes and C. W. Spangler, *Phys. Rev. B,* **1990**, 42, 11670.

37. N. C. Greenham, S. E. Burns, I. D. W. Samuel, R. H. Friend, S. C. Moratti and A. B. Holmes, *J. Mol. Cryst. And Liq. Cryst.,* **1996**, 283, 51.

38. I. D. W. Samuel, B. Crystall, G. Rumbles, P. L. Burn, A. B. Holmes and R. H. Friend, *Chem. Phys. Lett.,* **1993**, 213, 472.

39. W. J. Swatos and B. Gordon, *Amer. Chem. Div. Polym. Chem.,* **1990**, 31/1, 505.

40. J. D. Gagon, F. E. Capistran, J. Karaz, R. W. Lenz and S. Antoun, *Polymer,* **1987**, 28, 567.

41. J. B. Schlenoff and L. J. Wang, *Macromolecules,* **1991**, 24, 6653.

42. H. Kolshorn, H. Kretzschmann and H. Meier, *J. Praktische Chem-Chem. Ztg.,* **1994**, 336, 292.

Chapter 7

General Conclusions

At the current time conjugated polymers are exciting materials for use in light-emitting displays. Due to their many advantages, such as efficient electron-hole recombination and high level of brightness, conjugated polymers show real potential for use in commercial panel displays (see fig 8.1). For many of these materials, high electroluminescence efficiencies were consistent with their high absolute photoluminescence quantum yield, hence the importance of the integrating sphere technique. An experimental set-up was built to measure the absolute photoluminescence quantum yield in the solid state of all materials described in this thesis. The technique also proved useful in assessing new efficient materials.

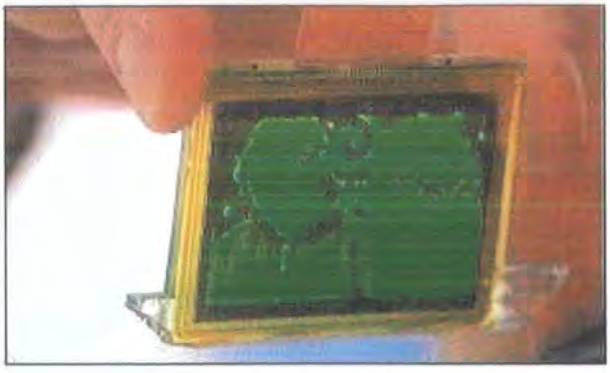

FIG. 8.1 *Miniature polymer display demonstrated by CDT Ltd.*

However, conjugated polymers still suffer from disadvantages such as poor photo-stability and the difficulty in obtaining pure blue emission, hence the need for developing new materials to overcome such obstacles. At the beginning of this project new conjugated dendrimers of different generations were studied in order to assess their potential for use in LEDs. The distyrylbenzene (DSB) based dendrimer consisted of a central core, branching units and functional surface groups. Each of these parts proved to play a different role, the core controlled the emission of the dendrimer while branches and surface groups affected transporting and processing properties. All generations gave strong blue photoluminescence with a reasonable photoluminescence quantum yield ranging between 20 and 36 % for different generations. They can be spin-coated from solution to give optical quality thin films. Moreover, they have been used as emissive layers in LEDs and emitted blue electroluminescence in all generations. The generation number was found to have a large effect on device performance. The most dramatic being nearly an order of magnitude increase in external quantum efficiency in going from the first to second generation dendrimer.

One of the most attractive features of these conjugated dendrimers was found to be the possibility of tuning their processing and electronic properties independently. Therefore to obtain different emission wavelengths, one had only to replace the dendrimer core by another compound emitting in a different region of the spectrum. An anthracene derivative and a porphyrin molecule were used as the cores in first and

second generation dendrimers while the branches and surface groups were the same as in the DSB-based dendrimer. The new dendrimers were soluble in common organic solvents and formed good quality films by spin coating. The films were strongly luminescent with photoluminescence quantum yields in the range of 50 % for the anthracene dendrimer. Monolayer LEDs were successfully fabricated and control of colour was demonstrated showing good potential for organic LEDs

The new molecular architecture where chromophores are implemented in the centre of a dendrimer proved to be successful in combining properties of small molecules and long polymers. The combination of the two structures offered the advantage of an extended colour range using different chromophores and the processibility of polymers for easy device fabrication. The processibility of theses dendrimers provides a way of making chromophores in solution-processible form which also offers a extended range of chromophores that could be used for LEDs. The dendritic molecular structure offered the possibility of controlling aggregation and optimising the optical, electronic, and processing properties independently, a feature that is desirable for improving device performance.

Conjugated polymers are known for their characteristic of tuning the emission wavelength by simply modifying the chemical structure of the polymer. However, unlike dendrimers, this can change the electronic and processing properties which can prove to be inconvenient in some cases. Nevertheless, it offers an alternative for colour tuning. In PPY for example, luminescence was obtained in the green-region of the visible spectrum. PPY demonstrated different behaviour to PPV as the photoluminescence quantum yield of spin coated films, which was measured to be 37 %, remained stable in air. Emission in PPY was also found to be different from that in solution. This is attributed to the torsion angle of the pyridyl rings. In the solid state the polymer chains are driven planar by inter-chain interactions.

Different alkoxide-substituted PPVs were studied and revealed the effect of different side chains on polymer properties.

APPENDIX

List of Publications

1. Measurement of time dependent quantum yield of poly(*p*-pyridine) and poly(*p*-phenylenevinylene)
M. Halim, I. D. W. Samuel, E. Rebourt and A. P. Monkman, *Synth. Met.*, **1997**, 84, 951.

2. Polypyridine as an efficient electron-transporting polymer for light-emitting diodes
S. Dailey, M. Halim, E. Rebourt, I. D. W. Samuel, and A. P. Monkman, *Proceedings of SPIE meeting*, 28-30 July **1997** San Diego, California.

3. Photophysical characterisation of poly(*p*-pyridine)
A. P. Monkman, M. Halim, S. Dailey, I. D. W. Samuel, M. Sluch, and L. E. Horsburgh. *Proceedings of SPIE meeting,* 28-30 July **1997** San Diego, California.

4. An efficient electron-transporting polymer for light-emitting diodes
S. Dailey, M. Halim, E. Rebourt, I. D. W. Samuel, L. Horsburgh, A. P. Monkman, J. Phys. Cond. Mat.,**1998**, 10, 5171.

5. Photo- and electro-luminescence of MEH-PPV Langmuir-Blodgett films
M. I. Sluch, C. Pearson, M. C. Petty, M. Halim and I. D. W. Samuel, *Synth. Met.*, **1998**, 94, 285.

6. Protonation effects on the photophysical properties of poly(2,5-*p*-pyridine diyl)
A. P. Monkman, M. Halim, I. D. W. Samuel and L. E. Horsburgh, **1998**, *J. Chem. Phys., 109, 23, 10372.*

7. Conjugated dendrimers for light-emitting diodes: effect of generation
M. Halim, J. N. G. Pillow, I. D. W. Samuel, and P. L. Burn, *in Press.*

8. Synthesis and characterisation of 2,5-dialkoxy-*p*-phenylenevinylene light-emitting polymers (LEPs)
P. C. Marr, J. A. Crayston, J. C. Walton, M. Halim and I. D. W. Samuel, *in Press.*

9. Conjugated dendrimers for LEDs: control of colour
M. Halim, I. D. W. Samuel, J. N. G. Pillow, and P. L. Burn, *Proceedings of ICSM meeting*, 12-18 July **1998**, Montpellier, France.

10. Controllig the photophysics of poly(*p*-pyridine) via doping
A. P. Monkman, M. Halim, and L. E. Horsburgh, *Proceedings of ICSM meeting*, 12-18 July **1998**, Montpellier, France.

11. Control of colour and charge injection in conjugated dendrimer/polypyridine bilayer LEDs
M. Halim, I. D. W. Samuel, J. N. G. Pillow, A. P. Monkman, and P. L. Burn, *Proceedings of ICSM meeting,* 12-18 July **1998**, Montpellier, France.

12. The effect of dendrimer generation on LED efficiency
M. Halim, P. L. Burn, J. N. G. Pillow, and I. D. W. Samuel, *Proceedings of ICSM meeting*, 12-18 July **1998**, Montpellier, France.

13. The photophysics of polypyridine
A. P. Monkman, M. Halim, L. E. Horsburgh, S. J. Pomfret, L. J. Hartwell, I. D. W. Samuel, and S. Dailey, *Proceedings of ICSM meeting,* 12-18 July **1998**, Montpellier, France.

14. Photophysical studies of isolated polypyridine chains
A. P . Monkman, M. Halim, L. J. Hartwell, L. E. Horsburgh, and S. Dailey, *Proceedings of ICSM meeting,* 12-18 July **1998**, Montpellier, France.

15. Synthesis of conjugated dendrimers
J. N. G. Pillow, M. Halim, I. D. W. Samuel, and P. L. Burn
Submitted to Macromolecules.

16. Synthesis of dialkoxy-*p*-phenylenevinylenes for light-emitting polymer devices
P. C. Madden, J. A. Crayston, J. C. Walton, M. Halim, and I. D. W. Samuel,
Proceedings of ICSM meeting, 12-18 July **1998**, Montpellier, France.